Volume 36 No. 1 | JNSChE Mar/Apr 2021 | ISSN 0794-6759

DOI: 10.51975/EFSD2591

JOURNAL OF THE NIGERIAN SOCIETY OF CHEMICAL ENGINEERS

Published by,
THE NIGERIAN SOCIETY OF CHEMICAL ENGINEERS
National Secretariat: Infinite Grace House, Plot 4, Oyetubo Street,
Off Obafemi Awolowo Way, Ikeja, Lagos State, Nigeria.
E-mail: nationalhqtrs@nsche.org, nsche_headquarters@yahoo.com
Website: https://www.nsche.org.ng; Journal URL: https://journal.nsche.org.ng
Submission of Manuscripts: nschejournal@yahoo.com and copy: stevmomoh@yahoo.com

JOURNAL OF THE NIGERIAN SOCIETY OF CHEMICAL ENGINEERS
A Publication on the Science and Technology of Chemical Engineering

EDITORIAL BOARD

2021 BOARD OF DIRECTORS AND OFFICIALS

INTERNAL AUDITORS

SUBSCRIPTION

a.	**Individual Member**	~~₦~~3,000.00
b.	**Overseas Subscribers**	US$100.00
c.	**Institution, Libraries, etc**	~~₦~~5,000.00

CHAPTER CHAIRMEN

Engr. G. H. Abubakar, *MNSChE*	Kogi
Engr. (Mrs.) Rosemary O. Imhanwa, *MNSChE*	Edo/Delta
Engr. I. A. Dirani, *MNSChE*	ABBYGOT
Prof. I. A. Mohammed-Dabo, *MNSChE*	Kaduna
Dr. M. S. Nwakaudu, *FNSChE*	Imo/Abia
Prof. G. O. Mbah, *FNSChE*	Anambra/Enugu/ Ebonyi
Dr. A. A. Ujile,*FNSChE*	RIVBAY
Engr. N. A. Akanji, *MNSChE*	Niger
Engr. O. O. Onugu, *FNSChE*	FCT/Nasarawa
Prof. E. A. Taiwo, *MNSChE*	Oyo/Osun/Kwara
Dr. K. F. K. Oyedeko, *FNSChE*	Lagos/Ogun
Engr. T. S. Soom, *MNSChE*	Benue Industrial
Dr. I. O. Oboh , *MNSChE*	Akwa Ibom/Cross River
Prof. E. I. Dada, *FNSChE*	USA

DOI: 10.51975/SRCX6538
Journal of the Nigerian Society of Chemical Engineers, 36(1), 2021

APPLICATION OF LOW-TEMPERATURE THERMAL ARC PLASMA REACTOR FOR PETROLEUM INDUSTRY WASTEWATER SLUDGE TREATMENT

***Abubakar M. A[1], Abdulkarim, B. I.[2] and Kefas, E. G.[3]**
[1,3] Department of Chemical Engineering, Kaduna Polytechnic, Kaduna, Nigeria
[2] Department of Chemical Engineering, University of Abuja, Nigeria
E-mail*: abualimoh67@gmail.com, balisa76@yahoo.com* & *egkefas@yahoo.com*

ABSTRACT
A large quantity of wastewater sludge is generated yearly. Traditional disposal methods are short of providing the much needed benign treatment. Thermal plasma is a promising treatment technique to address this problem. A 20 cm^3 capacity laboratory-scale thermal-arc plasma reactor was developed using a 4.5 kW TIG welding torch and was used to treat wastewater sludge. The design was based on a DC transferred-arc torch with argon gas as plasma forming gas. The reactor was tested with wastewater sludge from the petroleum industry. The plasma arc temperature was in the range of 356 – 1694 ^oC at an arc current of 100 – 190 A. Two products, flue gas and a vitreous slag were obtained. A mass reduction of 36.87 – 91.40% of the sludge was achieved at an arc current 150 – 190 A, which correspond to a plasma temperature range of 539 – 1603 ^oC. The mass reduction increased with treatment duration from 2 – 8 min. The mass reduction also increased with increasing arc current from 150 – 190 A at an interval of 20 A. Reduction in total organic carbon (TOC) was between 74.03 – 75.83%. The metal elements in the wastewater sludge were enriched after the plasma treatment. The composition of the flue gas is H_2, CO, O_2, CO_2, CH_4 and C_2 hydrocarbons. CO is the major component accounting for over 74%. The concentration of greenhouse gases (CH_4 and CO_2 combined) is less than unity. The system was able to gasify the organics in the wastewater sludge to combustible gases and vitrified the inorganics into a slag.

Keyword*: Thermal plasma, wastewater sludge, plasma temperature, mass reduction, TOC, carbon conversion*

1. INTRODUCTION

Thermal arc plasma technology has become a prominent waste treatment technique for a wide variety of waste because of the shortcomings of traditional waste disposal methods (Ali *et al.*, 2016). The plasma arc treatment technology has been identified as a potentially effective tool for producing less harmful by-products which can be used in building and road construction (Kourti *et al.*, 2011; Tu *et al.*, 2008). The innovative plasma technique involves subjecting waste material to high-temperature arc plasma such that the organics and the volatile species are gasified while the inorganics and non-volatiles are chemically bonded in a vitreous matrix, thereby making them resistant to leaching of heavy metals (Agon, 2015). Thermal arc plasma provides a suitable treatment technique for special waste disposal requirements. Advantages of thermal arc plasma treatment technique over conventional incineration include high-temperature regime, high waste volume reduction, low gas throughput, process flexibility in either oxidizing or a reducing environment, and can effectively treat a wide variety of waste types (Heberlein, 2002).

There is an increase in the documented research, in the last two decades, concerning the destruction of hazardous wastes using thermal arc plasma technique. The growing interest of academic research in such an area cannot be unrelated to the ability of the technique to reduce waste volume by over 80% and produce benign byproducts (Ali *et al.*, 2016; Heberlein and Murphy, 2008). The plasma gasification of the organic portion of sludge has attracted interest as a source of energy and spawned process developments for the treatment of sludge from different sources (Bień *et al.*, 2013; Celary and Sobik-Szołtysek, 2014; Cubas *et al.*, 2014; Kim and Park, 2004; Leal-Quirós and Villafañe, 2007; Li *et al.*, 2007; Li *et al.*, 2012; Li *et al.*, 2015a; Li *et al.*, 2015b; Mohai and Szépvölgyi, 2005; Mountouris *et al.*, 2008; Ramachandran and Kikukawa, 2002; Shie *et al.*, 2014; Sobiecka and Szymanski, 2014). Factors like treatment efficiency, plasma gas flow-rate, the treatment period of a batch operation, feed flowrate of continuous operation and inter-electrode separation were the subject of investigation.

Feasibility studies involving design and fabrication of thermal arc plasma reactors for hazardous waste destruction are also documented in the literature. In the USA a laboratory-scale thermal arc plasma reactor consisting of a highly instrumented furnace equipped with a 75 kW transferred arc plasma torch, was developed and used to study the physical and chemical behaviour of metal-spiked waste (nickel and chromium) in a high-temperature plasma regime (Cortez *et al.*, 1996). In Thailand, a 20 kW laboratory-scale, atmospheric-air DC plasma reactor was designed and fabricated using a non-transferred plasma torch and its performance was evaluated using electronic waste (Tippayawong and Khongkrapan, 2009). A research team in Brazil developed a small-scale, continuous-flow plasma reactor consisting of a torch with graphite electrodes and an integrated nebulization furnace. The reactor was used to eliminate carbon-tetrachloride from liquid waste (Cubas *et al.*, 2005). In the Durgapur city of West Bengal, a 20 kg/hr plasma reactor for the treatment of waste plastic was developed, and its performance on the pyrolysis of waste plastic and energy generation was studied (Punčochář *et al.*, 2012). Other similar studies involving the design and evaluation of thermal plasma reactor for hazardous waste destruction were reported (Barcza, 1986; Khongkrapan *et al.*, 2013; Szałatkiewicz *et al.*, 2012, 2013; Tang *et al.*, 2003; Townsend and Oehmig, 2014; Zhao *et al.*, 2001).

It is obvious from the above discussion that waste treatment using thermal plasma technology has gained ground, and laboratory/pilot scale plasma reactors have been developed and their performances for the destruction of hazardous waste were studied. However, to the knowledge of the authors, any attempt to develop a thermal arc plasma reactor that treats wastewater sludge from the petroleum industry it not available. The wastewater sludge from the petroleum industry is unique in its composition due to the presence of hydrocarbons, phenols and dissolved minerals (Diya'uddeen *et al.*, 2011). Thus, the present investigation was geared towards bridging this gap. In this study, a 20 cm^3 capacity laboratory-scale thermal-arc plasma reactor was developed and used to treat wastewater sludge from the petroleum industry.

2. MATERIALS AND METHOD

2.1. Thermal Plasma Reactor

The thermal plasma process system consists of a DC power source, a transferred arc plasma torch, a reaction chamber and a gas cooling and cleaning system. The process flow diagram of the system is shown in Fig.1. The equipment power rating and reactor capacity were based on a commercially available torch and 20 cm^3 of sludge respectively. The DC power source is a TIG (master weld, model: TP-2000) used commercially for arc welding, it supplies a voltage of 63 V and a variable current of 5 – 200 A to the plasma torch.

The transferred arc plasma torch was a Ø 2.4 mm tungsten rod (98% purity) inserted into the centre of a nozzle ejector. The torch was connected to the negative terminal of the DC power source. The nozzle ejector had an orifice opening through which argon gas (the plasma forming gas) flows. The torch was supported vertically at 10 cm distance above the anode electrode. The anode was a tungsten rod of Ø 10 mm and 35 mm length, placed concentrically at the centre of the reaction chamber. The reactor furnace was an aluminium block with a sculptured conical shaped chamber at the inner side and a cooling water jacket surrounding the chamber. The block had a dimension of 99 mm by 95 mm rectangular bottom and a height of 116 mm. The conically shaped chamber had a dimension of Ø 42 mm top, Ø 13 mm base and 20 mm depth. The furnace had a flue gas outlet and a glass window for temperature measurement. The gas cooling and cleaning system consisting of a cooling coil and particle gas filter were connected to the gas outlet. Photographs of the equipment components and the reactor setup are shown in Plate I. Specifications for TIG master weld and reactor system are shown in Tables 1 and 2 respectively

DOI: 10.51975/SRCX6538
Journal of the Nigerian Society of Chemical Engineers, 36(1), 2021

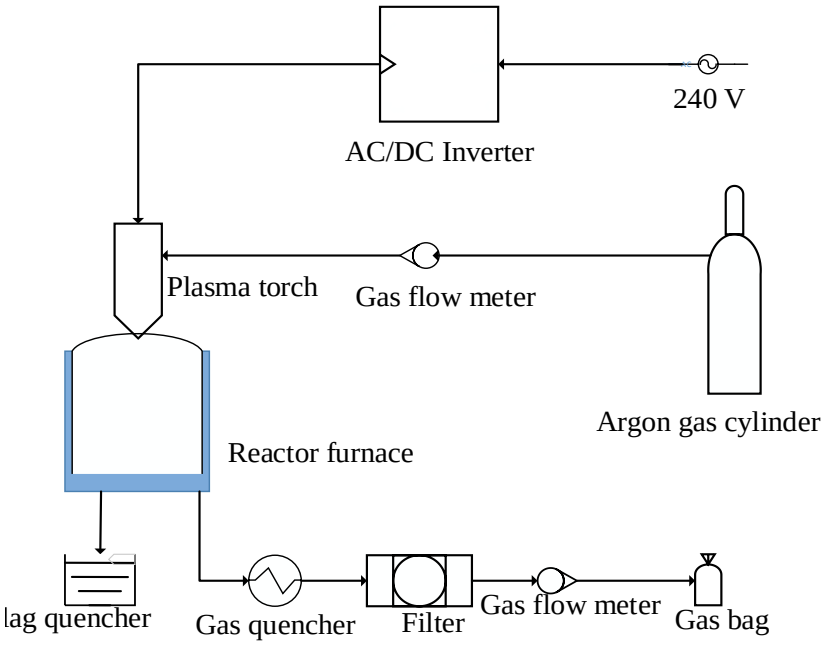

Fig. 1: Process flow diagram of the setup for plasma treatment of sludge

(a) The torch (b) reactor furnace (c) assembled chamber (d) complete setup

Plate I: Photographs of the equipment components and the reactor setup

Table 1: TIG master weld specifications

Specification	Input rating	Output rating
Model	TP – 2000	
Efficiency (%)	80	
Power (kW)	4.7	
Voltage (V)	220/230/240	63
Current (A)	31	5 – 200

2.2. Plasma Treatment of the Wastewater Sludge

A current of 100 A and argon flow-rate of 10 L/min were supplied to ignite and generate the arc plasma. The supplied current was increased gradually using a control nob while the plasma temperature was measured at intervals using an infrared thermometer (temperature range of 200 – 2200 ^{o}C). The same procedure was repeated with argon flow-rate of 5 L/min and 15 L/min. The result of temperature measurement is presented in Fig. 2. Samples of wet wastewater sludge were treated batch-wise in the thermal arc plasma generated at arc currents of 150, 170 and 190 A respectively. At each of the operating current 20 cm^3 of the sludge was treated for 2, 4, 6, 8 and 10 min respectively. The flue gas, after passing through the cooling coil and the particle dust filter, was collected in a Teflon gas bag and analyzed in an offline residual gas analyzer (model: MKS Cirrus 2). The reactor was allowed to cool to room temperature. The slag collected, weighed and analyzed using TOC analyzer (Model SSM-5000A) and AAS machine (model: Perkin Elmer, PinAAcle 900T).

Table 2: Reactor parts and specifications

Reactor furnace: rectangular aluminium block
Dimension: 99 mm by 95 mm bottom, 116 mm height
Reaction chamber: conical shape
Dimension: Ø 42 mm top, Ø 13 mm base and 20 mm depth
Reactor inner volume: 20 cm^3
Cathode: long tungsten rod (98% purity)
Dimension: Ø 2.5 mm and length 150 mm

Anode: tungsten rod (98% purity)
Dimension: Ø 10 mm and length 35 mm

3. RESULT AND DISCUSSION

3.1. Plasma Arc Temperature Profile

The thermal arc plasma ignited at an arc current of 100 A, bellow 100 A only vibration was observed. At an argon gas flow-rate of 15 L/min, when the plasma arc current was increased from 100 – 190 A, the plasma arc temperature increased from 356 – 1694 ^{o}C. This increase in temperature was not uniform all through. Between 100 – 140 A, the increase in temperature was gradual, from 372 – 627 ^{o}C respectively. However, from 140 – 190 A, the plasma arc temperature increased from 627 – 1694 ^{o}C. This trend of increased plasma arc temperature with increased plasma arc current was equally observed with argon gas flow-rate of 10 and 5 L/min as depicted in Fig 2. The plasma temperature also increased when the argon gas flow-rate increased from 5 – 15 L/min.

Kim *et al.* (2003) reported a temperature of range of 1520 – 1570 K in a steam plasma used for the treatment of polychlorinated biphenyls (PCBs). Similarly, Tang and Huang (2005) observed an increased in temperature from 1073 – 1773 K in a high-frequency (HF) plasma reactor used for pyrolysis of waste tyre powder. In both the two literature results, an increased in the plasma temperature with increased arc current were reported.

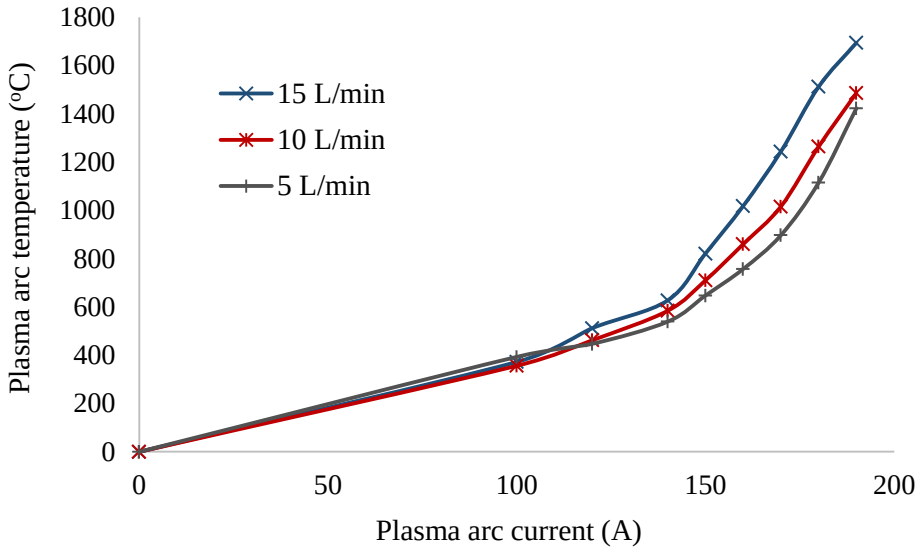

Fig. 2: Effect of plasma arc current and gas flow-rate on plasma temperature

3.2. Mass and Volume Reduction

The mass reduction achieved through the thermal plasma treatment of wastewater sludge from the petroleum industry was in the range of 36.87 – 91.40%. The obtained mass reduction was achieved at a relatively high plasma arc current (150 – 190 A). At 150 – 190 A, the plasma temperature ranges between 539 – 1603 ^{o}C. The high-temperature plasma environment decomposed the bulk of the sludge (the organic fraction) leaving behind small fraction (the inorganic) as a byproduct. There is a general increase in the mass reduction of the wastewater sludge with an increase in the plasma treatment duration as shown in Fig 3. At a plasma arc current of 190 A, the mass reduction increased from 44.78 – 91.40% when the plasma treatment duration increased from 2 – 10 min. Likewise, at 170 and 150 A, the mass reduction increased with increased plasma treatment duration.

The increase in the mass reduction is associated with the elevated temperature in the thermal plasma regime coupled with the limited amount of oxygen in the reaction chamber. The hydrocarbons in the wastewater sludge were gasified in the reducing environment by the elevated temperature plasma, into flue gases. Thereby, leaving the inorganics and heavy metals in the vitreous slag. The mass reduction was most significant between the 2nd and the 8th min, suggesting that the hydrocarbons were mostly gasified within the first 8 min of treatment. Similarly, mass reduction increased with increasing arc current from 150 – 190 A at an interval of 20 A. At

constant applied voltage, the current is proportional to the power. Thus, higher arc current leads to a higher power, which yielded more decomposition of the hydrocarbons.

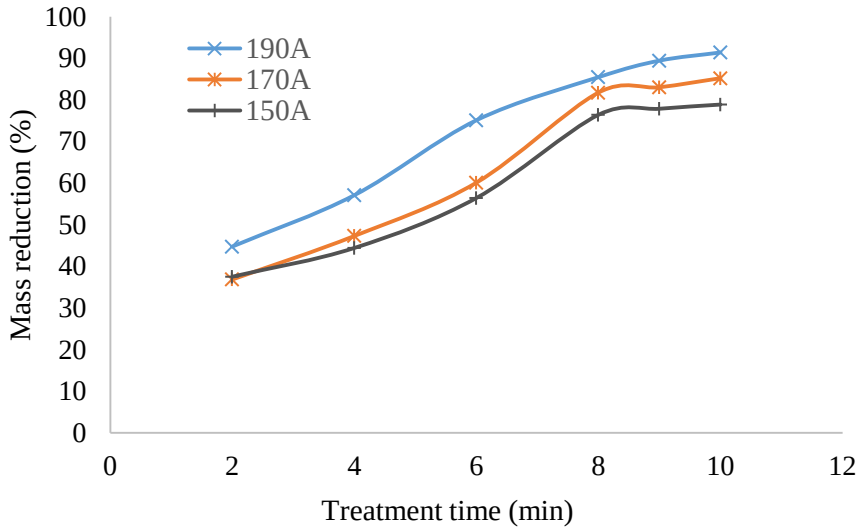

Fig. 3: Effect of treatment duration and arc current on mass reduction of sludge

3.3. Total Organic Carbon and Metal Composition

The measurement of the total organic carbon (TOC) in both the wastewater sludge and the product slag was conducted via the Total Organic Carbon-Solid Sample Module (TOC-SSM) machine (Model: SSM-5000A) (Ali *et al.*, 2017). Glucose was used as a standard for total carbon (TC) measurement while sodium carbonate was used as a standard for inorganic carbon (IC) measurement. Finally, TOC was calculated as the difference between the results of the measurements of TC and IC. The effectiveness of the thermal plasma reactor in treating the wastewater sludge was evaluated by determining the percentage carbon conversion using Equation 1. Carbon conversions of 74.03%, 75.83% and 75.86% were achieved with 150, 170 and 190 A respectively as shown in Table 3. These high carbon conversions are evidence of effective gasification of the hydrocarbon in the wastewater sludge by the thermal plasma. A similar result was reported by Li *et al.* (2015a) where a 100% carbon conversion of hydrocarbons was obtained when stormwater sludge was treated in an integrated thermal plasma system.

$$Carbon\ conversion(\%) = \left[1 - \frac{TOC\ of\ product\ slag}{TOC\ of\ sludge}\right] \times 100 \quad (1)$$

Table 3: Carbon conversion achieved in the treated wastewater sludge

Plasma arc current	TOC of sludge (%)	TOC of product slag (%)	Carbon conversion (%)
150	54.48	14.15	74.03
170	54.48	13.17	75.83
190	54.48	13.15	75.86

The metal concentrations in both the raw wastewater sludge and the product slag were determined via acid digestion according to US EPA method 3050 B as reported by Ali *et al.* (2019), the results are shown in Table 4. The metal elements in the wastewater sludge in major quantities were Al, K and Fe. Three other metal elements, Na, Mg and Zn were in small quantities while Cr, Mn, Ag and Hg were in trace quantities. After the thermal plasma treatment, the concentrations of the metals elements, except K, were significantly increased. The presence of large quantities of hydrocarbons in the wastewater sludge suppressed the concentration of the inorganics. After the gasification of the hydrocarbons, the inorganics became paramount in the products. The reduced concentration in the case of K could be as a result of vapourization of the metal because of its low melting point when compared with the other metals present.

3.4. Flue Gas Analysis

The composition of the flue gas obtained from the plasma treatment of wastewater sludge from the petroleum industry is shown in Table 5. The gas consists of H_2, CO, O_2, CO_2, CH_4 and C_2 hydrocarbons. The CO is the major component accounting for over 74%. At high temperature and in the presence of moisture (H_2O) hydrocarbon was converted to CO through water-gas reaction as shown in Equation 2. The concentration of oxygen in the flue gas is between 15 – 19%. There was the possibility of air getting into the reactor since it was not airtight. Concentrations of greenhouse gases (CO_2 and CH_4 combined) was very low, less than 1%. Even though there may be oxygen in the system, CO_2 was not stable at a temperature above 1400 ^oC and any quantity formed at the beginning of the process, when the temperature was lower than 1400 ^oC, may be converted to CO through Boudouard reaction shown in Equation 3.

$$C + H_2O \leftrightarrow CO + H_2 \quad (2)$$

$$C + CO_2 \leftrightarrow 2CO \quad (3)$$

Table 4: Metal concentrations in the wastewater sludge and the product slag

	Concentration (ppm)	
Metals	Wastewater sludge	Product slag
Na	21	34.4467
Mg	15.09	27.9125
Al	95.83	193.047
K	183.667	75.2154
Cr	1.6197	2.05181
Mn	0.1372	0.3487
Fe	327	620.989
Zn	12.4	25.5033
Ag	0.4630	0
Hg	1.3908	0.34387

Table 5: Composition of the flue gas

Component	Concentration (mol %)	
	1st run	2nd run
H_2	0.0051	0.0023
N_2	1.1729	1.3976
CH_4	0.5083	0.5125
CO	78.1940	74.5410
C_2^+	0.0195	0.0140
O_2	15.6388	18.6352
Ar	1.9549	1.8635
CO_2	0.0782	0.1398
NO_2	0	0.0056
SO_2	0.0043	0

4. CONCLUSION

A laboratory-scale thermal arc plasma reactor was developed to treat 20 cm^3 of wastewater sludge from the petroleum industry. The reactor was used to treat petroleum waste-water sludge. Temperature profile inside the plasma reactor increased with an increasing arc current and also with an increasing argon gas flowrate. A mass reduction of between 36.87 – 91.10% was achieved at a plasma temperature of 539 – 1603 ^oC. The mass reduction increased with an increase in the duration of treatment. The mass reduction also increased with an increase in plasma arc current from 150 – 190 A. A TOC reduction of 74.03%, 75.83% and 75.86% was obtained at an arc current of 150, 170 and 190 A respectively. The concentration of metals in the wastewater sludge increased after the plasma treatment. CO is the major component in the flue gas, accounting for over 74%. The concentration of greenhouse gases (CH_4 and CO_2 combined) was less than 1. The thermal plasma reactor gasifies the wastewater sludge from the petroleum industry into flue gases with slag as a

byproduct. The CO richen flue gas can be enriched with hydrogen to produce syngas.

5. RECOMMENDATION

Further research should look into the effect of cathode diameter on plasma temperature.

REFERENCES

Agon, N. (2015). *Development and study of different numerical plasma jet models and experimental study of plasma gasification of waste.* Ghent University.

Ali, A. M., Abu-Hassan, M. A., Ibrahim, R. R. K., Zaini, M. A. A., Abdulkarim, B. I., Hussein, A. S., Su, S. M. and Mohd-Halim, M. I. (2017). Characterization of Petroleum Sludge from Refinery Industry Biological Wastewater Treatment Unit. *The International Journal of Engineering and Science (IJES), 6*(9), 61 - 65. doi: 10.9790/1813-0609016165

Ali, A. M., Abu Hassan, M. A. and Abdulkarim, B. I. (2016). Thermal Plasma: A Technology for Efficient Treatment of Industrial and Wastewater Sludge. *IOSR Journal of Environmental Science, Toxicology and Food Technology (IOSR-JESTFT), 10*(11), 63 - 75. doi: 10.9790/2402-1011046375

Ali, A. M., Abu Hassan, M. A., Ibrahim, R. R. K., Jalil, A. A., Mat Nayan, N. H., Abdulkarim, B. I. and Sabeen, A. H. (2019). Analysis of Solid residue and Flue Gas from Thermal Plasma Treatment of Petroleum Sludge. *Journal of Environmental Chemical Engineering, 7*(4), 103207. doi: https://doi.org/10.1016/j.jece.2019.103207

Barcza, N. (1986). The development of large-scale thermal-plasma systems. *J. S. Afr. Inst. Min. Metall., 86*(8), 317-333.

Bień, J., Celary, P., Morzyk, B., Sobik-Szołtysek, J. and Wystalska, K. (2013). Effect of Additives on Heavy Metal Immobilization During Vitrification of Tannery Sewage Sludge. *Environment Protection Engineering, 39*(2). doi: 10.5277/EPE130204

Celary, P. and Sobik-Szołtysek, J. (2014). Vitrification as an alternative to landfilling of tannery sewage sludge. *Waste Management, 34*(12), 2520-2527. doi: http://dx.doi.org/10.1016/j.wasman.2014.08.022

Cortez, R., Zaghloul, H. H., Stephenson, L. D., Smith, E. D., Wood, J. W. and Cahil, D. G. (1996). Laboratory scale thermal plasma arc vitrification studies of heavy metal-laden waste. *Journal of the Air & Waste Management Association, 46*(11), 1075-1080.

Cubas, A. L. V., Carasek, E., Debacher, N. A. and De-Souza, I. G. (2005). Development of a DC-Plasma Torch Constructed with Graphite Electrodes and an Integrated Nebulization System for Decomposition of CCl4. *J. Braz. Chem. Soc., 16*(3B), 531-534.

Cubas, A. L. V., Machado, M. D.-M., Machado, M. D.-M., Gross, F., Magnago, R. F., Moecke, E. H. S. and De-Souza, I. G. (2014). Inertization of Heavy Metals Present in Galvanic Sludge by DC Thermal Plasma. *Environmental science & technology, 48*(5), 2853-2861. doi: 10.1021/es404296x

Diya'uddeen, B. H., Wan-Daud, W. M. A. and Abdul-Aziz, A. R. (2011). Treatment technologies for petroleum refinery effluents: a review. *Process Safety and Environmental Protection, 89*(2), 95-105.

Heberlein, J. (2002). New approaches in thermal plasma technology. *Pure and Applied Chemistry, 74*(3), 327-335.

Heberlein, J. and Murphy, A. B. (2008). Topical review: Thermal plasma waste treatment. *Journal of Physics D: Applied Physics, 41*, 1-20. doi: 10.1088/0022-3727/41/5/053001

Khongkrapan, P., Thanompongchart, P., Tippayawong, N. and Kiatsiriroat, T. (2013). Fuel gas and char from pyrolysis of waste paper in a microwave plasma reactor. *International Journal of Energy And Environment, 4*(6), 969 - 974.

Kim, H. and Park, D. (2004). Characteristics of Fly Ash/Sludge Slags Vitrified by Thermal Plasma. *J. Ind. Eng. Chem., 10*(2), 234-238.

Kim, S. W., Park, H. S. and Kim, H. J. (2003). 100 kW steam plasma process for treatment of PCBs (polychlorinated biphenyls) waste. *Vacuum, 70*(1), 59-66. doi: http://dx.doi.org/10.1016/S0042-207X(02)00761-3

Kourti, I., Devaraj, A. R., Butos, A. G., Deegan, D., Boccaccini, A. R. and Cheeseman, C. R. (2011). Geopolymers prepared from DC plasma treated air pollution control (APC) residues glass: Properties and characterisation of the binder phase. *Journal of Hazardous Materials, 196*, 86-92. doi: http://dx.doi.org/10.1016/j.jhazmat.2011.08.081

Leal-Quirós, E. and Villafañe, C. R. (2007). An Assessment of the Power Generated With

Plasma Processing of Sludge From Wastewater Treatment Plants. *IEEE Transactions On Plasma Science, 35*(6), 1622 - 1627.

Li, C., Lee, W., Huang, K., Fu, S. and Lai, Y. (2007). Vitrification of Chromium Electroplating Sludge. *Environmental science & technology, 41*(8), 2950-2956. doi: 10.1021/es062803d

Li, O. L.,Guo, Y., Chang, J. S., Urashima, K. and Saito, N. (2012). Treatment of Non-point Sources by a Thermal Plasma System Under DC Partial Transferred Mode. *International Journal of Plasma Environmental Science & Technology, 6*(1), 63 - 67.

Li, O. L., Guo, Y., Chang, J. S., Urashima, K. and Saito, N. (2015a). A new approach of nonpoint source pollution/stormwater sludge treatment by an integrated thermal plasma system. *International Journal of Environmental Science and Technology, 12*(5), 1769-1778. doi: 10.1007/s13762-014-0570-7

Li, O. L., Guo, Y., Chang, J.S., and Saito, N. (2015b). Thermal plasma treatment of stormwater sediments: comparison between DC nontransferred and partially transferred arc plasma. *Environ Technol, 36*(13), 1672-1679.

Mohai, I. and Szépvölgyi, J. (2005). Treatment of particulate metallurgical wastes in thermal plasmas. *Chemical Engineering and Processing, 44*, 225-229.

Mountouris, A., Voutsas, E. and Tassios, D. (2008). Plasma gasification of sewage sludge: Process development and energy optimization. *Energy Conversion and Management, 49*(8), 2264-2271. doi: http://dx.doi.org/10.1016/j.enconman.2008.01.025

Punčochář, M., Ruj, B. and Chatterj, P. K. (2012). Development of Process for Disposal of Plastic Waste Using Plasma Pyrolysis Technology and Option for Energy Recovery. *Procedia Engineering, 42*, 420-430. doi: http://dx.doi.org/10.1016/j.proeng.2012.07.433

Ramachandran, K. and Kikukawa, N. (2002). Thermal Plasma In-Flight Treatment of Electroplating Sludge. *IEEE Transactions On Plasma Science, 30*(1), 310-317.

Shie, J., Liau, Y., Lin, K. and Chang, C. (2014). *Thermal Treatment of Paper Sludge Using Torch Plasma*. Paper presented at the 2014 4th International Conference on Future Environment and Energy, IACSIT Press, Singapore.

Sobiecka, E. and Szymanski, L. (2014). Thermal plasma vitrification process as an effective technology for fly ash and chromium-rich sewage sludge utilization. *Journal of Chemical Technology & Biotechnology, 89*(7), 1115-1117. doi: 10.1002/jctb.4221

Szałatkiewicz, J., Szewczyk, R., Budny, E., Missala, T. and Winiarski, W. (2012). Determination of PID control parameters of plasmatron plasma reactor. *Journal of Applied Computer Science Methods, 4*(2), 31--39.

Szałatkiewicz, J., Szewczyk, R., Budny, E., Missala, T. and Winiarski, W. (2013). Construction Aspects of Plasma Based Technology for Waste of Electrical and Electronic Equipment (WEEE) Management in Urban Areas. *Procedia Engineering, 57*(Supplement C), 1100-1108. doi: https://doi.org/10.1016/j.proeng.2013.04.139

Tang, L. and Huang, H. (2005). Treatment of Waste Tyre Powder Using a High-frequency Capacitively Coupled Plasma Reactor. *Chinese Journal of Process Engineering, 5*(3), 295-300.

Tang, L., Huang, H., Zhao, Z., Wu, C. Z. and Chen, Y. (2003). Pyrolysis of Polypropylene in a Nitrogen Plasma Reactor. *Ind. Eng. Chem. Res., 42*, 1145-1150.

Tippayawong, N. and Khongkrapan, p. (2009). Development of a laboratory scale air plasma torch and its application to electronic waste treatment. *Int. J. Environ. Sci. Tech., 6*(3), 407-414.

Townsend, T. and Oehmig, W. (2014). *Development of a Bench-Scale Plasma Arc Vitrification Unit and the Exploration of Element Behavior in High Temperature Plasma Vitrification.* (PhD), University of Florida, Hinkley Center for Solid and Hazardous Waste Management. (Report # 81839)

Tu, W. A., Shie, J. L., Chang, C. Y., Chang, C. F., Lin, C. F., Yang, S. Y., Kuo, J. T., Shaw, D. G. and Lee, D. J. (2008). Pyrolysis of Rice Straw Using Radio-Frequency Plasma. *Energy & Fuels, 22*(1), 24-30. doi: 10.1021/ef7002848

Zhao, Z., Huang, H., Wu, C., Li, H. and Chen, Y. (2001). Biomass Pyrolysis in an Argon/Hydrogen Plasma Reactor. *Eng. Life Sci., 1*(5), 197 - 199.

DOI: 10.51975/LNDP7232
Journal of the Nigerian Society of Chemical Engineers, 36(1), 2021

SYNTHESIS AND CHARACTERIZATION OF NEEM-BASED ZINC OXIDE PHOTOCATALYST

***Gana, I. N.[1,2], Ohageria, V.U.[1], Akpan, U.G.[1], Ani, I.J.[1]**
[1]Department of Chemical Engineering, Federal University of Technology, Minna, Nigeria
[2]Headquarters Central Armament Depot, Tactical Air Command, Nigerian Air Force Base, Makurdi, Nigeria
[*]Corresponding Author: ugaekon@futminna.edu.ng; ganaisraelndamawo@gmail.com

ABSTRACT

The use of chemicals for the synthesis of photocatalyts poses threat to the environment. In this study, an active photocatalyst, Dalbejiya Dongoyaro (Azadirachta indica)-based zinc oxide (ZnO) was biosynthesized from zinc acetate dihydrate using sol gel and precipitation methods. The synthesized samples were characterized using Fourier Transfer InfraRed (FTIR), X-Ray Diffractometry (XRD), Brunauer Emmet Teller (BET), Energy Dispersive X-ray Spectroscopy (EDS) and Scanning Electron Microscopy (SEM) characterization techniques. The XRD and SEM analysis of the green synthesized and non-green synthesized ZnO demonstrated the formation of hexagonal wurtzite crystalline structure and agglomerated morphology. EDX analysis demonstrated the existence of Zn and O as the major constituents of the as-synthesized nanoparticles with traces of carbon which could be attributed to the carbon tape of the sample holder. The BET analysis displayed that the surface area of the ZnO nanoparticles increased from 23.75 to 97.08 cm^3/g after the green synthesis. Based on the surface area values, it can be derived that neem leaf extract enhanced the surface area of the green synthesized sample. Green synthesis is a promising route for the synthesis of photocatalyst nanoparticle which is environmentally friendly and sustainable method.

Keywords: *Zinc oxide, Neem leaf extract, Photocatalyt, Degradation, Bio-synthesis*

1.0 INTRODUCTION

Photocatalysis is a photoinduced reaction which is accelerated in the presence of a catalyst (Akpan & Hameed, 2009), and the catalyst should be small enough (probably in nano-range) to exert the requisite properties to function effectively. On the other hand, nanotechnology could be defined as the manipulation of matter through certain physical and/or chemical processes to produce materials that have specific properties which can be used in particular applications. Nanoparticles are particles that have at least one dimension less than 100 nm in size (Jeevanandam *et al*., 2018). Ahmed *et al*. (2016) defined "Nanomaterials" as those particles whose size lies in the dimension area of 1–100 nm. Nanomaterials are found to show enhanced properties based on morphology, size and distribution.

Nanotechnology is no doubt emerging as a vital area of study with its incredible applications in the areas of science, engineering, medicine, catalysis, pharmacy, electrochemistry, sensors, biomedicines, food technology, cosmetics, textile industry, optics, electronics, space industry, mechanics, energy science and optical devices. Nano-photocatalyts have equally gained much attention due to its structural and optical characteristics in the degradation of pollutants.

Zinc oxide and silver Nano-Particles (NPs) have attracted much interest in the research community among metal and metal oxide NPs, owing to their outstanding properties in terms of use in different areas such as antimicrobial, optical and catalytic properties (Espitia *et al*., 2016; Khan *et al*., 2016). ZnO NPs have shown different physical and chemical properties depending on the morphology. ZnO NPs have been synthesized by different methods such as sol–gel method, electrophoretic deposition, laser ablation, hydrothermal methods, electrochemical depositions, co-precipitation, ultrasound, chemical vapor deposition, thermal decomposition, combustion method and microwave-assisted combustion method (Ahmed *et al*., 2016). These physical and chemical methods have major shortcomings such as chemical poisoning and low surface area of the synthesized material. Therefore, any method that is environmentally friendly and that could result to improvement in the surface area of the synthesized ZnO NPs is urgently needed. However, in recent findings, ZnO NPs have also been synthesized by biological method using biological agents as reducing agents (Madhumitha *et al*., 2016 & Ahmed *et al*., 2016). ZnO NPs are non-toxic, semi-conducting materials having good photocatalytic behavior and high transparency. In addition, ZnO NPs produced from biological method have shown remarkable photocatalytic degradation of many dye pollutants like methylene blue, reactive dyes, direct dyes, disperse dyes, methyl orange, basic dyes, azo dyes, rhodamine blue

amongst others (Ghaly *et al*., 2014). Worthy of note is that ZnO NPs have gained special attention due to environmental concerns and it ability to degrade leading water pollutants particularly those in industrial effluents (Bhuyan *et al*., 2015).

Ahmed *et al*. (2015) in a meta-analysis reported the use of plant extract in the green synthesis of photocatalysts. These extracts include those of Ziziphora tenuior (Sadeghi & Gholamhoseinpoor, 2015), Abutilon indicum (Ashokkumar *et al*., 2013), Solanum tricobatum (Logeswari *et al*., 2013), Erythrina indica (Rathi Sre *et al*., 2015), Ocimum tenuiflorum (Logeswari *et al*., 2013), Spirogyra varians (Salari *et al*., 2014), Melia dubia (Ashokkumar *et al*., 2013), leaf extract of Acalypha indica with high antibacterial activities (Krishnaraj *et al*., 2010). Also, extracts of Sesuvium portulacastrum with nanoparticle size ranging from 5 to 20 nm (Nabikhan *et al*., 2010) have been identified as a source for the synthesis of nanoparticles as an alternative to the conventional methods. *Azadirachta indica* (Neem) leaf extract have been studied by Ahmed *et al*. (2016) and reported that the extract plays an important role in synthesis of ZnO NPs functioning as capping and stabilizing agent. They also noted that different capping agents can be used to stabilize ZnO particles imparting different properties, like size and morphology. They further reported that different surfactants have been employed in the synthesis of ZnO NPs, but the challenge with these surfactants is that they are difficult to degrade and are environmentally hazardous. Hence; the need to introduce green capping agents in the synthesis of ZnO NPs becomes imperative. Again it is important to bear in mind that synthesis of NPs is entirely dependent on biochemicals present in the precursor materials such as alkaloids, and others. Actually, the biochemicals present in the neem leaf extract can be a viable alternative.

The 'green' environment friendly methods being talked about in chemical and chemistry technologies are becoming increasingly popular and are much needed now because of the worldwide problems associated with environmental health (Thuesombat *et al*., 2014; Ahmed *et al*., 2016).

In the last ten years or more, researchers have showed interest in biological method to synthesize metal and metal oxide nanoparticles and the development of this biologically stimulated technique is growing as an important branch in the field of nanotechnology and nanoscience (Sharif *et al*., 2017). This so-called green synthesis of nanoparticles is gaining importance and has recently been suggested as potential alternative to physical and chemical methods because it is eco- friendly, non-toxic and safe reagents during the green-synthesis process while the use of Dalbejiya (Neem) leaf extract offers a biological method for the controlled and precise synthesis of several metallic nanoparticles with well-defined various shapes and sizes.

The bio-reduction of zinc ions into respective nanoparticles mediated by Dalbejiya leaf extract is chemically complex but environmentally benign. The role of neem leaf extract as reducing and mediating agent in the biosynthesis of ZnO nanostructures makes it indispensable in green technology (Bhuyan *et al*., 2015). On a general note, plant-extract-based and sodium hydroxide (NaOH)-enhanced simple precipitation processes are the most commonly used procedure in the synthesis of ZnO nanoparticles with NaOH as pH adjuster for the reaction mixture (Vishnukumar *et al*., 2018).

The wide variability of metabolites present in the Dalbejiya leaf extract have reducing properties or antioxidants that help in the immediate reduction of the zinc ions into nanostructured ZnO photocatalyst. Flavones, ketones, organic acids, amides and aldehydes are the main phytochemicals present in the Dalbejiya leaf extract which acts as bio-reductant out of which flavones, organic acids and quinones are water soluble phytochemicals that are actually responsible for the direct reduction of zinc ions into their respective nanostructures (Prathna *et al*., 2010; Bhuyan *et al*., 2015). Previous studies have further demonstrated that mild heating, followed by subsequent incubation of three types of benzoquinones (namely, cyperoquinone, dietchequinone and remirin) present in neem (mesophyte) leaf extract end up in the activation of quinones which results in particle size reduction (Bhuyan *et al*., 2015). Green synthesis is employed in this research because it is cheap, eco-friendly, and highly efficient method since it does not use toxic precursor as compared with the physical and chemical synthesis approach. This study seeks to synthesize ZnO nanoparticles with an increased surface area through green synthesis.

2.0 MATERIALS AND METHODS

2.1 Materials

Chemical and reagents such as the precursor [Zinc acetate dihydrate $[Zn(CH_3COO)_2]$-$2H_2O$], and sodium hydroxide (NaOH) were of analytical grade as supplied by Panlac Chemicals Nigeria Limited and were used directly without further purification.

Fresh leaves of Dalbejiya (*Azadirachta indica*) were randomly collected from different locations in Gidan Kwano, Bosso Local Government Area, Minna, Niger Sate, Nigeria. The collected leaves were gently washed with tap water and subsequently with de-ionized water, cut into pieces, sun-dried for seven days afterward grinded using plastic mortar and pestle. The resulting powder was stored in an air tight container for subsequent uses.

2.2 Method

Preparation of Dalbejiya Leaves Extract

Thirty gram (30 g) of the powder leaves was weighed into a beaker containing 300 ml de-ionized water. The mixture was placed for 15 min at 60 °C on a heating mantle. The extract which was allowed to cool at ambient temperature was filtered using Whatman No.1 filter paper. The obtained

extract (filtrate) was poured into a bottle and stored in a refrigerator at a temperature of 4 ^{o}C for further use. The method of Singh *et al*. (2019) was adopted.

Non-Green Synthesis of Zinc Oxide (ZnO) Nanoparticles

Zinc oxide nanoparticles was synthesized by slightly modifying the method of Bhuyan *et al*. (2015). One molar (1 M) of aqueous sodium hydroxide (NaOH) was prepared by adding 40 g of the crystals in 1000 ml of de-ionized water. To synthesize the non-green ZnO nanoparticles, 20 g of the Zinc acetate [$Zn(CH_3COO)_2$]-$2H_2O$] was added to 60 ml of de-ionized water in a beaker and stirred at 50 rpm for 60 min. The mixture then was divided into three equal volumes and with controlled drops of aqueous NaOH into each beaker, pH values of 8, 10 and 12 were measured using a pH meter. 20 ml of de-ionized water was subsequently added to each of the 3 beakers, stirred rigorously and allowed to settle for 30 min and then decanted after which the same volume of water was repeatedly added twice and decanted. The gel obtained were properly dried in an oven over night at 150 ^{o}C and then calcined at 350 ^{o}C for 2 h using muffle furnace.

Green Synthesis of Dalbejiya Based Zinc Oxide (ZnO) Nanoparticles

Zinc oxide nanoparticles were bio-synthesized following the method of Bhuyan *et al*. (2015). In the green synthesis of the Dalbejiya based ZnO nanoparticles, 20 g of Zinc acetate was added to 60 ml of de-ionized water in a beaker followed by 30 ml of the Dalbejiya (*Azadirachta indica*) extract and stirred for 60 min at a rotation speed of 50 rpm. The mixture then was divided into three equal volumes and was adjusted to pH 8, 10 and 12 as described in the non-green synthesis. Twenty (20) ml of de-ionized water was subsequently added to each beaker, stirred rigorously and allowed to settle for 30 min. The surfactant was decanted after which the same volume of water was repeatedly added twice and decanted. The gel obtained were properly dried in an oven over night at 150 ^{o}C, calcined at 350 ^{o}C for 2 h in a muffle furnace, cooled and stored for use.

Characterization of the Green (G) Synthesized and Non-Green (N) Synthesized ZnO Photocatalysts

The morphology, elemental composition, crystallography, Surface area and adsorption bands of the green and non-green synthesized ZnO nanoparticles were comprehensively examined using SEM, EDS, XRD, FT-IR and BET characterization techniques.

Measurement conditions for surface electron microscopy (SEM) and energy dispersive x-ray spectroscopy (EDXS)

About 0.05 mg of the synthesized green and non-green ZnO nanoparticle was sprinkled in a sample holder covered with carbon adhesive tape which was sputter-coated with gold-palladium (Au:Pd; 60:40) using Quorum T15OT for 5 min to the commencement of analysis. The sputter coated samples were characterized using Zeiss Auriga SEM. The secondary electron mode was activated for imaging and a homogeneous region on the sample was identified. The microscope was operated at 5 KeV for imaging with electron high tension (EHT) of 20 KeV detectors for EDS. The illumination angle was adjusted to 150° and the elemental composition of the sample was determined.

Measurement conditions for x-ray diffraction (XRD)

Approximately 1 g each of the green and non-green synthesized ZnO was crushed into powder and then dispersed into a rectangular aluminum sample holder with the aid of a well cleaned spatula. The sample holder containing the sample was clipped into the XRD instrument. Bruker AXS Advance diffractometer with 2θ range of 5 - 75°, a step size of 0.028°, and operating at 45 KV and 40 mA was used to collect the XRD data. Monochromatic copper (Cu) Kαl radiation with a wavelength of 0.154 nm was used as the X-ray source.

Experimental conditions for Brunner-Emmett-Teller (BET)

The analysis for the surface area, pore volume and pore size distribution of the samples was determined by Brunauer-Emmett-Teller technique using a NOVA 4200e surface area and pore analyzer instrument. Around 100 mg each of green and non-green ZnO photocatalysts powder was weighed and degassed by flowing N_2 at 90 °C for 1 h and then held at 350 °C for 2 h. As the temperature is increased, water vapour was adsorbed from the surface and pores of the sample. The sample was then cooled down and weighed again. The instrument uses physical adsorption and capillary condensation of N_2 principles to obtain information about the surface area and porosity of ZnO nanoparticles.

3.0 RESULTS AND DISCUSSION

3.1 Scanning Electron Microscopy (SEM) Analysis

SEM was employed to analyze the structure of nanoparticles that were synthesized. The SEM images in Figure 1 (a–b) show the changes in morphology of ZnO NPs. The photocatalysts formed are fairly spherical in shape and agglomerated tiny rods. However, the agglomeration was less for the green synthesized sample as compared with the non-green synthesized photocatalyst. Similar result was also obtained by Ungula and Dejene (2016).

3.2 Energy Dispersive X-ray Spectroscopy (EDXS) Analysis

EDX analysis (Table 1, Figures 2 and 3) was carried out to determine the elemental composition and stereochemistry of the synthesized zinc oxide nanoparticles. The EDS spectra in Figure 2 and Figure 3 indicate that the synthesized samples are composed of zinc and oxygen, and the route has pure ZnO phases. Theoretically, expected

stoichiometric mass percent of Zn and O are 80.3% and 19.7% (Bari *et al*. 2009). The green synthesized sample showed a closer theoretical value of Zn and O as shown in Table 1. This high purity of the ZnO NPs was further confirmed by XRD spectra. However, some traces of carbon element were found in the sample, which could be attributed to the carbon tape of the sample holder. Similar result was also reported by Gnanasangeetha and Thambwani (2013).

Table 1: Elemental Composition of the modified (G) and unmodified (N) ZnO samples

Photocatalyst	Zn	O	Total (%)
G-ZnO	88.19	11.81	100
N-**ZnO**	91.57	8.43	100

G = Green synthesized, N = Non-green synthesized

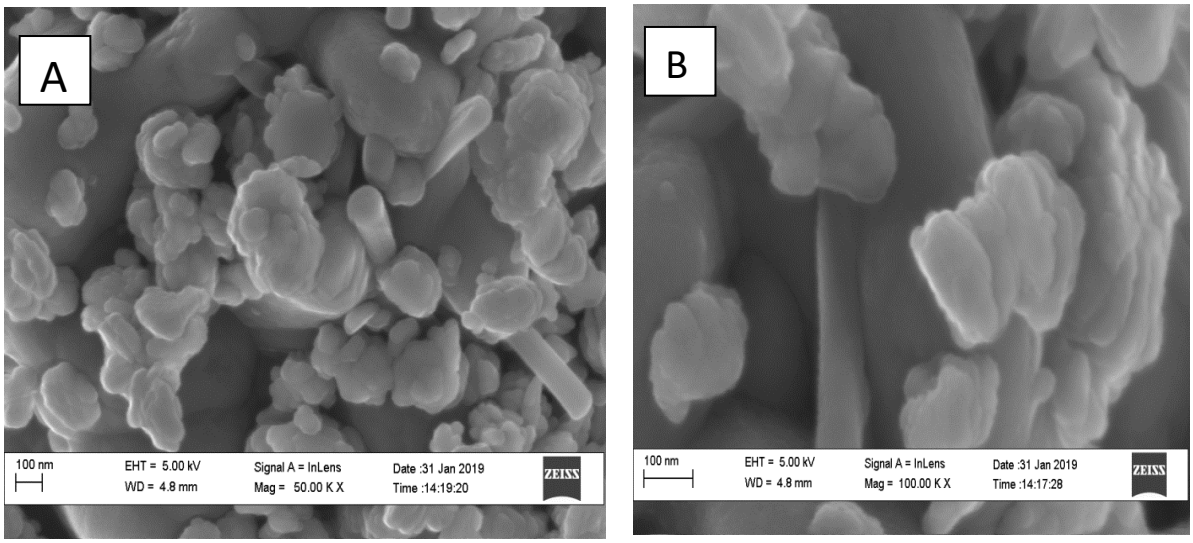

Figure 1: SEM images of (A) Green Synthesized ZnO and (B) Non – Green Synthesized ZnO

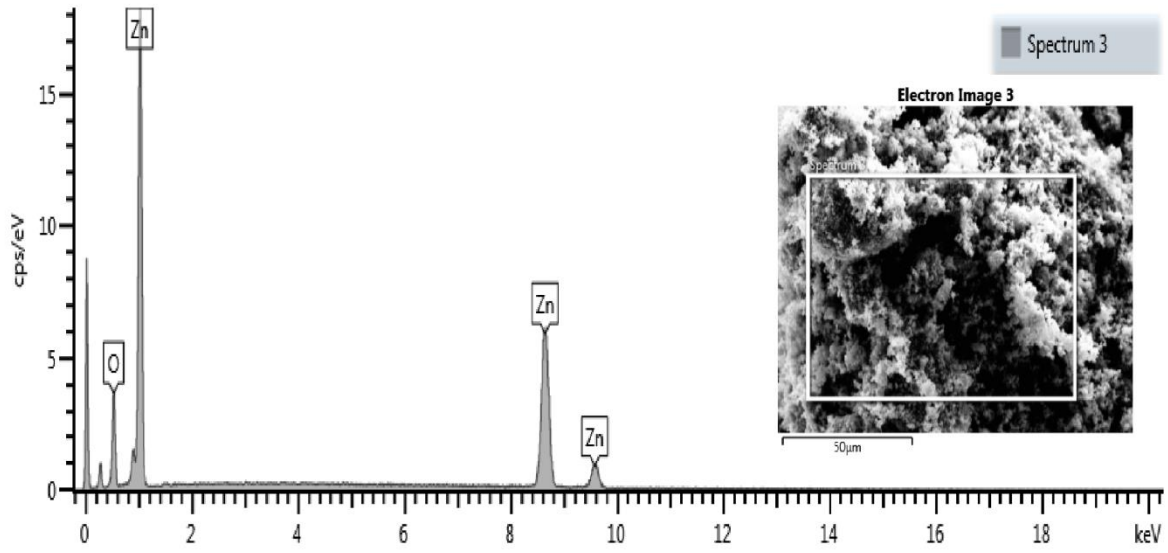

Figure 2: EDX Spectrum of Green synthesized ZnO

DOI: 10.51975/LNDP7232
Journal of the Nigerian Society of Chemical Engineers, 36(1), 2021

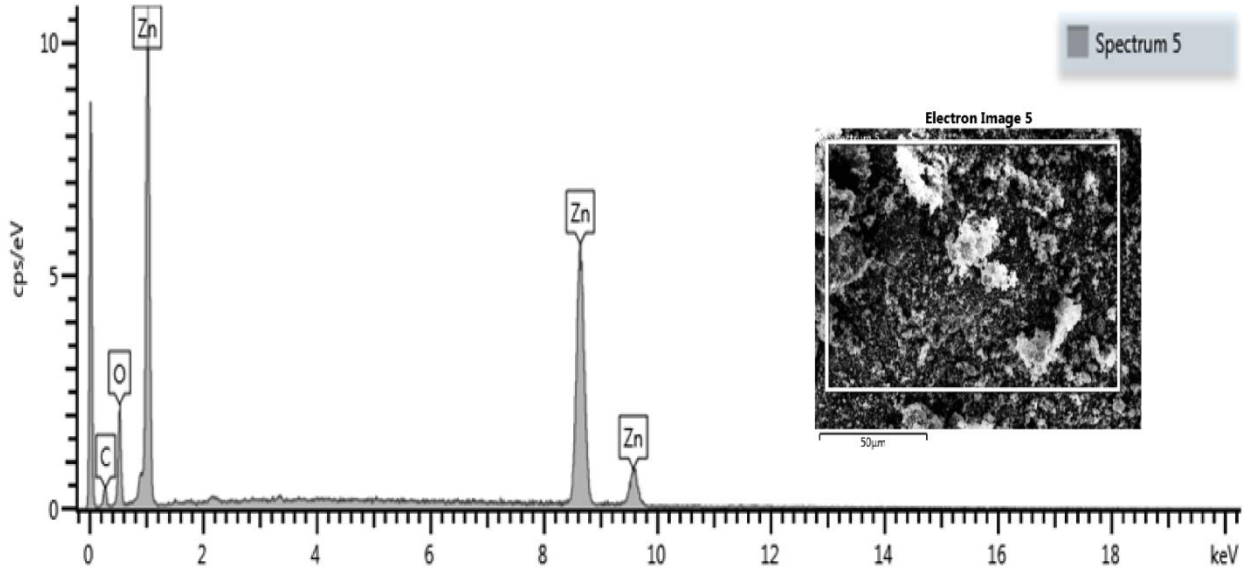

Figure 3: EDX Spectrum of the non-green synthesized ZnO

3.3 X-Ray Diffraction (XRD) Analysis

XRD analysis (Figure 4) was performed to investigate the crystal structure of the synthesized photo catalysts. The XRD patterns of the samples were recorded in the diffraction angle range 5° to 80°. The diffraction peaks at the characteristic planes (1 0 0), (0 0 2), (1 0 1), (1 0 2), (1 1 0), (1 0 3), (1 1 2) and (2 0 1) can be directly indexed to a hexagonal wurtzite crystalline structure of ZnO (Otal *et al.*, 2011). This Wurtzite crystalline structure also matched well with the Joint Committee on Powder Diffraction Studies Standards (JCPDS standard Card No.: 01-036-1451). No other peak was detected, indicating a high phase purity of the samples. The sharp and strong diffraction peaks in the XRD patterns of the zinc oxide nanoparticles synthesized confirm the high crystalline nature of the samples. Figure 4 also shows that the peak intensity increases for the green synthesized ZnO sample, which indicates an increased crystallinity of the modified sample compared to the non-green synthesized ZnO. Similar result was also obtained by Xing *et al.* (2017).

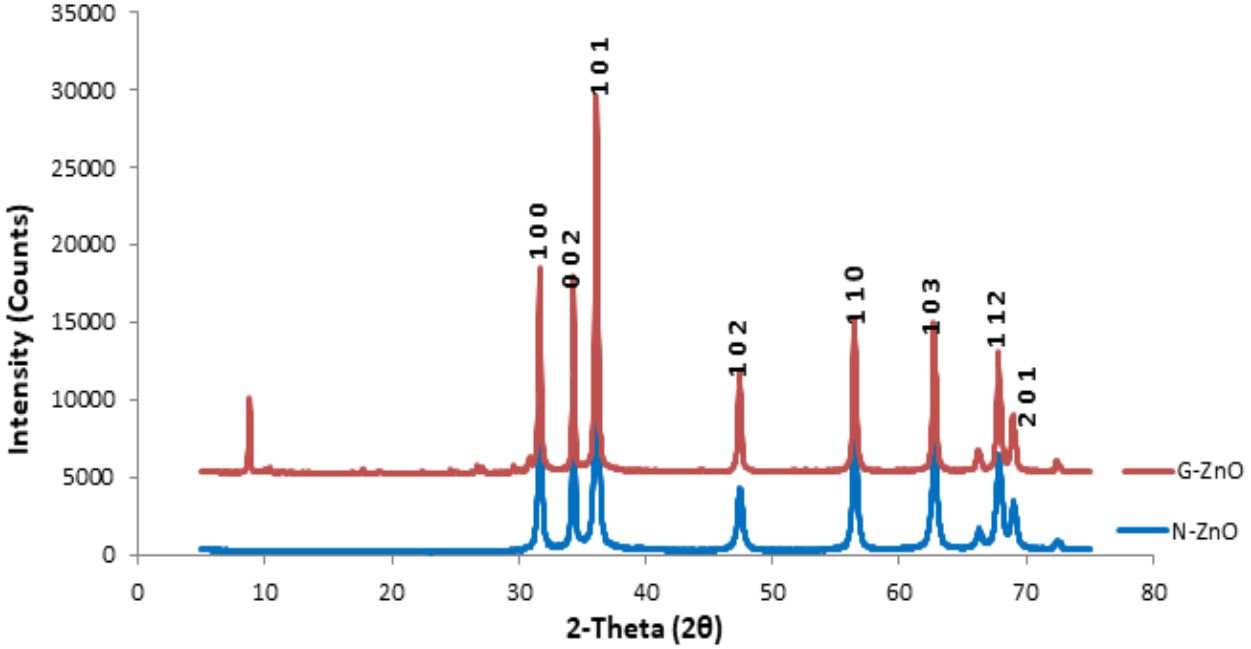

Figure 4: XRD patterns of the green synthesized (G-ZnO) and non-green synthesized (N-ZnO) ZnO samples

3.4. BET Surface Area Analysis

The BET surface area values of the synthesized ZnO nanoparticles are shown in Table 2. The result reveals that the BET surface area of 97.08 m^2/g was obtained for the green synthesized (G-ZnO) sample, an increase of four-folds compared to the value of 23.75 m^2/g for the non-green synthesized (N-ZnO) sample. Based on the surface area values, it can be adduced that neem leaf extract enhanced the surface area of the modified sample.

Table 2: The BET specific surface area, pore volume and pore size of photocatalysts

Photocatalyst	BET Surface Area (m^2/g)	Pore Volume (cm^3/g)	Pore Size (nm)
N-ZnO	23.75	0.01431	2.138
G-ZnO	97.08	0.04949	2.105

3.5 Fourier Transform Infrared (FT-IR) Analysis

FT-IR spectra for the green and non-green synthesized ZnO samples are presented in Figure 5.

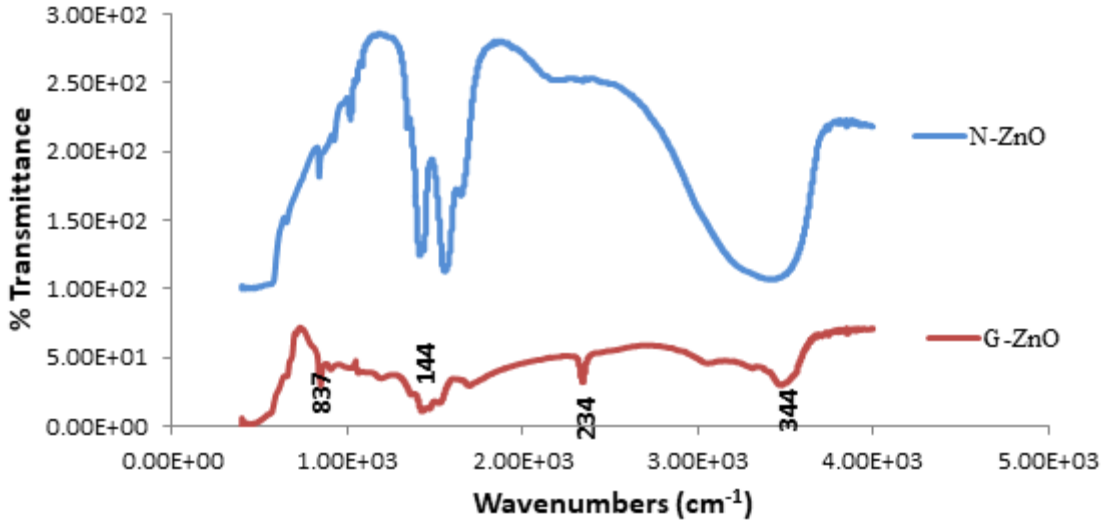

Figure 5: FT-IR spectra of the green synthesized (G-ZnO) and non-green synthesized (N-ZnO) nanoparticles

The peaks at 459 and 400 cm^{-1} identified the bending vibration of Zn-O in the green synthesized and non-green synthesized samples respectively. In addition, the result clearly indicates that –OH stretching around 3042 cm^{-1} and –CH stretching around 2340 cm^{-1} are responsible for strong capping on the green synthesized ZnO nanoparticles. This result matches with the reported result of biosynthesis of ZnO nanoparticles using *Acalypha indica* leaf extract (Gnanasangeetha and Thambwani, 2013).

4.0 CONCLUSION

Zinc oxide nanoparticles have been successfully synthesized via green route, an eco-friendly and inexpensive method for the bio-synthesis of ZnO using aqueous leaf extracts of Dalbejiya (*Azadirachta indica)*. The extracts act as reducing and stabilizing agents for the synthesis of ZnO nanoparticlesThe sharp and strong diffraction peaks in the XRD patterns of the zinc oxide nanoparticles confirm the high crystalline nature of the samples which is a desired property of the material. The EDS result revealed a successful synthesis of ZnO NPs and FT-IR spectra indicates the presence of –OH and –CH stretching which are responsible for strong capping on the green synthesized ZnO NPs. Green-synthesis chemistry of ZnO has fourfold improvement judging by its surface area (97.08 cm^2/g) in relation to the non-green-synthesized ZnO (23.75 $cm^{2/}/g$). From the results obtained, the ZnO nanoparticle is hereby proposed to be applied in the degradation of organic pollutants in wastewater, especially industrial effluents. This therefore, can be gainfully employed in environmental remediation.

ACKNOWLEDGEMENT

The authors wish to acknowledge the support of TETFund in conjunction with Federal University of Technology, Minna for providing 2017 IBRG grant No.: TETFUND/FUTMINNA/2016-2017/6thIBRP/12.

REFERENCES

Ahmed, S., Saifullah, Ahmad, M., Swami, B. L., & Ikram, S. (2016). Green synthesis of silver nanoparticles using Azadirachta indica aqueous leaf extract . *Journal of Radiation Research and Applied Sciences*, *9*(1), 1–7. https://doi.org/10.1016/j.jrras.2015.06.006

Akpan, U.G. & Hameed, B.H. (2009). Parameters

affecting the photocatalytic degradation of dyes using TiO_2-based photocatalysts: A review. *Journal of Hazardous Matrials, 170, 520-529.*

Ashokkumar, S., Ravi, S., & Velmurugan, S. (2013). Green synthesis of silver nanoparticles from Gloriosa superba L. leaf extract and their catalytic activity. *Spectrochimica Acta Part A: Molecular and Biomolecular Spectroscopy*, 115, 388-392.

Bari, A. R., Shinde, M. D., Vinita, D. & Patil, L. A. (2009). Effect of Solvents on the Particle Morphology of nanostructured ZnO. *Indian Journal of Pure and Applied Physics*, 47, 24-27.

Bhuyan, T., Mishra, K., Khanuja, M., Prasad, R., & Varma, A. (2015). Biosynthesis of zinc oxide nanoparticles from Azadirachta indica for antibacterial and photocatalytic applications. *Materials Science in Semiconductor Processing*, *32*, 55–61.

Espitia, P.J., Otoni, C.G., Soares, N.F.F. (2016). Zinc oxide nanoparticles for food packaging applications. *Antimicrobial Food Packaging*, 425–431.

Ghaly, A.E., Ananthashankar, R., Althab, M., & Ramakrishnam, V.V. (2014). Production, characterization, and treatment of textile wastewaters: a chritical review. *Journal of Chemical Engineering Process Technology*, 5,182-187.

Gnanasangeetha, D., Thambwani, D.S. (2013). Biogenic production of zinc oxide nanoparticles using Acalypha indica. *Journal of Chemistry, Biology and Physical Sciences*, 1, 238–246.

Jeevanandam, J., Barhoum, A., Chan, Y. S., Dufresne, A., & Danquah, M. K. (2018). Review on nanoparticles and nanostructured materials: History, sources, toxicity and regulations. *Beilstein Journal of Nanotechnology*, *9*, 1050–1074.

Khan, S.T., Musarrat, J., Al-Khedhairy, A.A. (2016). Countering drug resistance, infectious diseases, and sepsis using metal and metal oxides nanoparticles: current status. *Colloids and Surfaces B: Biointerfaces*, 146, 70–83.

Krishnaraj, C., Jagan, E.G., Rajasekar, S., Selvakumar, P., Kalaichelvan, P.T., & Mohan, N. (2010). Synthesis of silver nanoparticles using Acalypha indica leaf extracts and its antibacterial activity against water borne pathogens. *Colloids and Surfaces B: Biointerfaces*, 76, 50-56.

Logeswari, P., Silambarasan, S., & Abraham, J. (2013). Ecofriendly synthesis of silver nanoparticles from commercially plant powders and their antibacterial properties. *Sciencia Iranica*, 20, 1049-1059

Madhumitha, G., Elango, G., & Roopan, S.M. (2016). Biotechnological aspects of ZnO nanoparticles: overview on synthesis and its applications, *Appl. Microbiol. Biotechnol*., 100, 571–581.

Otal, E.H., Yoon, S., Aguirre, M., Weidenkaff, A. (2011). Metastability of heavy lanthanides in the ZnO wurtzite structure. *Journal of Alloys and Compounds*, 509, 364-366.

Prathna, T.C., Mathew, L. Chandrasekaran, N., Raichur, A.M. & Mukherjee, A. (2010). Biomimetic synthesis of nanoparticles: science, technology & applicability, Biomimetics Learning from Nature, (Chapter1).

Rathi Sre, P.R., Reka, M., Poovazhagi, R., Arul Kumar, M., & Murugesan, K. (2015). Antibacterial and cytotoxic effect of biologically synthesized silver nanoparticles using aqueous root extract of Erythrina indica lam. *Spectrochimica Acta Part A: Molecular and Biomolecular Spectroscopy*, 135, 1137-1144.

Salari, Z., Danafar, F., Dabaghi, S., & Ataei, S.A. (2014). Sustainable synthesis of silver nanoparticles using macroalgae Spirogyra varians and analysis of their antibacterial activity. *Journal of Saudi Chemical Society*, 20, 459-464.

Sharif, M.M., Shah, F.-H. Butt, M.S. & Sharif, H.R. (2017). Role of nanotechnology in enhancing bioavailability and delivery of dietary factors. *Nutrient Deliv*ery, 587–618.

Singh, A., Neelam, & Kaushik, M. (2019). Physicochemical investigations of zinc oxide nanoparticles synthesized from Azadirachta Indica (Neem)leaf extract and their interaction with Calf-Thymus DNA. *Results in Physics*, *13*, 1–9.

Thuesombat, P., Hannongbua, S., Akasit, S., & Chadchawan, S. (2014). Ecotoxicology and environmental safety effect of silver nanoparticles on rice (Oryza sativa L. cv. KDML 105) seed germination and seedling growth. *Ecotoxicology and Environmental Safety*, 104, 302-309.

Ungula, J. & Dejene, B.F. (2016). Effect of solvent medium on the structural, morphological and optical properties of ZnO nanoparticles synthesized by the sol–gel method. *Physica B*, 480, 26–30.

Vishnukumar, P., Vivekanandhan, S., Misra, M. & Mohanty, A.K. (2018). Recent advances andemerging opportunities in phytochemical synthesis of ZnO nanostructures. *Materials Science in Semiconductor Processing*, 80, 143–161.

Xing, Z., Chen, Y., Liu, C., Yang, J., Xu, J., Situ, Y. & Huang, H. (2017). Synthesis of core-shell ZnO/oxygen doped g-C3N4 visible light driven photocatalyst via hydrothermal method. *Journal of Alloys and Compounds*, 708, 853-861.

DOI: 10.51975/VEWJ4581
Journal of the Nigerian Society of Chemical Engineers, 36(1), 2021

MIL-53(FE) / COW BONE CHAR COMPOSITE FOR CHROMIUM REMOVAL FROM TANNERY WASTEWATER

***Ajayi O. A.[1], Nanbyen S.[1]. Oladipo A.A.[2] and Nwafulugo, F. U.[3]**

[1]Department of Chemical Engineering, Ahmadu Bello University, Zaria. Kaduna State.
[2]Department of Environmental Engineering, Cyprus Science University, Girne, TRCN Mercin 10, Turkey.
[3]Federal Polytechnic, Oko, Anambra State, Nigeria**Corresponding Author:** segeaj@gmail.com

ABSTRACT

MIL-53(Fe)/Cow bone char composite, prepared via the sol-gel method was used for the removal of chromium from real tannery effluent having an initial concentration of 40mg/l. The characteristics of MIL-53(Fe)/Cow bone char were studied using X-ray diffraction (XRD), Fourier transform infrared spectroscopy (FTIR), thermo gravimetric analysis (TGA) Boehm titration and scanning electron microscopy (SEM-EDX). Adsorption capacity of MIL-53(Fe)/Cow bone char composite for chromium was 19.61 mg/g with a removal efficiency of 87.8% at an optimal bed height of 2.4cm (2.0g) for MIL-53(Fe)/Cow bone char composite, time of 2 minutes and pH_{pzc}=5.4.The kinetic studies showed that the adsorption data were well fitted to the pseudo second-order model with high correlation coefficient R^2=0.9911. Furthermore, the adsorption isotherm equilibrium studies confirmed that the Langmuir model best described the adsorption process of chromium onto MIL-53(Fe)/Cow bone char composite. Analysis of data with Dubinin–Radushkevich and Temkin isotherms showed that adsorption of chromium onto MIL-53(Fe)/Cow bone char composite is physical in nature.

1. INTRODUCTION

Wastewater discharge from industrial sectors such as agriculture, textile, tanneries, pulp and paper contribute largely to environmental pollution when untreated. It may contain heavy metals like cadmium and chromium that are toxic, mutagenic, carcinogenic and cause hormonal disorder to human life.

Tannery waste is generated in huge amount during the tanning process by leather industries all over the world (Mohammed *et al*., 2017). The used and non-useable hides and skins along with the excess chemicals and water used in the process constitute solid and liquid wastes in the tannery (Mohammed *et al*., 2017), which when untreated affect streams, groundwater, land and sewers in which they are discharged. Important pollutants associated with the tanning industry include chlorides, tannins, chromium, sulphate, sulphides and increasing use of synthetic chemicals such as pesticides, dyes and finishing agents.

Several adsorbents have been investigated including zeolite, cow bone, activated carbon, banana peel, sugarcane bagasse, rice husk, palm kernel shell, coconut shell etc. Modern technology employs the use of composites that have extraordinary combination of properties (Araoye, 2015). One of the materials used are the metal organic framework (MOFs) with carbon-based materials.

Recently, metal of organic framework materials (MOFs) with high porosity and high surface area have gained application in adsorption, membrane separation, sensing, catalysis and proton conduction, owing to their water stable structure (Wang *et al*., 2016). They have adjustable surface properties, and have more abundant and controllable porous structures compared to conventional porous materials such as zeolite, silica and activated carbon (Jiao *et al*., 2017).

Cow bones used in this research constitutes a waste of natural resources especially in developing countries. Cow bones which are obtainable from slaughtered cows in abattoirs are readily available in Nigeria and are usually burnt or sold to feed mill for the production of animal feeds. Cow bone char consists mainly of 57–80% tricalcium phosphate,6–10% calcium carbonate and 7–10% carbon (Fawell, 2006).

The use of MIL-53(Fe)/cow bone char composite for the removal of chromium in tannery wastewater through the process of adsorption has not been harnessed and thus, will be used in this present study.

2. MATERIALS AND METHODS

2.1 Materials and Instruments

All chemical reagents, namely: Iron (III) chloride hexahydrate ($FeCl_3.6H_2O$), Terephthalic acid (H_2BDC) N,N'-Dimethylformamide (DMF, 99.8%), Ethylene glycol and Sodium hydroxide were of analytical grade

(≥98%). Cattle bones were collected at Zango abattoir, Zaria, Nigeria. Deionized water was obtained from the PTDF Laboratory, Department of Chemical Engineering Ahmadu Bello University, Zaria. Tannery wastewater was collected from the Nigerian Institute of Leather and Science Technology (NILEST), Zaria, Nigeria.

2.2 Synthesis of MIL-53(Fe)

MIL-53(Fe) powder was prepared via a modified previously reported method (Dan *et al*., 2017; Oladipo, 2018). A mixture of Iron (III) chloride hexahydrate ($FeCl_3.6H_2O$) (1.35g), 1,4-benzenedicarboxylic acid (H_2BDC) (0.83g), and N,N'-Dimethylformamide (DMF) (112 ml) were mixed and stirred at room temperature using a magnetic stirrer until it became clear, then the reaction mixture was transferred into a 100ml Teflon-lined stainless steel autoclave and heated at 180°C for 10h. After the heat treatment, the autoclave was allowed to cool to room temperature and the resultant suspension was filtered and the orange MIL-53(Fe) powder residue was washed with 200ml deionized water and allowed to dry at 150^0C in the oven for 24 hours in order to remove the DMF in the pores. The resulting sample was stored at room temperature in a covered glass container until the time of study. The functional groups, surface morphology, crystal structure and surface area were determined using FTIR spectrophotometer, SEM, XRD and BET respectively for the as-prepared MIL-53(Fe).

2.3 Preparation of bone char

Cow bone char was prepared via a previously reported method (Patel *et al*., 2015). Cattle bones collected at Zango abattoir, Zaria, Nigeria were parboiled with NaOH, washed thoroughly with water several times and dried at 100 ^{o}C for 1hour. The dried bones were carbonized at a temperature of 500 ^{o}C for a residence time of 1hour resulting into bone char. The bone char was further ground to powder using a ceramic mortar and pestle followed by sieving to a particle size of 75 µm with an electric sieve shaker.

2.4 Synthesis of MIL-53(Fe)/Cow bone char composite

The composite was prepared via a previously reported method (Oladipo, 2018). 4.2 g of the as-prepared MIL-53(Fe) was suspended into 100 ml ethylene glycol in a flask and stirred for 1hour. And then, 3.2 g of cow bone powder was added to the above suspension, followed by continuous stirring with heating for 190 mins at 100 ^{o}C for solvent evaporation. The resulting solid was washed severally with 160ml deionized water and 40 ml ethanol and decanted with a suction pump and sinter glass. It was further dried in the oven at 80 ^{o}C for 5hours and finally calcined at 500 ^{o}C for 1h and cooled, sieved and stored in desiccator.

2.5 Treatment of tannery wastewater by fixed-bed system

The dynamic sorption studies were carried out in a plastic column of 1.2 cm in diameter and 7.5 cm in length. Different masses of 0.5 g, 1.25 g and 2.0 g of composite was packed into the column, achieving a bed height of 0.6 cm, 1.5 cm and 2.4 cm respectively. The tannery wastewater with an initial concentration of 40 mg/l was allowed to pass over the adsorbent bed at different times of 2 mins to 16 mins. The initial and final chromium concentration in the effluent samples was determined by atomic absorption spectroscopy (SHIMADZU, Model-AA6800 AAS).The amount of heavy metal adsorbed (q_t) at any given time (t) and at equilibrium (q_e) can be expressed as Equations (1) and (2) respectively (Chowdhury *et al*., 2013; Agoyi *et al*., 2015).

$$q_t = \left(\frac{C_o - C_t}{m}\right)V \quad (1)$$

$$q_e = \left(\frac{C_o - C_e}{m}\right)V \quad (2)$$

While the percentage of heavy metal adsorbed is expressed as equation 3:

$$\% = 100\left(\frac{C_o - C_t}{C_o}\right) \quad (3)$$

Where:

C_0 is the initial chromium concentration (mg/l)

C_t is the chromium concentration at time t (mg/l)

C_e is the molar equilibrium concentration of the solute remaining after adsorption (mg/l)

M is the mass of the adsorbent (g)

V is the volume of solution used (l)

2.6 Column desorption of MIL-53(Fe)/cow bone char composite and regeneration studies

Desorption studies were performed with MIL-53(Fe)/cow bone char composite that was saturated with tannery wastewater of pre-determined chromium concentrations. The flow rate was adjusted to 5 ml/min at a bed height of 2.4 cm. After the column had reached exhaustion, the exhausted MIL-53(Fe)/cow bone char composite was regenerated using 0.05 M NaOH. After elution, the bed was washed with distilled water until the pH stabilised close to neutral (7.0). Three cycles of

sorption-desorption-regeneration were carried out to evaluate the MIL-53(Fe)/cow bone char composite capacity. The chromium removal percentage was determined in each cycle.

3. RESULTS AND DISCUSSION

3.1 Physicochemical characteristics of tannery wastewater

From Table 1, the total suspended solids concentration in the sample tannery wastewater was 5920 mg/l. Hence tannery industrial waste cannot be discharged into the environment. Similarly, total dissolved solid concentration was 7160 mg/l indicating that the tannery wastewater contain soluble solids as well as floating solids. The result of Table 1 shows a COD and BOD concentration of 1600 mg/l and 170mg/l respectively. This is due to the use of inorganic chemicals. The pH of wastewater is the strength of acidity or alkalinity of the wastewater, which is the measure of hydrogen ion concentration in the wastewater (Oke *et al*., 2006).

Table 1: Physicochemical Parameters of Tannery Wastewater

S/n	Parameter	Unit	Result
1	pH	-	6.8
2	Dissolved Oxygen (DO)	mg/l	210
3	Biological Oxygen Demand	mg/l	170
4	Total Dissolved Solids	mg/l	7160
5	Total Suspended Solids	mg/l	5920
6	Chemical Oxygen Demand	mg/l	1600
7	Total Chromium Concentration	mg/l	40
8	Electrical Conductance	µmhos/cm	190
9	Color	Hazen Unit	1200

3.2 Characterization of samples

Fig. 1 presents the XRD pattern of the synthesized MIL-53(Fe), the diffraction lines appeared at 2θ of 8.9 (101), 11.2, 14.5, 17.5 (002), 23.5 (302), were identical to those reported for standard MIL-53(Fe) (Araya *et al.*, 2017; Oladipo, 2018) and no other lines were observed indicating that the pure crystalline phase of MIL-53(Fe) was synthesized. The XRD pattern of bone char is consistent with the standard crystalline hydroxyapatite and distinct diffraction peaks were observed at the 2θ of 26.3°, 28.2°, 32.1°, 37.9°, 43.2°, 47.8°, 49.4°, 50.4° and 62° which is agrees with the JCPDS card no: 82-1943. The XRD pattern of the MIL-53 (Fe)/char exhibits the coexistence of both MIL-53 (Fe) and bone char phases, no any impurity peaks detected, and thus indicated the high purity of the composite. While the characteristic diffraction peaks of MIL-53(Fe) reduced in intensity in the composite with no shift, the retained bone char peaks became more crystalline in nature in the composite and the structure of MIL-53(Fe) remain unchanged after the deposition of CBC (Hu *et al*., 2017).

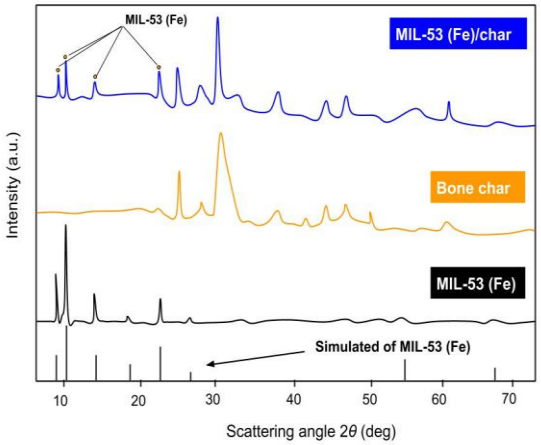

Fig. 1: XRD patterns for samples

The morphology and spectra of elemental analysis of cow bone char, MIL-53(Fe) and MIL-53(Fe)/cow bone char composite are reported in Fig.2. The micrograph for cow bone char clearly shows that the sample had undergone significant structural changes due to the thermal

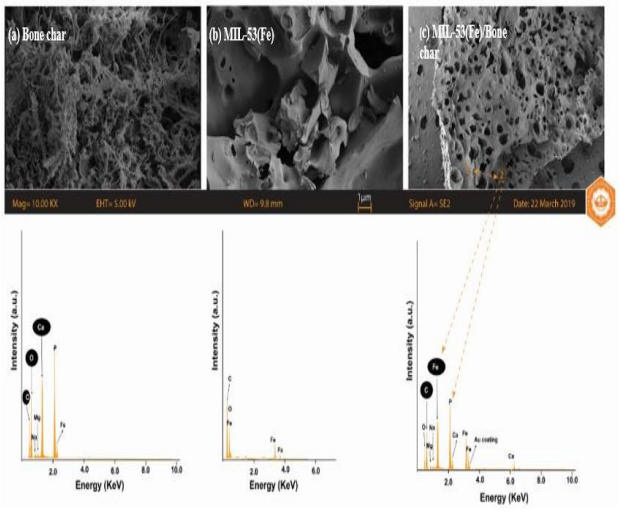

Fig. 2: SEM-EDX images for samples

treatment at 500 ^{o}C which indicates that the thermal treatment creates more pores on the surface and increases the surface area (Mendoza-Castillo *et al*., 2014). Cow bone char exhibits a distinct morphology from the MIL-53 (Fe). As seen, the cow bone char is characterized by a highly dense continuous fibrous-like structure with crunchy textural surface and its chemical composition includes the presence of carbon, oxygen, phosphorus, and calcium, which are the main components of hydroxyapatite (Mendoza-Castillo *et al*., 2014) with minor traces of sodium, iron and magnesium. These results are consistent with the results of X-ray diffraction (see Fig. 1).

In contrast, the MIL-53 (Fe) morphology is homogeneous and characterized by well-defined smooth surface and pronounced polyhedron-like crystalline structure and its chemical composition include the presence of Iron (Fe), carbon and oxygen as depicted on the physicochemical characteristic for the sample in Table 2 as reported by Oladipo *et al*. 2017).

The surface of the MIL-53(Fe)/cow bone char is relatively smooth with heterogeneous meso and micro-pores and thick cuticle-like edges because of hetero-junctions of the pores of cow bone char onto the MIL-53(Fe) structure and the thermal treatment of the composite, which increased the porosity of the structure. Its chemical composition includes the presence of carbon, oxygen, phosphorus, calcium from the hydroxyapatite structure of cow bone char and Iron with minor traces of sodium, iron and magnesium.

The FTIR spectra are shown in Figs. 3, 4 & 5 respectively. For the MIL-53(Fe), a broad vibration at around 3480 cm^{-1}was attributed to the stretching vibrations of the O–H of water molecules adsorbed on the surface. The asymmetric (γ_{as}C-O) and symmetric (γ_s C-O) stretching of carboxyl group could be described by the appearance of sharp vibrations at 1525 cm^{-1} and 1380 cm^{-1} respectively indicating the presence of dicarboxylate linkers within the framework (Oladipo, 2018). The carbonyl groups (C=O) of the carboxylate ligand (COO) were visible at 1696 cm^{-1}, whereas a very sharp peak at 750 and 696 cm^{-1} corresponds to the Csp^2-H (C=C-H) bending vibrations, which belong to the benzene rings of carboxylates. The characteristic coordination bonds between Fe^{3+} cations and -OOC-C_6H_4-COO- carboxylate anions were observed at a very low wave number of 545 cm^{-1} which implies the existence of a Fe-oxo-bond present in the MIL-53(Fe) structure that exists between the carboxylic group of terephthalic acid linker and the inorganic iron(III) metal (Zhang *et al*., 2016; Oladipo, 2018). The MIL-53(Fe) spectrum clearly exhibited the characteristic absorption peaks and thus confirms the formation of MIL-53(Fe) structure (Oladipo, 2018).

For the cow bone char, the C-O stretching vibrations at 1453 with a shoulder at 1421 cm^{-1} has been assigned to CO_3^{2-} group indicating that CO_3^{2-} is present (Patel *et al*., 2015). The bands at 1041 and 962 cm^{-1} has been assigned to the P-O stretching vibrations of PO_4^{3-} group. The bands at 600, 561 and 475 cm^{-1} corresponds to PO_4^{3-} bending vibrations (Patel *et al*., 2015).

The intensity of the characteristic absorption peaks of MIL-53 (Fe) were decreased, the peak at 1380 cm^{-1} become narrower and the Fe-O band was widened at 545cm^{-1} (Oladipo, 2018). The bands at 1026 and 963 cm^{-1} is seen to also appear which is assigned to the P-O stretching vibrations of PO_4^{3-} group from the hydroxyapatite structure of the bone char. The broad vibration from the MIL-53(Fe) is seen to disappear in the spectra of the composite as a result of sintering at 500 ^{o}C and thus, becoming broader.

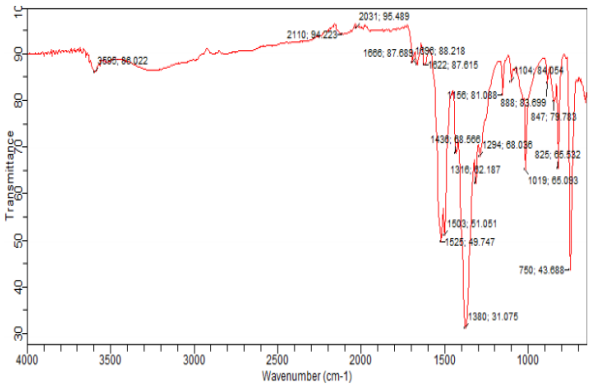

Fig. 3: FTIR for MIL-53(Fe)

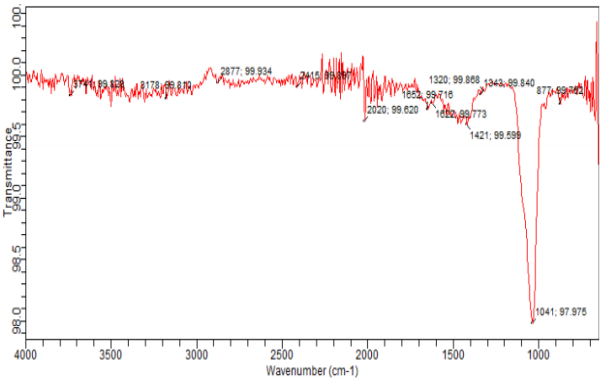

Fig. 4: FTIR for Cow bone char

DOI: 10.51975/VEWJ4581
Journal of the Nigerian Society of Chemical Engineers, 36(1), 2021

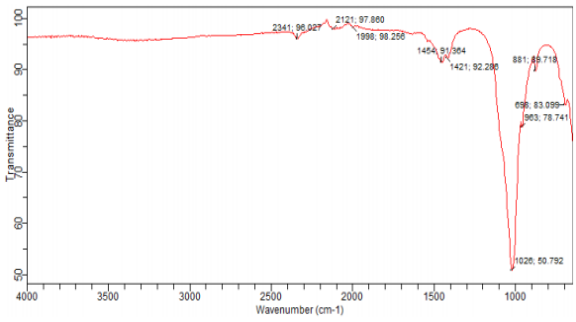

Fig. 5: FTIR for MIL-53(Fe)/Cow bone char composite

The thermal stability of MIL-53(Fe), cow bone char and MIL-53(Fe)/cow bone char composite was studied by means of TG analysis using the TG 209 F1 Libra machine at a heating rate of 10 ^{o}C/min with nitrogen gas as shown in Figures 6, 7 and 8 respectively.

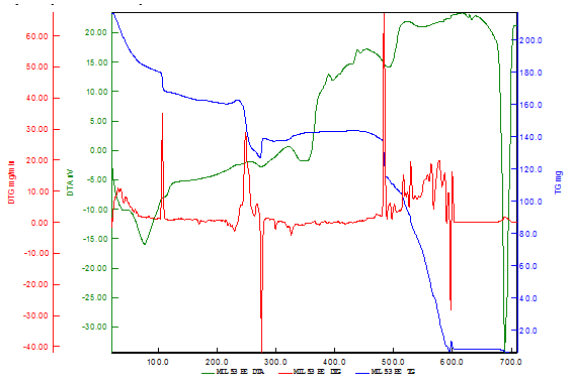

Fig. 6: DTA/TGA curves for MIL-53(Fe)

For MIL-53(Fe), the DTA/ TG profile shown in Fig.6 exhibits an endothermic peak between~90 ^{o}C to 110 ^{o}C with a minimal weight loss up to 180 mg which is as a result of evaporation of moisture from the surface of the MIL-53(Fe). The weight loss became constant from 160 mg in the temperature range of 120 ^{o}C to 280 ^{o}C which was due to free DMF occupation inside the pores. The loss was continued at the exothermic peak between 280 ^{o}C to 480 ^{o}C which can be attributed to the degradation of the organic ligand, H_2BDC. A low rate of decomposition was observed between 520 ^{o}C to 680 ^{o}C followed by a sharp decrease in weight due to complete decomposition of MIL-53(Fe).

Thermal analysis was used to investigate the high temperature behavior of cow bone char shown in Fig.7.

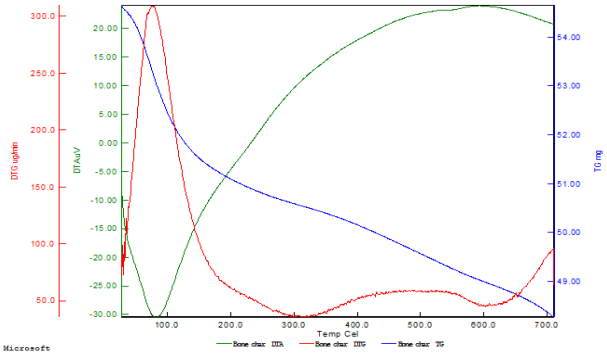

Fig. 7: DTA/TGA curves for cow bone char

The endothermic loss at 50 ^{o}C to 150 ^{o}C corresponds to the removal of absorbed moisture. The exothermic losses at 150 ^{o}C to 550 ^{o}C are attributed to the degradation of the organic substances, fats and collagen. The endothermic loss at 600 ^{o}C to 700 ^{o}C corresponds to the decomposition into calcium oxide from calcium carbonate. This result is consistent with those obtained by Patela *et al*. (2015).

Thermal analysis was used to investigate the high temperature behavior of MIL-53(Fe)/cow bone char composite as shown in Fig. 8

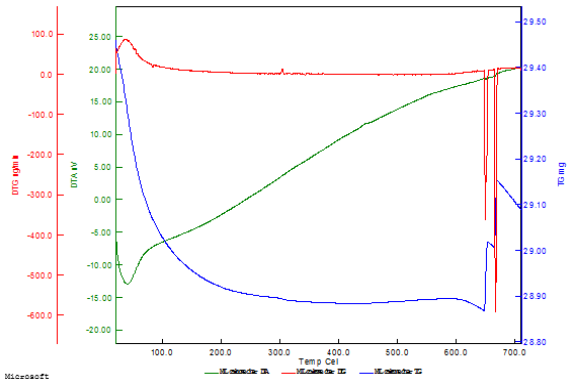

Fig. 8: DTA/TGA curves for MIL-53(Fe)/Cow bone char composite

The first endothermic peak between 50 ^{o}C to 90 ^{o}C is attributed to the evaporation of moisture from the surface of the composite as seen in the individual thermal characteristics of MIL-53(Fe) and cow bone char. The second weight loss peak occurred at above 200 ^{o}C which was as a result of decomposition of MIL-53(Fe) to amorphous Fe_2O_3, the degradation of the organic ligand as seen in MIL-53(Fe) and also the degradation of the organic substances in the cow bone.

3.3 Analysis of samples

Table 2 shows the results for ultimate and proximate analysis of all samples as well as specific surface area and pore parameters of the samples. The prepared cow

bone char has a high surface area of 108.2 m^2 g^{-1}compared to that of MIL-53(Fe) with 69.5 m^2g^{-1}, while the composite recorded 125.6 m^2 g^{-1}. In terms of pore size, the synthesized MIL-53(Fe) has a higher value of 13.9 nm compared to that of cow bone char of 8.94 nm which explains the network structure of MIL-53(Fe) as highly flexible and opens up its pores to guest host (breathing effect), though having a small surface area compared to other metals (Janiak and Jana, 2010; Oladipo, 2018). And on introduction of cow bone char to the composite structure, there was a reduction in the pore size to 11.2 nm. The results obtained confirm that the composite have mesoporous structures suitable for the entrapment of the reactive species, chromium and subsequent enhancement of the adsorption process reactive species (Oladipo, 2018).

The elemental analysis indicates the presence of P_2O_5 higher in cow bone char than in the MIL-53(Fe)/cow bone char composite having 38.66% and 22.78% respectively with an absence in MIL-53(Fe) structure. This result is depicted on the SEM-EDX analysis of the samples. The percentage content of Iron (Fe) is seen to be higher in MIL-53(Fe) with 8.16% and MIL-53(Fe)/bone char composite with 8.23% compared to bone char having 0.07% of Fe.

Table 2: Properties of Samples

Property	**Cowbone char**	**MIL-53(Fe)**	**MIL-53(Fe)/Char**
Total surface area (m^2 g^{-1})	108.2	69.5	125.6
Pore size (nm)	8.94	13.9	11.2
Total pore volume (cm^3 g^{-1})	0.589	0.789	0.981
Micropore volume (cm^3 g^{-1})	0.237	0.396	0.325
Density (g cm^{-3})	0.69	0.89	1.12
Carbon content (%)	13	15.3	22.4
pHpzc (zero point charge)	6.7	4.5	5.4
P_2O_5 (%)	38.66		22.78
N_2 (%)	0.89		0.32
Fe (%)	0.07	8.16	8.23
Ca (%)	26.55		11.89
Mg (%)	0.67		0.23
SO_4 (%)	0.89		0.23
S(%)	0.38		0.004
Cation exchange capacity (meq g^{-1})	7.5	4.56	6.56

3.4 Adsorption column studies

3.4.1 Effect of time of collection

The contact time was determined for different flow rates of 5 ml/min and 15ml/min as shown in Fig. 9 & 10. The percentage removal of chromium increased up to 4 minutes having a maximum removal at 87.9% and 80.94% respectively following a reduction up to 14 minutes and there after no further changes was observed.

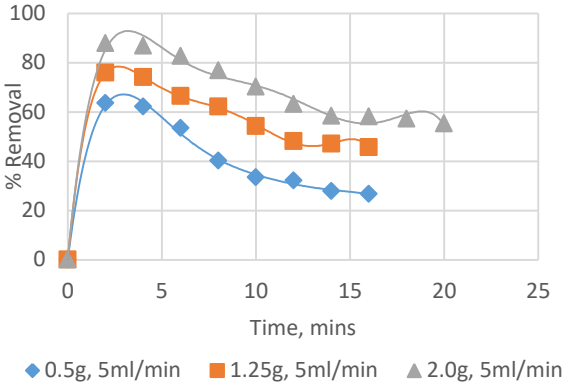

Fig. 9: Chromium removal with time (5ml/min)

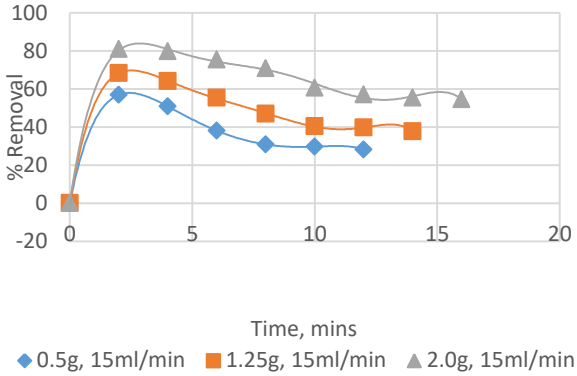

Fig.10: Chromium removal with time (15ml/min)

3.4.2 Effect of flow rate on breakthrough curve

The breakthrough curve in Figure 11 showed that at lower flow rate of 5ml/min, the surface of the composite was readily available for adsorption and more molecules were adsorbed as there was sufficient contact time with chromium molecules. Thus, having a higher adsorption percentage as well as a shallow adsorption zone and breakthrough and exhaustion were not quickly reached. While at higher flow rate, there was an increase in rate of mass transfer, shorter contact time and a steeper curve with relatively early breakthrough and exhaustion time which resulted in less adsorption uptake was observed. The observations drawn is in agreement with those reported by (Ghribi and Chlendi, 2011; Chowdhury *et al*., 2013; 2015; Dutta and Basu, 2014).

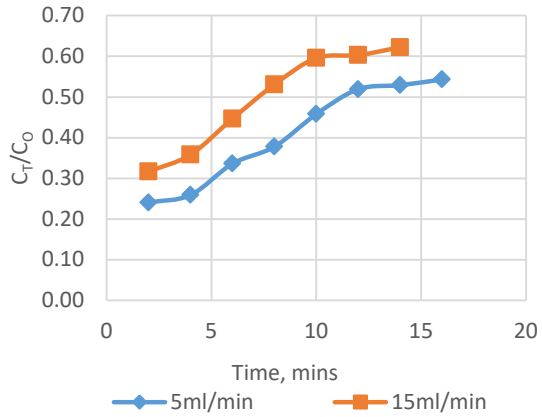

Fig.11: Breakthrough curve for chromium removal

3.4.2 Effect of bed height on chromium adsorption

Figure 12 shows the effect of bed height on chromium adsorption obtained for three different bed depths of 0.6 cm, 1.5 cm and 2.4 cm at 5 ml/min with an inlet concentration of 40 mg/l. A higher uptake was observed at a higher bed height of 2.4cm, as more adsorbate was passed down the bed, the adsorbent bed became saturated at which there was a reduction in the individual bed efficiency to about 58%. This observation is in agreement with those reported by (Ghribi and Chlendi, 2011; Chowdhury *et al*., 2013; 2015).

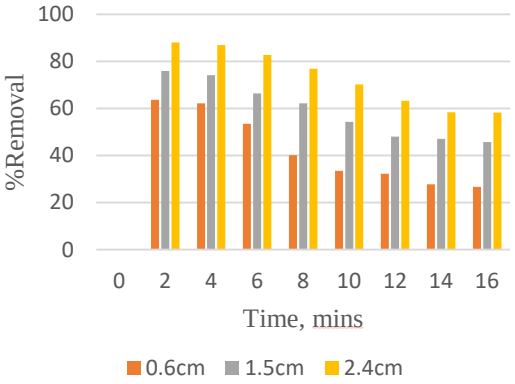

Fig.12: Bed height effect on adsorption of chromium

3.4.4 Equilibrium adsorption isotherm study

Table 3 and 4, the determination of coefficients (R^2) of the linear form of Langmuir model turned out to be satisfactory having an R^2> 0.9893 and 0.9933 respectively at a bed height of 2.4 cm.

Also, the maximum monolayer adsorption capacity of 19.61 mg/g was found at this same bed height of 2.4 cm compared to other bed heights which indicate uniform monolayer coverage. R_L values determined were found to be in the range $0<R_L<1$ which explains that the chromium ions is favorably adsorbed and the values of the equilibrium constant K_L were lower than unity which quantitatively reflects the strong affinity between the chromium ions and the MIL-53(Fe)/cow bone char composite.

K_F was determined to be 13.5515 mg/g, 6.63461 mg/g and 4.8759 mg/g which explains the random distribution of cow bone char between the crystallites of MIL-53(Fe) which may introduce heterogeneity onto the surface (Ghanizadeh *et al*., 2012) and a favorable sorption capacity.

From the Temkin plot, the heat of adsorption of chromium ions onto the composite was seen to be higher at 0.6 cm and reduced at 1.5 cm with a slight increase at 2.4 cm for both flow rates indicating an exothermic process. Also, the b values are lower than 80 kJ/mol which indicates that the adsorption of chromium ions onto MIL-53(Fe)/cow bone char composite is a physical adsorption process and consistent with FTIR analysis.

The mean energy of adsorption for chromium onto MIL-53(Fe)/cow bone char composite were all below 8 kJ/mol with R^2 values all at 0.9 and demonstrates that the adsorption of chromium onto MIL-53(Fe)/cow bone char is physisorption and plays an important role.

Table 3: Isotherm parameters for chromium adsorption onto MIL-53(Fe)/CBC composite

Isotherm	Adsorption Parameters, 0.6cm, 5ml/min	Adsorption Parameters, 1.5cm, 5ml/min	Adsorption Parameters, 2.4cm, 5ml/min
Langmuir	Q_m=4.2753mg/g K_L=0.087L/mg R_L= 0.22273 R^2=0.9579	Q_m=8.326mg/g K_L=0.170L/mg R_L= 0.12807 R^2=0.9850	Q_m=19.61mg/g K_L=0.368L/mg R_L=0.06361 R^2=0.9893
Freundlich	K_F=13.5515 1/n=1.20 n=0.830 R^2=0.9696	K_F=6.63461 1/n=0.62 n=1.596 R^2=0.9735	K_F=4.8759mg/g 1/n=0.35 n=2.824 R^2= 0.9608
Temkin	A_T=49.9198L/g b_T=196.586 B=12.603J/mol R^2= 0.9942	A_T=75.8987L/g b_T=275.601 B=8.9897J/mol R^2= 0.9896	A_T=174.354L/g b_T=246.206 B=10.063J/mol R^2= 0.978
Dubinin-Radushkevich	β=0.00004 Q_m=5.5384mg/g E=111.8J/mol R^2=0.9056	β=0.00001 Q_m=10.4093mg/g E=223.6J/mol R^2=0.8805	β=0.000002 Q_m=14.0202mg/g E=500J/mol R^2=0.8019

3.4.5 Kinetics of adsorption

Three kinetic models were employed to describe the sorption rates for chromium and obtained results are presented in Table 5.

Table 4: Isotherm parameters for chromium adsorption onto MIL-53(Fe)/CBC composite

Isotherm	Adsorption Parameters, 0.6cm, 15ml/min	Adsorption Parameters, 1.5cm, 15ml/min	Adsorption Parameters, 2.4cm, 15ml/min
Langmuir	Q_m=3.88048mg/g K_L=0.074L/mg R_L= 0.25306 R^2=0.9767	Q_m=6.21891 mg/g K_L=0.116L/mg R_L= 0.17683 R^2=0.9811	Q_m=17.67mg/g K_L=0.259L/mg R_L= 0.08792 R^2=0.9933
Freundlich	K_F=17.374mg/g 1/n=1.37 n=0.726 R^2=0.9829	K_F=9.053mg/g 1/n=0.88 n=1.135 R^2=0.9782	K_F=6.857mg/g 1/n=0.46 n=2.183 R^2= 0.9818
Temkin	A_T=47.7674L/g b_T=182.55 B=13.572J/mol R^2= 0.9969	A_T=58.1506L/g b_T=226.345 B=10.946J/mol R^2= 0.9937	A_T=110.757L/g b_T=201.691 B=12.284J/mol R^2= 0.9910
Dubinin-Radushkevich	β=0.00006 Q_m=4.8105mg/g E=91.2871J/mol R^2=0.9446	β=0.00002 Q_m=7.87505 mg/g E=158.114J/mol R^2=0.9133	β=0.000005 Q_m=12.59mg/g E=316.228J/mol R^2=0.9011

The equilibrium adsorption of chromium onto MIL-53(Fe)/cow bone char composite could be best described with the pseudo-second order kinetic model judging by the R^2 values depicted in Table 5.

Table 5: Kinetic model parameters for chromium adsorption onto MIL- 53(Fe)/CBC composite.

Model	Kinetic parameters
Lagergren Pseudo First-order	k_1 (min^{-1})= 0.2096 q_1 (mg/g)=14.047 R^2=0.963
Pseudo second-order	k_2 ($gmg^{-1}min^{-1}$) =0.04304 q_2 (mg/g)=12.3762 R^2=0.9911
Intraparticle diffusion	k_{ad}($mgg^{-1}min^{-1(1/2)}$ =3.0312 C_i(mg/g)=26.353 R^2=0.9503

CONCLUSIONS

In the present work, MIL-53(Fe)/Cow bone charcoal composite, was successfully prepared via the sol-gel method and was tested for the removal of chromium from real tannery effluent. The adsorption process was found to be efficient below the pH_{pzc} of 5.4. The kinetic studies showed that the adsorption data were fitted well to the pseudo second-order model with high correlation coefficient R^2=0.9911. The adsorption isotherm equilibrium studies confirmed that the Langmuir model best described the adsorption process of chromium onto MIL-53(Fe)/Cow bone char composite. Adsorption capacity of MIL-53(Fe)/Cow bone char composite for chromium was 19.61mg/g with a removal efficiency of 87.8% at an optimal bed height of 2.4cm (2.0g) for MIL-53(Fe)/Cow bone char composite. A result from analysis of data with Dubinin–Radushkevich and Temkin isotherms showed that adsorption of chromium onto MIL-53(Fe)/Cow bone char composite is physical in nature.

REFERENCES

Agoyi O.R., Igboro S.B., Okuofo C.A. (2015). *Performance of Cow bone Char in Fixed-Bed Column for the Treatment of Industrial Wastewater*. Kaduna State: Department of Water Resources and Environmental Engineering, Ahmadu Bello University, Zaria.

Araoye, B. O. (2015). A Study of the Development, Characterisation and Degradability of Polyester/Nano-Locust Bean Pods Ash Composite. Ahmadu Bello University, Zaria, Department of Metallurgical and Materials Engineering.

Chowdhury, T, L. Zhang , J. Zhang and S. Aggarwal. (2018). Removal of Arsenic(III) from Aqueous Solution Using Metal Organic Framework-Graphene Oxide Nanocomposite. *Nanomaterials (8)*, 1-18.

Chowdhury, Z. Z., Zain,S.M., Rashid,A. K., Rafique,R. F., & Khalid, K. (2013). Breakthrough Curve Analysis for Column Dynamics Sorption of Mn(II) Ions from Wastewater by Using Mangostana garcinia Peel-Based Granular-Activated Carbon. *Journal of Chemistry*, 1-8. doi:http://dx.doi.org/10.1155/2013/959761

Fawell, J. (2006). Fluoride in drinking-water (1st published. ed.). *WHO ISBN 9241563192.*, 47.

Ghader Ghanizadeh, Ghorban Asgari, Abdol Motaleb Seid Mohammadi and Mohammad Taghi Ghaneian. (2012). Kinetics and Isotherm Studies of Hexavalent Chromium Adsorption from Water using Bone Charcoal. *Fresenius Environmental Bulletin*, 1296-1302.

Janiak, C and Jana K. V.. (2010),. MOFs, MILs and more: concepts, properties and applications for porous coordination networks (PCNs). *New Journal of Chemistry, 34*, Pages 2337–2684. Retrieved from www.rsc.org/njc

Oke,I. A., Otun, J. A., Okuofu,C. A. and Olarinoye,N. O. (2006). Characteristics of Tanning Industries in Nigeria for Aquatic Animals and Plants. *Research Journal of Agriculture and Biological Sciences, 2(5)*, 209-217.

Oladipo, A. A. (2018). MIL-53 (Fe)-based photo-sensitive composite for degradation of organochlorinated herbicide and enhanced reduction of Cr(VI). *Process Safety and Environmental Protection (116)*, 413-423.

Mohammed, SSD; Orukotan, AA; Abdullahi, H. (2017). Physicochemical and Bacteriological Assessment of Tannery Effluent from Samaru-Zaria, Kaduna State, Nigeria. *Journal of Applied Science and Environmental Management (4), 21*, 734-740. doi:10.4314/jasem.v21i4.14

DOI: 10.51975/XMTI1916
Journal of the Nigerian Society of Chemical Engineers, 36(1), 2021

OPTIMISATION OF MICROWAVE PRETREATMENT CONDITIONS OF ORANGE AND PLANTAIN PEELS FOR POLYGALACTURONASE PRODUCTION BY *ASPERGILLUS AWAMORI* CICC 2040

Adedeji, O.E.[1,2] and Ezekiel, O.O.[2]

[1]Department of Food Science and Technology, Federal University Wukari, PMB 1020, Wukari, Nigeria,
[2]Department of Food Technology, University of Ibadan, Ibadan, Nigeria.
[*]Corresponding author: jdadedeji@gmail.com

ABSTRACT

This study investigated the optimisation of microwave pretreatment of orange and plantain peels for polygalacturonase (PG) production, by Aspergillus awamori CICC 2040, using response surface methodology. The microwave pretreatment factors interacted were particle size (PS) (<0.4250, 0.4250<PS<0.8025, and 0.8025<PS<1.1800 mm), microwave power (240, 480 and 720 W) and time (2.50, 6.25, and 10.00 min.). These factors were interacted to determine combinations for maximum polygalacturonase activity (MPA). Pretreated orange and plantain peel powders were inoculated with 10^6 spores/mL Aspergillus awamori CICC 2040, incubated at 28^{o}C for 5 days, and crude polygalacturonase was extracted and its activity determined. Same microwave pretreatment combination, 0.8025<PS<1.1800 mm, 720 W and 10.00 min, gave MPA for orange and plantain peels. The MPA from orange and plantain peels was 26.21 and 26.72 U/mL, respectively. F and p values obtained for orange peel powder were 35.42 and 0.00, respectively while those obtained for plantain peel powder were 5.71 and 0.006, respectively. R^2 and R^2 (adjusted) of 96.96 and 94.22%, respectively were obtained for PG activity produced using orange peel powder while 90.71 and 79.04% were recorded for PG activity produced using plantain peel powder. Optimised microwave pretreatment conditions of orange and plantain peels for MPA from Aspergillus awamori CICC 2040 were established.

***Keywords**: Aspergillus awamori, Fruit peel, Microwave, Optimisation, Polygalacturonase, Pretreatment,*

INTRODUCTION

Polygalacturonase (PG) (E.C. 3.2.1.15) is a pectinase involved in the degradation of polygalacturonan in plant's cell walls through the hydrolytic breakdown of glycosidic bonds that bind galacturonic acid moieties (Heerd et al, 2012). Polygalacturonase is used in food, paper and pulp, animal feed, waste management, and pharmaceutical industries (Tapre and Jain, 2014) and represents 10% of estimated commercialised enzymes (Anuradha et al, 2014). Polygalacturonase has been produced via solid-state fermentation and submerged fermentation processes (Khatri et al, 2015).

In recent times, there has been considerable interest in the use of food wastes and agricultural residues as substrates for the production of bio-products, both from economic and environmental viewpoints. The utilisation of agricultural residues is increasing due to the high cost of traditional feedstocks (Wadhwa et al, 2015). The environmental concern of un-utilized wastes stems from the generation of hazardous materials that are released to nature as a result of their degradation. This results in environmental pollution, which has both short and long term effects (Obi et al, 2016). Different pectin-rich agricultural by-products have been used as substrates for PG production (Ptichkina et al, 2008; Anuradha et al, 2010; Anuradha et al, 2014) and among these, orange and plantain peels have enjoyed high preference due to their wide availability (Li et al, 2015; Castillo-Isreal et al, 2015).

The utilisation of agricultural residues and fruit processing wastes as substrates for microorganisms for subsequent elaboration of bio-products are limited due to high concentration of lignin, cellulose, and hemicelluloses, which are physical barriers that limit microbial and enzymatic hydrolysis of biomasses (Yu et al, 2015). Specifically, lignin is known to adsorb enzyme thereby reducing its degradation efficiency (Ju et al, 2013). Cellulose has been considered a factor that limits accessibility of microorganisms to agricultural residues. The severity of this occurrence is dependent on residue's surface area, crystalline, and amorphous ratio of cellulose as well as its degree of polymerisation (El-shishtawy et al, 2015). Previous studies demonstrated

that the bio-conversion rate of residues is dependent on properties of cellulose (Li et al, 2015; Yang et al, 2017; Lai et al, 2017).

Properties of enzymes e.g. cellulase and xylanase produced from pretreated agricultural by-products are well documented (Rahnama et al, 2013; Salihu et al, 2015). Increased PG activity was reported for alkaline-pretreated highly ligno-cellulosic materials (wheat straw and palm leaves) using *Trichoderma reesei* under SSF (El-Shishtawi et al, 2015). The findings of Li et al (2015) showed that the microwave pretreatment of orange peel before the production of exo-pectinase, by *Aspergillus japonicus* under submerged fermentation, resulted in a significant increase in the activity of the enzyme. However, information on the properties of PG produced from *Aspergillus* species using pretreated pectin-rich agricultural by-products under solid-state fermentation is sparse. Furthermore, there is paucity of information on the optimisation of microwave pretreatment operation conditions of agricultural residues for improved PG production. Hence, the objective of this study was to optimise microwave pretreatment conditions of orange and plantain peels for maximum PG activity from *Aspergillus awamori* CICC 2040 using response surface methodology.

MATERIALS AND METHODS

Materials

Peels of orange (*Citrus sinensis* L. Osbeck) and plantain (*Musa paradisiaca* Linn.) were obtained from small-scale food processing factories in Ibadan, Nigeria. Fungal strain, *Aspergillus awamori* CICC (China Centre of Industrial Culture Collection) 2040 was obtained from China National Research Institute of Food and Fermentation, Beijing, China. All reagents used were of analytical grade.

Methods

Production of orange and plantain peel powders

The orange and plantain peels were blanched (80 ^{o}C for 3 min), rinsed, and dried in a hot air oven (NL9023A, Genlab Ltd, Cheshire, England) at 60 ^{o}C for 48 h. The dried peels were milled into powders and sieved into 3 different particle sizes with the aid of 0.4250, 0.8025, and 1.1800 mm sieves (United States Pharmacopoeia Standard Sieves). The powders were packaged in polyethylene containers (ZipLock, China) and stored at -20 ^{o}C for subsequent analyses (Adedeji and Ezekiel, 2019).

Microwave pretreatment of orange and plantain peel powders

The microwave pre-treatment was carried out based on the procedure reported by Inan et al (2016). Substrate flour (5% w/v) was added to distilled water in a container and the mixture was treated in a laboratory microwave oven (NX-802, Nexus, Beijing, China, with 25 L capacity, 800 W power output and frequency of 2450MHz) at varying power level for different pre-treatment time. Thereafter, the residue was oven-dried (NL9023A, Genlab Ltd, Cheshire, England) at 60 ^{o}C to a final moisture content of 10 %.

Experimental design for microwave pretreatment of orange and plantain peels

Face centered central composite design under the response surface methodology (RSM) was used for the evaluation of three independent variables. Factors interacted were particle size, PS (<0.4250, 0.4250<PS<0.8025, 0.8025<PS<1.1800 mm), microwave power (240, 480, and 720 W) and pretreatment time (2.50, 6.25, and 10.00 min). The factors were interacted to determine combination for maximum polygalacturonase activity.

Culturing of microorganism

The fungal strain was maintained on malt extract agar (MEA) at 28^{o}C for 6 days. Inoculums for the experiments were prepared from heavily sporulated MEA slants.

Solid state production of polygalacturonase

Solid state fermentation procedure described by Dey et al (2014) was adopted. Orange peel powder (OPP) and plantain peel powder (PPP) were mixed with Czapek-dox medium (2.5 g/L $NaNO_3$, 1 g/L KH_2PO_4, 0.5 g/L KCl and 0.5 g/L $MgSO_4.2H_2O$) at pH 4.0 in ratio 1:2 (w/v) in a 250 mL Erlenmeyer flask and autoclaved (121^{o}C, 15 psi) for 15 min. Subsequently, the substrate was inoculated with 10^6 spores/mL of the culture and incubated in an incubator (CLN115, Pol Eko Aparatura, Poland) at 28^{o}C for 5 days. After this, fermented mass was suspended in distilled water to form a 50 g/L suspension. The suspension was placed in an incubator (CLN115, Pol Eko Aparatura, Poland) at 30 ^{o}C for 1 h and centrifuged (K24IR, Centurion Scientific Ltd, UK) at 2200 × g for 10 min. The supernatant was separated using Whatman No. 1 filter and PG assay conducted. Enzyme was stored at -20^{o}C until required.

ANALYSES

Determination of polygalacturonase activity

Activity of PG was determined based on the procedure outlined by Dey et al (2014). A 0.5 mL each of PG and 0.5% polygalacturonic acid was prepared in acetate buffer (pH 5.0) and the mixture incubated in a water bath (NL42OS, Genlab Ltd, Cheshire, England) at 50 ^{o}C for 10 min. Thereafter, a 3 mL of freshly prepared 3, 5 di-nitro salicylic acid solution was added and the mixture heated at 90 ^{o}C for 15 min. The mixture was rapidly cooled and absorbance read at 575 nm with the aid of UV/VIS spectrophotometer (Jenway 6850, Cole-Parmer, Staffordshire, UK). One unit of PG activity was calculated as the amount of enzyme required to release 1 µmol of D-galacturonic acid per minute of reaction (µmol/min). A blank was prepared by mixing buffer, DNS and distilled water, and subjected to similar treatment as the enzyme solution. Polygalacturonase activity was expressed in unit of activity per mL (U/mL).

Statistical analyses

Experiments were conducted in triplicates and means of measured values were used to generate the response (PG activity). A linear equation was fitted to the data by multiple regression procedure (Equation 1)

$$Y = \alpha_0 + \sum_{i=1}^{n} \alpha_i X_i + \sum_{i=1}^{n} \alpha_{ii} {X_i}^2 + \sum_{i=1}^{n-1} \sum_{i=1}^{n} \alpha_{ij} X_i X_j \quad (1)$$

Where Y represents predicted response, PG activity (U/mL), X_1, X_2, X_3…….Xn are independent variables, α_0 is a constant, and αi, αii and αij are linear, squared and interaction effects, respectively. Multiple regression model was evaluated with the aid of analysis of variance and quality of fit was tested by determining the coefficient of determination (R^2). These were achieved using the Minitab software, version 16.2.1 (Stat-Ease Inc., USA).

RESULTS AND DISCUSSION

Optimisation of microwave pretreatment condition of orange and plantain peels for polygalacturonase production

Table 1 shows the PG activity produced from *Aspergillus awamori* CICC 2040 using microwave (MW) pretreated orange and plantain peels. Polygalacturonase activity ranged from 6.97 (Run 3) to 26.21 U/mL (Run 8) and 10.22 (Run 13) to 26.72 U/mL (Run 8) on OPP and PPP, respectively. Results obtained showed that MW pretreatment variables: substrate particle size, MW power and pretreatment time had significant ($p < 0.05$) effect on PG activity. For OPP and PPP, maximum PG activity of 26.21 and 26.72 U/mL, respectively were obtained at Run 8, which corresponded to a substrate particle size of 0.8025<PS<1.18 mm, MW power of 720 W and pretreatment time of 10 min. The similarity observed may be due to the high efficiency of microwave pretreatment, which probably resulted in substrates with similar properties. Microwave treatment has been described as a technology with a high degree of heating efficiency and uniformity (Nomanbhay et al, 2013). Predicted PG activity of 24.70 and 26.03 U/mL for OPP and PPP, respectively showed that both the experimental and predicted values were highly correlated. The lowest PG activity of 6.97 U/mL was recorded for OPP with <0.425 mm particle size pretreated at 720 W for 2.5 min (Run 3). However, Run 13 which corresponded to PG activity produced from PPP with particle size of 0.8025<PS<1.18 mm, 480W MW power and pretreatment time of 2.5 min gave the lowest value of 10.22 U/mL.

Analysis of variance (Table 2) showed the adequacy of the models in the characterisation of the independent variables. F and p values obtained for OPP were 35.42 and 0.00, respectively while those obtained for PPP were 5.71 and 0.006, respectively. These values implied that the models were significant ($p<0.05$). R^2 and R^2 (adjusted) of 96.96 and 94.22%, respectively were obtained for PG activity produced from OPP while 90.71 and 79.04% were respectively recorded for PG activity produced form PPP. This suggested that 96.96% and 90.71% of the variation in the predicted and experimental data of PG obtained from pretreated OPP and PPP, respectively were covered by the models. For PG activity produced from OPP, X_2 (MW power), X_3 (pretreatment time), ${X_3}^2$ (pretreatment time × pretreatment time), and X_2X_3 (MW power × pretreatment time) were significant ($p < 0.05$) in the model. The quadratic equation after deleting the terms that were not significant ($p>0.05$) is presented in Equation 2.

$$Y = 25.89 - 0.069X_2 - 3.83X_3 + 0.17X_3^2 + 0.004X_2X_3 \quad (2)$$

The following terms were significant ($p < 0.05$) in the regression model for PG activity produced from MW-pretreated PPP: X_1 (particle size), X_2 (MW power), ${X_1}^2$ (particle size × particle size), X_1X_2 (particle size × MW power) and X_1X_3 (particle size × pretreatment time). The residual terms in the model are shown in Equation 3.

$$Y = 5.71 - 75.93X_1 - 0.08X_2 + 28.60X_1^2 + 0.03X_1X_2 + 1.85X_1X_3 \quad (3)$$

Effect of microwave pretreatment conditions of orange and plantain peels on polygalacturonase activity

The activity of PG as influenced by the synergistic effect of substrate particle size and MW power on OPP and PPP are presented in Figure 1a and b, respectively. The PG activity obtained from both OPP and PPP increased with increasing MW power and substrate particle size. For both peels, maximum PG activity was obtained at the highest boundary of MW power and substrate particle size. Li et al (2015) reported 11.8% increase in exo-pectinase activity from *Aspergillus japonicus* using OPP pre-treated at high MW power of 630 W and substrate particle size of 0.850 mm. According to Woldesenbet et al (2012), microwave radiation at high power level results in accelerated rupturing of substrates, due to high thermal energy dissipation, which makes polysaccharides to be more susceptible to microbial proliferation.

DOI: 10.51975/XMTI1916
Journal of the Nigerian Society of Chemical Engineers, 36(1), 2021

Table 1. **Activity of polygalacturonase produced by *Aspergillus awamori* on microwave-pretreated orange and plantain Peels**

				PG activity (U/mL)			
	Independent variables			From orange peel		From plantain peel	
Run	Particle size (mm)	Power level (W)	Time (min)	Experimental	Predicted	Experimental	Predicted
1	<0.425	240	2.5	14.04	15.42	22.84	23.68
2	0.8025<x<1.18	240	2.5	25.43	24.27	11.29	10.52
3	<0.425	720	2.5	6.97	6.05	19.69	17.32
4	0.8025<x<1.18	720	2.5	17.12	18.15	13.27	16.19
5	<0.425	240	10	10.13	8.97	22.22	19.44
6	0.8025<x<1.18	240	10	15.04	15.83	14.27	16.79
7	<0.425	720	10	13.55	14.59	15.74	16.66
8	0.8025<x<1.18	720	10	26.21	24.70	26.72	26.03
9	<0.425	480	6.25	7.13	6.79	15.09	18.48
10	0.8025<x<1.18	480	6.25	15.43	16.27	20.56	16.58
11	0.425<x<0.8025	240	6.25	14.99	15.13	15.80	15.99
12	0.425<x<0.8025	720	6.25	14.53	14.88	18.22	17.44
13	0.425<x<0.8025	480	2.5	15.62	15.29	10.22	9.59
14	0.425<x<0.8025	480	10	14.51	15.34	12.36	12.39
15	0.425<x<0.8025	480	6.25	13.06	12.93	13.33	13.45
16	0.425<x<0.8025	480	6.25	13.11	12.93	13.06	13.45
17	0.425<x<0.8025	480	6.25	13.01	12.93	13.25	13.45
18	0.425<x<0.8025	480	6.25	13.16	12.93	13.12	13.45
19	0.425<x<0.8025	480	6.25	13.00	12.93	13.42	13.45
20	0.425<x<0.8025	480	6.25	13.21	12.93	13.35	13.45

Table 2. **Analysis of variance of fitted models of polygalacturonase from microwave-pretreated orange and plantain peels**

		Orange peel					Plantain peel			
Source	DF	Sum of square	Mean square	F-value	P-value	DF	Sum of square	Mean square	F-value	P-value
Model	9	396.79	44.09	35.42	0.00	9	305.55	33.95	5.71	0.006
X_1	1	224.71	12.98	10.43	0.09	1	8.97	109.25	18.37	0.002
X_2	1	0.16	39.52	31.75	0.00	1	5.21	59.74	10.05	0.01
X_3	1	0.01	39.67	31.87	0.00	1	19.60	0.96	0.16	0.70
X_1^2	1	8.26	5.37	4.31	0.07	1	103.79	45.68	7.68	0.02
X_2^2	1	28.38	11.93	9.58	0.01	1	17.49	29.34	4.92	0.051
X_3^2	1	15.68	15.68	12.59	0.005	1	16.64	16.36	2.80	0.125
X_1X_2	1	5.30	5.30	4.26	0.07	1	72.36	72.36	12.17	0.006
X_1X_3	1	1.97	1.97	1.58	0.24	1	55.13	55.13	9.27	0.012
X_2X_3	1	112.28	112.28	90.19	0.00	1	6.37	6.37	1.07	0.325
Residual error	10	12.45	12.45			10	59.47	5.95		
Lack of fit	5	12.41	2.48	353.84	0.227	5	59.37	11.86	604.92	0.183
Pure error	5	0.04	0.01			5	0.10			
Total	19	409.24				19	365.03			
R^2	96.96%					90.71%				
R^2 (adj)	94.22%					79.04%				

X_1- particle size; X_2- Microwave power; X_3- pretreatment time; DF- degree of freedom

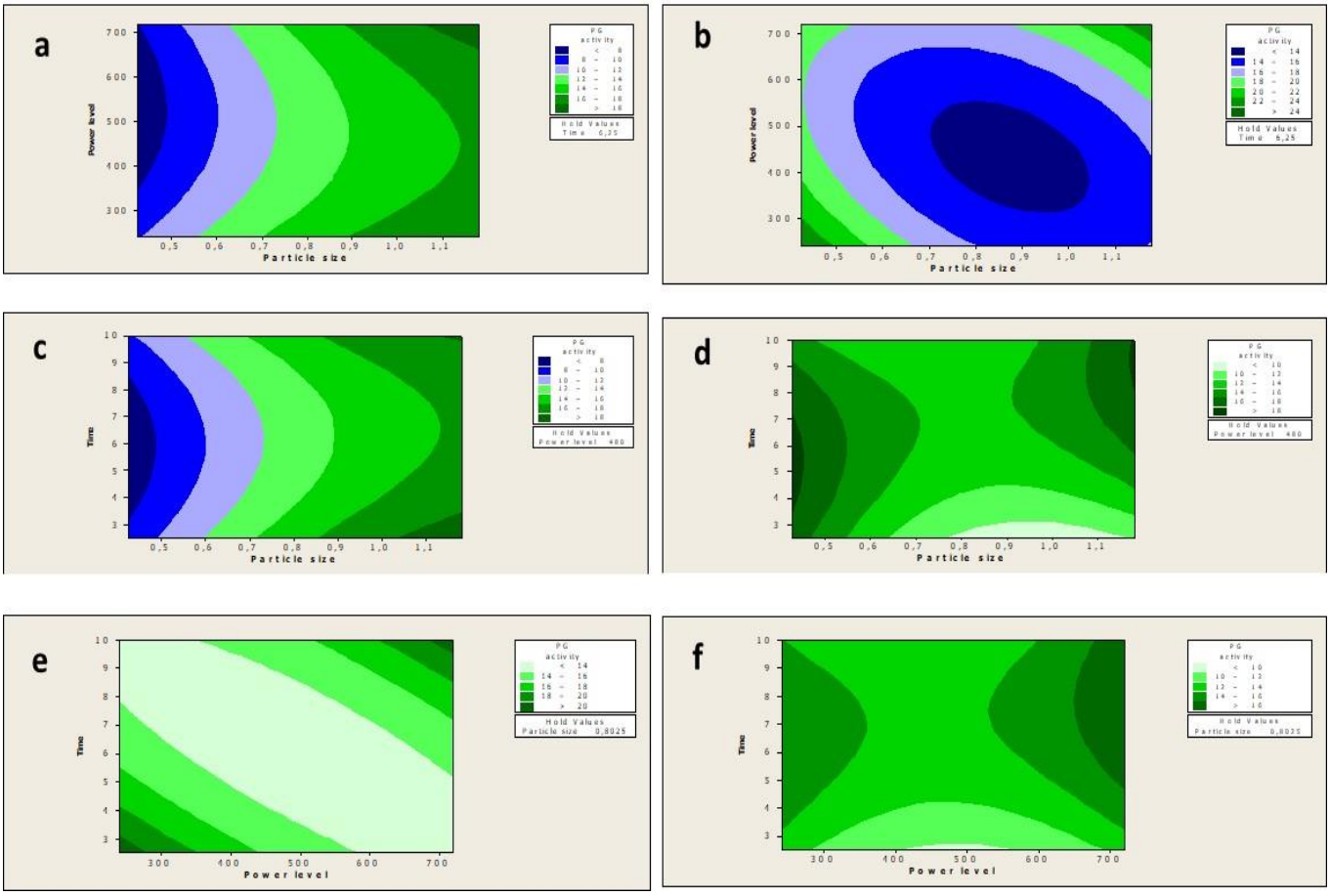

Figure 1. Effect of microwave pretreatment condition on PG activity (a) effect of particle size and NaOH molarity on PG activity produced using pretreated orange peel, (b) effect of particle size and NaOH molarity on PG activity produced using pretreated plantain peel, (c) effect of particle size and time on PG activity produced using pretreated orange peel, (d) effect of particle size and time on PG activity produced using pretreated plantain peel, (e) effect of NaOH molarity and time on PG activity produced using pretreated orange peel, (f) effect of NaOH molarity and time on PG activity produced using pretreated plantain peel.

The iinteractive effect between substrate particle size and pre-treatment time on PG activity produced from OPP and PPP is shown in Figures 1c and d, respectively. The activity of PG produced using OPP increased with increasing particle size irrespective of the pre-treatment time. The findings of Inan et al (2016) also showed an increase in sugar concentration with increasing particle size of barley straw (x < 1.0 mm) irrespective of pre-treatment time (2.5 – 10 min). Low PG activity recorded in OPP with small particle size could be due to the disintegration of pectin molecules, the main inducer substrate for PG production, as a result of intensive size reduction operation. For PG produced using PPP, maximum activity was produced at substrate particle size of >1.0 mm and pre-treatment time of 6 – 10 min.

Figures 1e and f are contour plots showing the interaction between MW power and pretreatment time on the activity of PG. The activity of PG from OPP increased between MW power of 480 and 720 W, and pretreatment time 7 to 10 min. In a similar pattern, PG activity from PPP increased with increasing MW power and pretreatment time. Differences in substrate composition may be responsible for the variation. This study is in agreement with the work of Inan et al (2016) who observed a decrease in total sugar from barley straw pretreated at a microwave power level of 300 W and pretreatment time of 2.5 min. This result did not agree with the report of Tiwari et al (2017) who reported maximum enzymatic hydrolysis of mango peel obtained at MW power of 450 W and exposure time of 4 min.

Model validation for microwave pre-treatment of orange and plantain peels

The percentage deviation for experimental and predicted data of OPP and PPP was 4.81 and 2.58%, respectively. Suitability of the model in fitting the experimental data was thus validated since these values were less than 5.0% (Ezekiel and Aworh, 2018).

CONCLUSIONS

This study established microwave pretreatment conditions of orange and plantain peels for maximum PG activity. The same microwave pretreatment conditions, i.e. 720 W microwave power, 0.8025<PS<1.1800 mm particle size and pretreatment time of 10 min, gave maximum PG activity. Besides, the maximum PG activity from orange (26.21 U/mL) and plantain (26.72 U/mL) peels was very similar. For the PG activity produced from OPP, the terms including X_2 (MW power), X_3 (pretreatment time), X_3^2 (pretreatment time × pretreatment time) and X_2X_3 (MW power × pretreatment time) were significant ($p<0.05$) in the model, however, X_1 (particle size), X_2 (MW power), X_1^2 (particle size × particle size), X_1X_2 (particle size × MW power) and X_1X_3 (particle size × pretreatment time) were significant for the PG activity produced from PPP.

ACKNOWLEDGEMENT

Special thanks go to the Tertiary Education Trust Fund of the Federal Republic of Nigeria for the Academic Staff Training and Development Fellowship (FUW/REG/S.39/vol.1/024) granted to Olajide Emmanuel Adedeji.

REFERENCES

Adedeji, O.E., & Ezekiel, O.O. (2019). Pretreatment of selected peels for polygalacturonase production by *Aspergillus awamori* CICC 2040: Purification and application in mango juice extraction. *Bioresource Technology Reports*, 7: 100306.

Anand, G., Yadav, S. and Yadav, D. (2016). Purification and characterization of polygalacturonase from *Aspergillus fumigatus* MTCC 2584 and elucidating its application in retting of *Crotalaria juncea* fiber. *3 Biotech*, 6: 201-207.

Anuradha, K., Padma, P.N., Venkateshwar, S. and Reddy, G. (2010). Fungi isolates from natural pectic substrates for polygalacturonase and multi enzyme production. *Indian Journal of Microbioliology*, 50: 339-344.

Anuradha, K., Padma, P.N., Venkateshwar, S. and Reddy, G. (2014). Selection of nutrients for polygalacturonase production by Aspergillus awamori MTCC 9166 using Placket-Burman design. *Indian Journal of Biotechnology*, 13: 502-507.

Castillo-Israel, K.A.T., Baguio, S.F., Diasanta, M.D.B., Lizardo, R.C.M., Dizon, E.I. and Mejico, M.I.F. (2015). Extraction and characterization of pectin from Saba banana [Musa 'saba'(*Musa acuminata* x *Musa balbisiana*)] peel wastes: A preliminary study. *International Food Research Journal*, 22(1): 190-195.

Dey, T.B., Adak, S., Bhattacharya, P. and Banerjee, R. (2014). Purification of polygalacturonase from *Aspergillus awamori* Nakazawa MTCC 6652 and its application in apple juice clarification. *LWT - Food Science and Technology*, 59: 591-595.

El-Shishtawy, R.M., Mohamed, S.A., Asiri, A.M., Gomaa, A.M., Ibrahim, I.H. and Al-Talhi, H.A. (2015). Saccharification and hydrolytic enzyme production of alkali pretreated wheat bran by *Trichoderma virens* under solid state fermentation. *BMC Biotechnology*, 15: 37-50.

Ezekiel, O.O. and Aworh, O.C. (2018). Simultaneous saccharification and cultivation of *Candida utilis* on cassava peel. *Innovative Food Science and Emerging Technology*, doi: https://doi.org/10.1016/j.ifset.2018.02.009.

Heerd, D., Yegin, S., Tari, C. and Fernandez-Lahore, M. (2012). Pectinase enzymecomplex production by *Aspergillus spp*. in solid-state fermentation: a comparative study. *Food and Bioproduct Processing*, 90: 102-110.

Inan, H., Turkay, O. and Akkiris, C. (2016). Microwave and microwave-chemical pretreatment application for agricultural waste. *Desalination and Water Treatment*, 57(6): 2590-2596.

Ju, X., Engelhard, M. and Zhang, X., (2013). An advanced understanding of the specific effects of xylan and surface lignin contents on enzymatic hydrolysis of lignocellulosic biomass. *Bioresource Technology*, 132(3): 137-145.

Khatri, B.P., Bhattarai, T., Shrestha, S. and Maharjan, J. (2015). Alkaline thermostable pectinase enzyme from *Aspergillus niger* strain MCAS2 isolated from Manaslu Conservation Area, Gorkha, Nepal. *SpringerPlus*, 4: 488-496.

Lai, C., Tang, S., Yang, B., Gao, Z., Li, X. and Yong, Q. (2017). Enhanced enzymatic saccharification of corn stover by in-situ modification of lignin with poly (ethylene glycol) ether during low temperature alkali pretreatment. *Bioresource Technology*, 244: 92-99.

Li, P., Xia, J., Shan, Y., Nie, Z. and Wang, F. (2015). Effect of surfactant and microwave-assisted pretreatment on orange peel on extracellular enzymes production by *Aspergillus japonicas* PJ10. *Applied Biochemistry and Biotechnology*, 176: 758-771.

Nomanbhay, S.M., Hussain, R. and Palanisamy, K. (2013). Microwave-assisted alkaline pretreatment and microwave assisted enzymatic saccharification of oil palm empty fruit bunch fiber for enhanced fermentable sugar yield. *Journal of Sustainable and Bioenergy Systems*, 3: 7-17.

Obi, F.O., Ugwuishiwu, B.O. and Nwakaire, J.N. (2016). Agricultural waste concept, generation, utilization and management. *Nigeria Journal of Technology*, 35(4): 957 – 964.

Ptichkina, N.M., Markinaa, O.A. and Rumyantseva, O.A. (2008). Pectin extraction from pumpkin with the aid of microbial enzymes. *Food Hydrocolloloids*, 22: 192–195.

Rahnama, N., Mamat, S., Shah, U.K., Ling, F.H., Abdulrahman, N.A. and Ariff, A.B. (2013). Effect of alkali pretreatment of rice straw on cellulose and xylanase production by local *Trichoderma harzianum* SNRS under solid state fermentation. *Bioresources*, 8(2): 2881-2896.

Salihu, A., Abbas, O., Sallau, A.B. and Alam, Z. (2015). Agricultural residues for cellulolytic enzyme production by *Aspergillus niger*: effect of pretreatment. *3 Biotech*, 5: 1101-1106.

Tapre, A.R. and Jain, R.K. (2014). Pectinases: enzymes for fruit processing industry. *International Food Research Journal*, 21(2): 447-453.

Tiwari, G., Sharma, A. and Sharma, S. 2017. Saccharification of Mango peel wastes by using microwave assisted alkali pretreatment to enhance its potential for bioethanol production. Centre for Rural Development and Technology, Indian Institute of Technology Delhi, Hauz Khas,New Delhi-110016, India.

Wadhwa, M., Bakshi, M.P.S. and Makkar, H.P.S. (2015). Wastes to worth: value added products from fruit and vegetable wastes. *CAB Reviews*, 10: 43-68.

Woldesenbet, F., Virk, A.P., Gupta, N. and Sharma, P. (2012). Effect of microwave irradiation on xylanase production from wheat bran and biobleaching of eucalyptus kraft pulp. *Applied Biochemistry and Biotechnology*, 167: 100–108.

Yang, M., Wang, J., Hou, X., Wu, J., Fan, X., Jiang, F. and Zhang, J. (2017). Exploring surface characterization and electrostatic property of Hybrid Pennisetum during alkaline sulfite pretreatment for enhanced enzymatic hydrolysability. *Bioresource Technology*, 244: 1166-117.

Yu, H., Li, X., Zhang, W., Sun, D., Jiang, J. and Liu, Z., 2015. Hydrophilic pretreatment of furfural residues to improve enzymatic hydrolysis. *Cellulose*, 22(3): 1675-1686

DOI: 10.51975/QRVL2337
Journal of the Nigerian Society of Chemical Engineers, 36(1), 2021

METROLOGY APPLICATIONS IN CHEMICAL ENGINEERING: A BRIEF REVIEW

Momoh, S. O.[1] and Abia-Etoh, E.[2]
[1]National Agency for Science and Engineering Infrastructure (NASENI), The Presidency,
Idu Industrial Area, P. M. B. 391, Garki, Abuja
[2]Weight and Measures Department, Federal Ministry of Industry, Trade and Investment,
Lagos Office.
Corresponding author: stevmomoh@yahoo.com

ABSTRACT

Metrology, while often confused with the science of measuring weather (meteorology), is a very widely used field. Metrology is mainly concerned with (i) establishing the units of measurements, reproducing these units in the form of standards, and ensuring the uniformity of measurements, (ii) developing methods of measurement, analysing the accuracy of methods of measurement, establishing uncertainty of measurement, researching into the causes of measuring errors, and eliminating these. Although as engineers and scientists, we make use of measurement to quantify the physical and chemical properties of objects, and design systems to conform to standards based on unit of measurement, the principles of measurement science (metrology) is not too familiar to most engineers and scientists. The focus of this brief review is to bring to fore the (i) meaning and definitions of metrology, (ii) importance of measurement, and (iii) the importance of metrology applications in chemical engineering and engineering in general.

***Key words**: Metrology, measurement, process control, process development, engineering design.*

1. INTRODUCTION

1.1 Metrology: Meaning and Definitions

The word "**Metrology**" may appear strange to many people. At best, most people assume it to mean the same as "**Meteorology**" or another way of writing "**Meteorology**". The two words are quite different in eamning. Meteorology is the study of the Earth's atmosphere and the variations in temperature and moisture patterns that produce different weather conditions. It is a branch of the atmospheric sciences with a major focus on weather forecasting; whereas Metrology is the study of measurement.

The study of measurement is a basic requirement in any field of science and technology, most importantly in engineering and manufacturing. Since metrology is the study of measurement, it is expected to enforce, validate and verify predefined standards for traceability, accuracy, reliability, and precision. All of these are factors that would affect the validity of measurement.

The word metrology indeed has a long tradition and is derived from the Greek word for measure. It is well-known saying that the knowledge about anything is complete only when it can be expressed in numbers. Thus for every kind of quantity measured, there must be a unit to measure it and express it in numbers of that unit. Furthermore, in order that this unit is followed by all and not just the one who is taking the measurements, there must be a universal standard; and the various units for various parameters of importance must be standardised (*WikiHow, 2019*).

Metrology is basic to the economic and social development of a country. It is concerned with providing accurate measurements which impact our economy, health, safety and general well-being. Trade and currency exchanges are possible because there are units of measurements.

Metrology also includes ways of establishing and maintaining the accuracy of measurement devices, such as by comparing them with more accurate standards.

1.2 Three sub-field of Metrology

Metrology is divided into three basic overlapping activities. The first being the definition of units of measurement, second the realisation of these units of measurement in practice, and last traceability, which is linking measurements made in practice to the reference standards. These overlapping activities are used in varying degrees by the three basic sub-fields of Metrology. The sub-fields are scientific or fundamental metrology, which is concerned with the establishment of

units of measurement, Applied, technical or industrial metrology, the application of measurement to manufacturing and other processes in society, and Legal metrology, which covers the regulation and statutory requirements for measuring instruments and the methods of measurement *(Wikipedia, 2021*).

As a further explanation, Scientific Metrology deals with the organization and development of measurement standards and with their maintenance. As you might expect, scientific metrology is deeply involved with research and new technologies for industries concerning government, healthcare, and research for commercial products.

Industrial metrology's purpose is to ensure that instruments, used in a wide variety of industries, are functioning properly. An example of this type of metrology might be seen in the production of products for the commercial industry, the testing and designing of aircraft, the functioning of large machinery, or even in factories using rotating equipment during the manufacturing of their products.

Legal Metrology is concerned with the measurements that influence economic transactions. This field does not use physical tools as the other fields of metrology use. Instead it focuses on the buying and selling of materials for economic studies and law enforcements.

The focus in this review is on the metrology applications in engineering and with chemical engineering as the main focus. (*Wikipedia, 2021, Jaychris, 2019*)

1.3 Importance of Measurement

Measurement is a quantitative comparison between a known quantity and an unknown quantity. Therefore, a measurement is the process of determining quantity of something (say size or length). Measurement is part of our daily life. It is used in all our movement, in our research work, our industry. How does one know the distance, the time, the height and the width of any geometrical shape? How does one know his size to buy clothes? How does one differentiate between cm, inch, foot, meter, mile and km? How could we deal with studying the universe without measurement? How do chemical engineers compare quality of products and ascertain their safety for use? So, measurement is an important part of human beings' lives and endeavours.

Indeed, without the ability to measure, it would be difficult for scientists to conduct experiments or form theories. Not only is measurement important in science and the chemical industry, it is also essential in engineering, farming, construction, manufacturing, commerce, and numerous other occupations and activities.

It is impossible to describe anything without measuring it. Measurement provides a standard for everyday things and processes. From weight, temperature, length even time is a measurement and it does play a very important role in our lives. The money or currency we use is also a measurement. And think of the rumble that can be caused if it was not there.

Scientists and engineers use many skills as they investigate the world around them. They make observations by gathering information with their senses. Some observations are simple. For example, a simple observation would be figuring out the color or texture of an object. However, if scientists want to know more about a substance, they may need to take measurements. Indeed, measurement is perhaps one of the most fundamental concepts in science. (*The Importance of Measurement*). A standard measurement system is important because it allows scientists and engineers to compare data and communicate with each other about their results. Indeed, one of the activities of engineers is to generate data from the experimental models and using it for betterment of people by generalising the results. Data like properties of materials, stresses, forces, etc must be done with maximum precision possible. As your precision increases you would have better design than previous. Measurement is comparison of available data with set standards or specimen which are agreed upon globally. Therefore, you cannot have data or information without any reference to compare it.

The international today's society relies on a proper measurement infrastructure, which in much extent depends on the properly trained people. There is no doubt that quality of measurements is an important issue in modern society influencing quality of life and border-crossing trade. Most important decisions are based on data obtained from measurement (*Bulska & Taylor, 2003*).

2.0 THE IMPORTANCE OF METROLOGY APPLICATIONS IN CHEMICAL ENGINEERING

The role of metrology in the various phases of a products lifecycle is very important (*ASQ, 2019*). Chemical engineers should have a proper understanding

of metrology concepts, basic statistics, reliability statistics and measurement uncertainty.

A quantitative analysis of design based on sound metrology principles will help engineers and scientists to design better products and services. In order to evaluate multiple solutions to the design, physical measurements are made and the data analyzed. Predictions need to be made on how well the design will perform to its specifications before full scale production begins. Tests are performed using prototype models, computer simulation, designed experiments, destructive and non-destructive tests, scale models and stress tests among the many other methods of evaluation.

In the broader sense, metrology is not limited to length measurement but is also concerned with the industrial inspection and its various techniques. Due to big industrial revolution and great advancement, industrial inspection does not simply mean the fulfilling of the specifications laid down by the manufacturers. Rather inspection in real sense is concerned with the checking of a product at various stages in its manufacture right from the raw material form to the finished products and even assembled parts in the form of machine also *(WikiHow, 2019).*

Let us discuss in brief how metrology plays a role in some critical areas of chemical engineering operations.

2.1 In Manufacturing and Chemical Analysis

Anything that has to do with manufacturing is the main domain of a chemical engineer. Chemical engineers design chemical plant equipment and devices and troubleshoot processes for manufacturing chemicals and products, such as gasoline, synthetic rubber, plastics, detergents, cement, paper, pulp just to name a few by applying principles and technology of chemistry, physics, and engineering. They are most often employed by large-scale manufacturing plants to maximize productivity and product quality while minimizing costs. Chemical engineers therefore must design systems that led themselves to ease and accurate measurements at all times. In design you must have idea of measurement.

Chemical engineering has its offshoot in science and particularly in chemistry which involves the use of various precision measuring machines. Chemical engineers use chemistry and engineering to turn raw materials into usable products on a large-scale, industrial setting.. In all of these processes, both physical and chemical measurement are critical to compare data obtained with international standards in helping to determining safety and quality of products to human life. Therefore, they work with a lot of experimental method and instrumentation to analyse processes and products quality.

2.2 In Process Control

Process control, for example, is all about controlling a chemical process or running machinery. Process Control can be manual or automatic, continuous or discrete. It is all about monitoring and controlling certain set of process variables (i.e. temperature, flow, level, pressure, etc) that leads to control of the whole process. If we can't measure then we can never control. Almost all control method works on the basis of the error of the process variable. For example in PID (proportional–integral–derivative controller**)** control, *Error=set point - measured value*. We can't get error without measuring process variables. We called it feedback. So measurement is most important parameter for controlling of any process. For in controlling any process it is necessary to know the current amount or the quantity of the controlled variable. Thus, we need to sense that variable (Pressure, temperature, flow, level, etc). For this purpose measuring instruments are necessary in process control. The measuring instrument measures, converts it to Electrical signals and gives it to controller for taking proper action of the final control element to control the process the way we want. And unless we measure the value to a precision needed in our control system, we cannot change the output of the system manually or in automatic, as required to keep the process in the required state. *(James E. Potzick, 2010).* Similarly, the conformance of parts and assemblies to geometrical specifications is assessed by physical measurements (*NRC, 1995*).

2.3 In Product Development

Chemical engineers do not really use much of chemical laboratory equipment in the industry. It should be stressed that, even in the university, chemical engineering laboratory equipment often consists of pilot scale systems where potential chemical engineers learn about unit operations and chemical process steps such as distillation, separation, crystallization, evaporation, filtration, polymerization, mixing, homogenization, cooling, heating, polymerization and chemical reactions. Practicing chemical engineers generally work with larger scale equipment in a pilot facility or in a production plant where they can evaluate how equipment and system changes impact physical and chemical transformations. Chemical engineers receive

training and develop understanding of fluid flow, heat transfer, mass transfer, thermodynamics, chemistry, physics, advanced mathematics and control theory, which they use to optimize and design chemical processes. (*Gary Kardys, 2017*)

Although chemical engineers evaluate processes on pilot scale equipment, bench top chemical laboratories are necessary when chemical engineers are involved in product development and in research activities. Every stage of a chemical process involves checking on safety, product quality, level of effluents emission in solid, liquid and gaseous form, etc. To ensure compliance, there are needs for measurements, either analytically and otherwise; and may involve developing methods of measurement and analysing the accuracy of the methods of measurement. The need for compliance to standards in process and product manufacturing industries, places upon a chemical engineer a burden to design unit operations and processes that strictly adhere to standards.

For an example, for product formulation, characterization and quality testing, the chemical engineers use analytical testing machines. Analytical testing, which is also referred to as materials testing, is a broad term used to describe various techniques that are used to identify the chemical makeup or characteristics of a particular sample. Chemical analysis equipment is used to determine, characterize, and quantify chemical components in gas, liquid, and solid samples. Bioanalysis, nanotechnology, clinical chemistry, environmental and materials analysis, and forensics represent a few of the many areas of use for chemical analysis instruments.

Examples of such analytical instruments include mass spectrometers, chromatographs (e.g. GC and HPLC), titrators, spectrometers (e.g. AAS, X-ray, and fluorescence), particle size analyzers, rheometers, Refractometers, viscometers, evaporators and calorimeters, elemental analyzers (e.g. salt analyzers, CHN analyzers), thermal analyzers, and more. In the chemical laboratory, you will have also basic measuring equipment like graduated cylinders, volumetric flasks, Pipettes, Burets, Thermometers, balances, and many more.

2.4 Equipment categories of interest to chemical engineers

Gary (2017) provides a list of equipment categories and their descriptions (shown in Appendix 1) that are of interest to chemical engineers. These serve as process components and equipment required for process engineering projects, and sometimes helps to determine quality of products. The list included the following: Equipment for

- Instrumentation and equipment used to control the properties and degree of purity of air;
- Remediation of environmental factors equipment;
- Processing equipment such as centrifuges, clarifiers, and several filter technologies used to filter or separate media of different materials or sizes;
- Flow measurement instruments used to determine flow rate;
- Materials Processing Equipment.

Alpha (2016) gave description of some of the Chemical Testing Equipment. These include:

- **Abrasion Testers** - widely used for testing abrasion resistance of plastic materials
- **Adhesion Tester** - to determine the flexibility and adhesion of coatings to painted metallic surface.
- **Automatic Pigment Muller** - widely used for accurate and fast evaluation of color strength, color matching, dispersion, particle hardness and particle size, color comparison, tint and tone of paints.
- **Corrosion Cabinet** - to determine their resistance to environmental elements
- **Density Measuring Equipment** – for determining the mass per unit volume of a substance
- **Dew Point Apparatus** - is commonly used for determining vapor content of gaseous fuels by measuring their dew point temperature.
- **Existent Gum Steam Generator** - used for measuring evaporation residue in aviation fuels, motor gasolines and other volatile distillates on the basis of standard test procedures
- **Flash Point Apparatus** - apparatus is a petroleum testing equipment for determining the flash point of fuels, lube oils, solvents and other liquids
- **Flexural Strength Tester** - to determine the flexure or bending properties of plastic materials.
- **Freezing Point Apparatus** - used to determine the temperature below which solid hydrocarbon crystals are formed in case of **aviation fuels**.
- **Impact Testing Equipment** - used in the plastic industry evaluates the effect of varying degrees of impact on plastic materials and components.
- **Liquid Bath** - **Liquid Bath** is an instrument commonly used in petroleum industry to determine the tendency of aviation fuels and gasoline to form

gum in storage conditions. It is also used to measure the oxidation stability of fuels.

- **Mandrel Bend Testers** - This equipment is used to determine elasticity, elongation and adhesion properties of paint on sheet metal.
- **Melting Point Tester** - **Melting point** is defined as the temperature at which a substance changes into liquid state from solid state.
- **Oxygen Index Apparatus** - **Oxygen index apparatus** is used to determine the oxygen index of plastic materials.

A chemical engineer may not be involved directly in the design and manufacture of these measuring equipment, but must be conversant with their use in analyzing his results; and should be able to detect when the system malfunction giving wrong results.

Because of the growing importance of metrology in chemical engineering, some Chemical Engineering departments of Universities have research units dealing with issues of design of measuring equipment. For example, the Department of Chemical Engineering and Biotechnology of the University of Cambridge (*University of Cambridge, 2019*) has a metrology research group whose research focus is addressing challenges of measurement and quantitative analysis of chemical and biochemical systems. In their website, it stays "Challenges in healthcare require new solutions in imaging and measurement and our skills are also central to investigations into structure-function relationships for catalysis and reaction engineering, and build on core understanding of chemical reactions and physical phenomena in designing sustainable new processes. The Department is home to the Measurement and Image Analysis Centre, the Laser Analytics Group and Cambridge Analytical Biotechnology and also the Magnetic Resonance Research Centre (MRRC). It leads 'Cam-bridge-Sens', the University strategic Network that brings together sensing activities across the University and it is active in promoting a sustainable healthcare model where the primary point of care will move towards the home, powered by technology for remote diagnosis and monitoring." Some of their current research include: Development of novel data acquisition techniques, Microstructural and composition data derived from MRI, Terahetz, X-ray and atomic force microscopy, Electrochemical, optical and acoustic sensors and biosensors, Development of high resolution microscopy techniques, Diagnosis through biomarker discovery, Analytical recognition ligand design and synthesis, Smart material design, etc.

2.5 Use of metrology in Nanotechnology.

The growing interest in applying nanomaterials to societal needs is now urging that increasing attention be given to the development of scientific and applied metrology to address nanomaterials as the newly developing field of nanometrology. This multidisciplinary field spans many disciplinary fields, such as chemistry, physics, materials science, biology, and engineering, chemical engineering in particular. Nanomaterials embrace the full range of traditional materials classes. The distinction between metrology in general and metrology on the nanoscale stems from the different properties of materials on the nanoscale as compared to their bulk counterparts. Of course, new ideas need new measurements and this is where the novel class of materials, the nanomaterials, is playing an important role. (*Jorio & Dresselhaus, 2010*)

3.0 MEASUREMENT IN ENGINEERING DESIGN

As stated above, *measurement* is a quantitative comparison between a known quantity and an unknown quantity. *Measurement* helps an engineer and indeed a chemical engineer to quantify the physical and chemical properties of objects and systems. In *engineering*, it can help you with manufacture of various parts thereby ensuring proper fit between components. An engineering designer must be conversant with measurement principles.

In Reverse Engineering, which is the ability to replicate the machine designs, construct, testing and publication of a manufacturing layout thereby developing requisite skills and technology in its manufacture and mass production, requires accurate measurement of components parts that are taken apart for study and replication. Chemical engineers also used the concept of Reverse Engineering to design and manufacture equipment components/parts from the existing one. Because in a manufacturing plant there will be need to replace a particular unit/parts of an equipment that may no longer be supported by the Original Equipment Manufacturer (OEM) due to its obsolesce. There will then the need for Reverse Engineering of such components. Measurement equipment like the following are very useful in giving accurate measurement of the parts. . (*Sanja , 2013*).

i. **Coordinate Measuring Machines, CMM** - A coordinate measuring machine (CMM) is a device used in the measurement of the physical geometrical characteristics of an object. These machines can be manually controlled by an operator

or they may be computer controlled. Measurements are defined by a probe attached to the third moving axis of this machine.

ii. **Contour graph**. A contour plot is a graphical technique for representing a 3-dimensional surface by plotting constant z slices, called **contours**, on a 2-dimensional format. That is, given a value for z, lines are drawn for connecting the (x,y) coordinates where that z value occurs.

iii. **Surface texture examination machine**. Surface finish, also known as surface texture or surface topography for examining the roughness of a surface.

iv. **VMM (Vision System)** – Vision Measuring Machine, VMM are non-contact type of measuring machines which use Optics as source of inspection.

4. CONCLUSION

Measurements have been carried out for as long as civilization has existed. Metrology is basic to the economic and social development of a country. It is concerned with providing accurate measurements which impact our economy, health, safety and general well-being. Without accurate measurement, important decisions may be faulty.

Even though we have been applying the concept in our day to day practice as engineers, some of us still lack the

basic understanding of the concept of Metrology and its role in engineering. This brief review is able to bridge this gap by reviewing what metrology is all about and its uses in chemical engineering in particular and engineering in general.

Indeed, without the ability to measure, it would be difficult for scientists to conduct experiments or form theories. Not only is measurement important in science and the chemical industry, it is also essential in farming, engineering, construction, manufacturing, commerce, and numerous other occupations and activities. Indeed in all human endeavour.

REFERENCES

Alpha Chemika laboratory (2016). *Chemical Testing Equipment*. Retrieved July 13, 2019 from https://www.alphalabchem.com/chemical-testing-equipment/.

ASQ (2019). *Metrology Applications for Engineers and Scientists.* Retrieved July 13, 2019 from https://asq.org/training/metrology-applications-for-engineers-and-scientists-metappwpt.

Bulska E., Taylor P. (2003)., Anal. and Bioanal. Chem., in print.

Gary Kardys (2017).*What Chemical Lab Equipment is Most Popular Among Engineers?* Retrieved July 13, 2019 from https://insights.globalspec.com/article/5219/what-chemical-lab-equipment-is-most-popular-among-engineers.

James E. Potzick (2010). *Metrology and process control: dealing with measurement uncertainty.* Retrieved July 13, 2019 from https://www.google.com/search?client=firefox-b-d&channel=crow&q=process+control+and+metrology.

Jaychris (2019). *What is Metrology? What Does Metrology Mean?*. Retrieved July 13, 2019 from https://www.brighthubengineering.com/manufacturing-technology/63936-what-is-metrology/.

Jorio,A. and Dresselhaus, M.S (2010) in *Encyclopedia of Materials: Science and Technology*, 2010. *Nanostructured Materials: Metrology*. Retrieved July 13, 2019 from https://www.sciencedirect.com/topics/chemistry/metrology.

NRC (1995). *Unit Manufacturing Processes: Issues and Opportunities in Research*. A publication of National Research Council by National Academic Press. Retrieved July 13, 2019 from https://www.nap.edu/read/4827/chapter/18#158

Sanjay Kumar (2013). *What is metrology in engineering?* Retrieved July 13, 2019 from https://www.quora.com/What-is-metrology-in-engineering.

The Importance of Measurement. Retrieved July 13, 2019 from https://msdlt.instructure.com/courses/108/files/2589/download?verifier...wrap=1.

University of Cambridge (2019). *Department of Chemical Engineering and Biotechnology*. Retrieved July 13, 2019 from https://www.ceb.cam.ac.uk/research/strategy/metrology.

WikiHow (2019). *What Is Metrology.* Retrieved July 13, 2019 from https://what-when-how.com/metrology/what-is-metrology.

Wikipedia (2021). *Metrology.* Retrieved March 25, 2021 from https://en.wikipedia.org/wiki/Metrology.

APPENDIX 1: LIST OF EQUIPMENT CATEGORIES (SHOWN IN APPENDIX 1) OF INTEREST TO CHEMICAL ENGINEERS AND THEIR DESCRIPTIONS (Gary, (2017))

Chemical Process Equipment Category	Description
Air Quality (3,093 suppliers)	Instrumentation and equipment used to control the properties and degree of purity of air. These types of equipment include dust collectors, oxidizers, scrubbers and adsorption equipment.
Environmental Equipment (5,544 suppliers)	Equipment involved in the remediation of environmental factors. Specific aspects covered include water and wastewater treatment, air and groundwater quality analysis, waste processing, and pollution control.
Filtration and Separation Products (5,092 suppliers)	Processing equipment such as centrifuges, clarifiers, and several filter technologies used to filter or separate media of different materials or sizes.
Flow Sensing (2,642 suppliers)	Flow measurement instruments are used to determine flow rate by monitoring the amount of media passing during a specific time. Devices within this category can monitor liquids, gases or solids, and measure in units of mass, velocity or volume.
Fluid Processing Equipment (3,351 suppliers)	Any piece of equipment used to monitor, distribute and store process and industrial fluids.
Gas Handling Equipment (1,008 suppliers)	Any piece of equipment used to monitor, distribute, generate, compress and store process and industrial gases.
Heating and Cooling Equipment (13,466 suppliers)	Ovens, furnaces, induction heaters, welding equipment, heat exchangers, fans, blowers, refrigerators, baths and other equipment for heating or cooling materials.
Hose, Pipe and Tubing (4,820 suppliers)	Hose, pipe and tubing covers the broad spectrum of fluid transfer lines.
Hose, Pipe, and Tubing Accessories (4,518 suppliers)	Hose, pipe, and tubing accessories make up the infrastructure necessary to convey all manner of materials in a process line.
Industrial Heaters and Heating Elements (2,520 suppliers)	Electrical resistance heaters or their internal elements; designed to provide an integrated thermal source for products or systems.
Industrial Machine Safeguarding (1,510 suppliers)	Components or systems that protect industrial machinery, operators or moving parts from injury or damage from electrical, mechanical or other potential hazards.
Materials Processing Equipment (3,617 suppliers)	Extruding, casting, forging, compacting, heat treating, molding, rolling or other processing machines and components used for metals, polymers or other materials.
Pressure Regulators (1,249 suppliers)	Pressure regulators are used to maintain a constant outlet pressure or flow.
Process Controllers (4,849 suppliers)	Instruments for monitoring and automatically revising process parameters such as temperature, pressure, force, humidity, level and flow.
Pumps (5,243 suppliers)	Machines and devices used for the raising, compression or transference of a variety of materials.
Safety and Personal Protective Equipment (3,655 suppliers)	Safety equipment guards personnel or areas from hazardous conditions or mitigates damage. Personal protective equipment protects individuals from personal injury.
Safety Sensors and Switches (733 suppliers)	Safety sensors and switches are used in machines and other industrial applications to safeguard equipment and prevent personal injury.
Tanks and Vessels (2,241	Equipment used to contain or store materials prior to, during, and after their processing.

Chemical Process Equipment Category	Description
suppliers)	
Vacuum Equipment (2,530 suppliers)	Vacuum equipment is used for degassing, welding, and the manufacturing of thin films, semiconductors, optics and specialty materials.
Valve Actuators and Positioners (946 suppliers)	Devices designed to automatically control and monitor the position of valves, in relation to their open or closed positions.
Valves (6,133 suppliers)	Devices that regulate the flow of gases, liquids, or loose materials through piping by opening, closing, or obstructing ports or passageways.
Viscosity Sensing (210 suppliers)	Instruments and sensors for measuring the viscosity (resistance to flow) or viscoelastic properties of liquid or molten glass and plastic.
Web Handling and Processing Equipment (1,157 suppliers)	Equipment for handling, processing and converting continuous webs of textiles, paper, plastic films, metal sheet or other materials.

DOI: 10.51975/WMOV5566
Journal of the Nigerian Society of Chemical Engineers, 36(1), 2021

AN OVERVIEW OF HYDROGEN FUEL FROM BIOMASS GASIFICATION - COST EFFECTIVE ENERGY FOR DEVELOPING ECONOMY

Osuolale, F. N.[1], Babatunde, K. A.[1], *Agbede, O. O.[1], Olawuni, A. F.[1], Fatukasi, A. J.[1], Adewunmi, A. E.[1], Oladipo, C. J.[1] and Osuolale, O. M.[2]

[1]Department of Chemical Engineering, Ladoke Akintola University of Technology, Ogbomoso, Oyo State, Nigeria
[2]Department of Civil Engineering, Ladoke Akintola University of Technology, Ogbomoso, Oyo State, Nigeria
*Correspondence: ooagbede@lautech.edu.ng; Tel.: +234-806-550-2864

ABSTRACT

Hydrogen has the potential to be a clean and sustainable alternative to fossil fuel especially if it is produced from renewable sources such as biomass. Gasification is the thermochemical conversion of biomass to a mixture of gases including hydrogen. The percentage yield of each constituent of the mixture is a function of some factors. This article highlights various parameters such as operating conditions; gasifier type; biomass type and composition; and gasification agents that influence the yield of hydrogen in the product gas. Economic evaluation of hydrogen from different sources was also presented. The hydrogen production from gasification process appears to be the most economic process amongst other hydrogen production processes considered. The process has the potential to be developed as an alternative to the conventional hydrogen production process.

1.0 INTRODUCTION

Biomass is the largest renewable energy and it has a major share of about 90% of the total energy supply in the remote and rural areas of developing world (Demirbas, 2001). While burning of fossil fuel converts carbon that has been confined underground (as crude oil, coal and gas) to carbon dioxide (CO_2) thereby increasing CO_2 in circulation and hence the greenhouse gas (GNG) effects, the combustion of biomass recycles the CO_2 captured during photosynthesis and thus maintains the CO_2 balance in the atmosphere (Ahmad *et al*., 2016). Biomass can therefore be said to possess a zero CO_2 net emission (Mohammed *et al.*, 2011).

Most often, biomass is from agricultural by products but sometimes, it could be directly cultivated (McKendry, 2002a). The routes to convert biomass into useful products will depend on the form of the biomass. For agricultural residues, forest residues and wood, thermo-chemical conversion routes are the widely-used methods to extract energy from biomass. Thermochemical processes can be categorized into combustion, pyrolysis and gasification where the syngas and bio-oil produced as intermediate products can be subsequently converted to valuable fuels and chemicals. Combustion is the direct burning of biomass in air to convert the chemical energy in biomass to heat, electricity or mechanical power. The energy efficiency of this process is between 10-30% (Ni *et al*., 2006). Pyrolysis is the burning of biomass in the absence of air. Slow pyrolysis gives high yield of charcoals whereas rapid heating of biomass at high temperature (fast pyrolysis) gives products in the liquid, gaseous and solid states (Cao *et al*., 2020; Yang *et al*., 2018). Gasification is the conversion of biomass into a combustible gas mixture (syngas) by heating in a gasification medium such as air, oxygen or steam. Gasification of biomass leads to the production of syngas of which carbon monoxide, methane, and hydrogen are some of the constituents (Brachi *et al*., 2018; Qiu *et al*., 2018).

Of all the three thermochemical routes, gasification is being considered in this research work as a promising technology to treat biomass. This is because it produces minimal emissions, can be easily adapted to treat different materials and the process conditions can be altered selectively to isolate different gaseous products (Sikarwar *et al*., 2017; Molino *et al.*, 2018). Furthermore, gasification is likely to be commercially viable based on the consideration of overall conversion efficiency and proven operational history and

performance (Barbuzza *et al*., 2019; Catalan-Martinez *et al*., 2018; Qiu *et al*., 2018).

Hydrogen - one of the constituents of syngas has been dubbed the energy carrier of the future and has gained reputation as a potential substitute to fossil fuels. This is because hydrogen, when combusted or used in a fuel cell, does not emit greenhouse gas (GHG), it has a high energy content on a mass basis when compared to gasoline or natural gas and it can be easily and efficiently converted to electricity using fuel cells. Hydrogen, as a high efficiency low polluting fuel, can be used for transportation, heating and power generation (Orhan *et al.*, 2011). Hydrogen is also a raw material for chemical, petroleum and agro-based industries (Lewis *et al.*, 2009 and Naterer *et al.*, 2010).

Converting biomass to aqueous and gaseous fuel most especially hydrogen could be a more efficient way of utilizing biomass. This is good for developed nations because the problem of GHG emissions will be dealt with and for developing nations with power generation problems by providing access to electricity and power supply from relatively available sources.

This study is focused on highlighting the potential of hydrogen generated from biomass gasification to be effective solution to the menace of inadequate power supply in rural areas. It could also serve as source of energy generation for both small and medium scale industries. This is much more apt for a developing nation like Nigeria which has an agrarian based economy. The vast amount of biomass as agricultural byproducts and abundant virgin land that could be put to use for more cultivation of biomass is a great motivation for this study.

2.0 HYDROGEN PRODUCTION

Although abundant on earth as an element, hydrogen is almost always found as part of another compound, such as water (H_2O) and some other compounds, and must be separated from the compounds that contain it. Once separated, hydrogen can be used in diverse ways. In addition, hydrogen can be produced using diverse resources. The environmental impact and energy efficiency of hydrogen depends on how it is produced. Figure 1 depicts some sources through which hydrogen can be generated.

2.1 Production from Natural Gas: Hydrogen can be produced from natural gas through three different chemical processes. Steam reforming involves the endothermic conversion of methane and water vapour into hydrogen and carbon monoxide as given in equation 1. The product gas CO can be further converted to CO_2 and H_2 through the water-gas shift reaction as given in equation 2 (Holladay *et al.,* 2009).

$$CH_4 + H_2O + heat \rightarrow CO + 3H_2 \quad (1)$$

$$CO + H_2O \rightarrow CO_2 + H_2 + heat \quad (2)$$

Partial oxidation involves the production of hydrogen through the partial combustion of methane with oxygen rich gas to yield carbon monoxide and hydrogen according to equation 3 (Ahmed *et al*., 2017). The CO can be further converted through the water-gas shift reaction of equation 2 (Cormos *et al*., 2018).

$$CH_4 + \frac{1}{2}O_2 \rightarrow CO + 2H_2 \quad (3)$$

Autothermal reforming is a combination of both steam reforming and partial oxidation. This method of producing hydrogen has developed technology and has been commercialized. However, the hydrogen generated from this source can only be sustainable if it is from renewable source such as biogas or syngas (Dincer and Acar, 2015).

2.2 Electrolysis: An electric current splits water into hydrogen and oxygen. If the electricity is from renewable sources, such as solar or wind, the resulting hydrogen will be considered renewable as well, and have numerous environmental benefits. Electrolysis is considered as the easiest method of hydrogen production since it yields high level hydrogen purity and requires simple equipment (Badwal *et al*., 2013). It however has low efficiency (Nikolic *et al.,* 2010) and contributes only about 4% of overall hydrogen production (Chakik and Mikou, 2017; Santos *et al.,* 2013).

$$H_2O + electricity \rightarrow H_2 + \frac{1}{2}O_2 \quad (4)$$

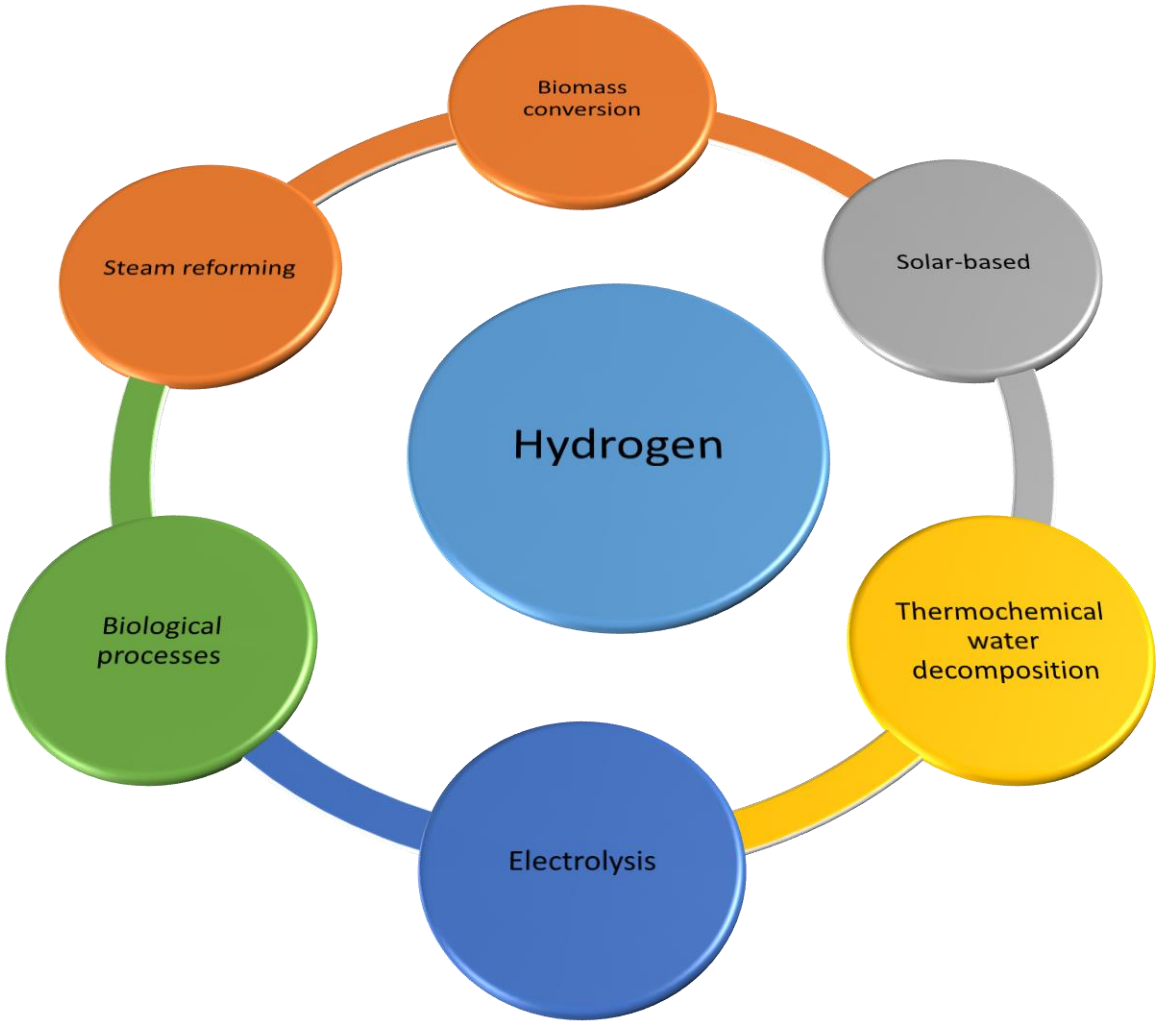

Figure 1: Some hydrogen production processes

2.3 Solar-based Hydrogen Production: Solar energy is readily available at no cost to produce hydrogen; therefore, it may lead to a future clean alternative fuel (hydrogen) for transportation. Direct solar water decomposition, or photolytic, processes use light energy to split water into hydrogen and oxygen (Contreras *et al.*, 1999; Do Sacramento *et al.*, 2008). These processes are currently in the very early stages of research but offer long-term potential for sustainable hydrogen production with low environmental impact such as the threatening global warming effects (Liu *et al.*, 2020).

2.4 Biological Processes: Microbes such as bacteria and microalgae can produce hydrogen through biological reactions, using sunlight or organic matter. These technology pathways are at an early stage of research, but in the long term have the potential for sustainable low-carbon hydrogen production. Biological hydrogen can be produced in an algae bioreactor (Hemschemier *et al.*, 2009).

2.5 Thermochemical Water Decomposition for Hydrogen Production: This is an emerging and promising technology for large-scale production of

hydrogen and it is commonly called thermochemical cycles. This is done using intermediate compounds and sequence of chemical reactions to split water into hydrogen and oxygen without polluting the atmosphere (Naterer *et al*., 2009). Many thermochemical cycles have been identified but only a few have been proven to be feasible (McQuillan, 2002).

2.6 Gasification: This conversion route is the focus of this study. It is discussed extensively in the next section.

3.0 BIOMASS GASIFICATION

Gasification is the conversion of biomass into a gaseous product that mainly consist of hydrogen (H_2), and carbon monoxide (CO) with lower amounts of methane (CH_4), carbon dioxide (CO_2), water (H_2O), nitrogen (N_2) and higher hydrocarbons (C+) in the presence of gasifying agents. The gasifying agents could be air, oxygen or steam or a mixture of these components. Gasification is carried out at temperatures between 500 and 1400 ^oC and at atmospheric pressure of 101.325 kPa up to an elevated pressure of 3300 kPa (Ciferno and Marano, 2002). The reactions taking place in the gasifier are summarized in equations 5-7 (Mckendry, 2002b).

$C + \frac{1}{2}O_2 \rightleftharpoons CO$ (partial oxidation) (5)

$C + O_2 \rightleftharpoons CO_2$ (complete oxidation) (6)

$C + H_2O \rightleftharpoons CO + H_2$ (water gas reaction) (7)

The hydrogen and steam can undergo further reaction during gasification as given in equations 8 and 9:

$CO + H_2O \rightleftharpoons CO_2 + H_2$ (water gas shift reaction) (8)

$CO + 3H_2 \rightleftharpoons CH_4 + H_2O$ (methane formation) (9)

The arrows indicate that the reactions are in equilibrium and can proceed in either direction depending on the conditions of reaction (temperature, pressure and concentration)

Main products of gasification are synthesis gas (syngas), char and tars. The content depends on the feedstock, oxidizing agent and the conditions of the process. The gas mainly consists of CO, CO_2, H_2, CH_4 and other hydrocarbons. The gasification process can be summarized as given in equation 10:

$$\gamma C_a H_b O_c + \varphi H_2O \xrightarrow{heat} d\,H_2 + eCO + fCO_2 + gCH_4 + tar \quad (10)$$

where $\gamma C_a H_b O_c$ is the general chemical representation of the biomass.

The syngas produced consists of a mixture of CO_2 (8-10%), H_2 (18-20%), CO (18-20%), CH_4 (2-3%) and traces of other light hydrocarbon and steam (Simonyan and Fasina, 2013). This can be burnt directly or used as a fuel for gas engines and gas turbines in generating electricity (Ben-Iwo *et al*., 2016).

A few parameters have effects on the quality and quantity of the syngas production during gasification. These are discussed as follows.

3.1 Effects of Temperature

Temperature appears to have the greatest influence on the performance of the gasifiers. The composition of the volatiles produced from a gasifier depends on the degree of the equilibrium attained by various gasification reactions. All the gasification reactions are normally reversible and the equilibrium point of any of the reaction can be shifted by changing the temperature. Hydrogen production reactions (water gas shift reaction) is endothermic, a higher gasification temperature will favor the production of hydrogen (Nanda *et al.*, 2016a).

A study of steam gasification of almond shells in a continuous fluidized bed reactor reported the yield of hydrogen as above 50% of the syngas composition (Rapagna and Latif, 1997). The temperature was increased from 600 to 800 ^oC. Similarly, Lv *et al.* (2004) reported an increase in hydrogen production from 21-39 vol.% when the gasification temperature was varied from 700 to 900 ^oC. Sawdust and fluidized bed reactor were the feedstock and type of gasifier, respectively. For all cases considered, the higher temperature favoured higher concentrations of syngas and hydrogen yield but lower concentration of char and heavy tar. The increase in hydrogen yield at higher temperature was due to tar thermal cracking reaction which also decreases the tar concentration (Skoulou *et al.*, 2009). The gasification temperature needed to be selected carefully as a tradeoff between the char conversion and the H_2 output. However, other research shows that high H_2 yield can be obtained at low temperature (600^oC) by using 90% steam content (Gao *et al*., 2008). Table 1 gives indication of the influence of temperature on hydrogen yield for selected biomass.

Table 1: Hydrogen production of biomass at different gasification temperature (Source: Nanda *et al.*, 2016a; Safari *et al.*, 2018; Lu *et al.*, 2008; Nanda *et al.*, 2016b)

Biomass	Temperature (^oC)	Hydrogen yield (mol/kg)
Orange peel	400	0.08
Orange peel	500	0.58
Orange peel	600	0.91

Biomass	Temperature (^oC)	Hydrogen yield (mol/kg)
Pine wood	300	0.22
Pine wood	400	0.69
Pine wood	500	1.14
Almond shell	380	3.95
Almond shell	400	4.55
Almond shell	420	5.43
Almond shell	440	6.45
Almond shell	460	7.85
Corn cob	550	2.55
Corn cob	600	5.31
Corn cob	650	9.08

3.2 Effects of Biomass Feed Stock

Table 2 shows the hydrogen production from gasification of different biomass subjected to the same conditions. The type of feed stock can be seen to affect the yield of hydrogen at the same process conditions. Sugarcane bagasse from table 2 yielded 1.66 mol/kg hydrogen, while coconut shell yielded 2.17 mol/kg hydrogen at the same process conditions. The general chemical representation of biomass as given in equation 10 indicates that the chemical composition of varying biomass is not the same. Ultimate analysis is often used for the chemical analysis of biomass feedstock. The chemical analysis usually lists the carbon, hydrogen and oxygen of the dry biomass sample on a weight percentage basis. The composition of hydrogen in the biomass feedstock may influence the yield of hydrogen in the gasified biomass.

Method of gasification also influences the yield of hydrogen. In the table, hydrogen yield with supercritical water gasification of biomass is much lower than steam gasification of the same biomass. For example, the yield of hydrogen for cotton stalk was 4.19 mol/kg with supercritical water gasification while steam gasification of the same biomass yielded 8.26 mol/kg of hydrogen, about 97% increment. The same goes for corn stalk with about 111% increment in hydrogen yield for steam gasification process.

Table 2: Hydrogen production from different biomass subjected to the same conditions. (Source: Nanda *et al.*, 2016a; Yanik *et al.*, 2007, Wei *et al.*, 2014; Pala *et al.*, 2017)

Biomass	Hydrogen (mol/kg)	Conditions
Sugarcane bagasse[#]	1.66	400^{o}C
Coconut shell[#]	2.17	400^{o}C
Cotton stalk[#]	4.19	500^{o}C
Corn stalk[#]	4.15	500^{o}C
Cotton stalk*	8.26	650^{o}C
Sawdust*	9.02	650^{o}C
Corn stalk *	8.79	650^{o}C
Wood residue	27.86	900^{o}C
Coffee bean husk	34.32	900^{o}C

[#]supercritical water gasification

*Steam gasification

3.3 Effects of Equivalence Ratio

The ratio between the theoretical and practical air demand in steam gasification process utilizing air or O_2 is termed the equivalence ratio (ER). For each kind of biomass, there is a theoretical O_2 demand needed to achieve the combustion based on its contents of combustible materials and since in most cases, gasification is based on realizing relatively partial combustion, a fraction of this ratio is only used. A ratio of 0.15-0.35 has been investigated (Mohammed, 2010). The tar and char yields were discovered to decrease as the ER increased. This is because more oxygen in the gasifier caused the oxidation of the char and tar, and invariably led to the production of more CO and CO_2, and less H_2. Optimum value of the ER for a particular gasification process should be noted. Beyond this optimum, carbon conversion efficiency and gasification efficiency will start to decrease (Gao *et al.*, 2012; Zhao *et al.*, 2010; Xiao *et al.*, 2007).

3.4 Effects of Steam/Biomass (S/B) Ratio

The steam biomass ratio could be varied either by changing the biomass feed rate while keeping the steam flow constant or vice versa. Result from previous researches show an increase in hydrogen production as the ratio increases. However, when S/B ratio is further increased beyond a certain point, hydrogen production declined. The critical S/Bs are generally between 0.70 and 3.41 depending on the conditions (Zhang *et al.*, 2016b). Previous researches by Mahishi and Goswami, (2007); Kalinci *et al.* (2009); Inayat *et al.* (2010) and Moneti *et al.* (2016) obtained optimum yield of hydrogen at steam/biomass ratios of 3, 0.6-10, 2, and 2-3, respectively. Increasing the S/B ratio decreases slightly the CO and favours the water gas shift reaction that results in more hydrogen production. Operating the gasifier at a very high S/B might not be energy efficient since the increase in the production of hydrogen at this

state may not justify the cost of increasing the steam (Pallozzi *et al.*, 2016).

3.5 Effects of Gasifier

Gasifiers are classified mainly on the basis of their gas solid contacting mode and gasifying medium. Based on the gas solid contacting mode, gasifiers are broadly divided into three principal types:

(i) fixed or moving bed gasifier
(ii) fluidized bed gasifier
(iii) entrained-flow bed gasifier

Each type of gasifier has different ranges of appropriate reaction condition and feedstock. There is an appropriate range of application for each. The moving-bed (updraft and downdraft) type often used for smaller units (10 MW) contains a large amount of tars in its product gas due to flow of biomass and the produced gas (Luo *et al.*, 2009; Li *et al.*, 2009). The fluidized-bed (bubbling and circulating) type is more appropriate for intermediate units (100 MW). Feed stock with high ash content can cause stickiness in the fluidized agent and reduce the fluidity of the inert bed material (Siedleck, 2011). The entrained-flow reactors are used for large capacity units (500 MW). The operating temperatures and pressure of the entrained flow reactor are higher than that of the fluidized bed and the fixed bed (Ghassemi *et al.*, 2016). Several studies have compared the advantages and various gasifiers applying different criteria such as use of material, energy efficiency, technology and environmental impacts. The general consensus is that there was no significant advantage of one reactor type over the other. However, for decentralized power generation and distribution to remote and rural areas as well as for small scale industries fixed bed gasifier such as downdraft gasifier which are typically small scale unit with power generation capacity of up to 10 MW could be used (Li *et al.*, 2009).

3.6 Effects of Catalyst and Biomass Composition

Reactions catalysts have positive effects on the yield of hydrogen. Previous works indicated increase in the yield of hydrogen when a catalyst was added to the reaction (Nanda *et al.*, 2016b; Gong *et al.*, 2014). The catalysts are known for cracking tars to produce gaseous products.

Biomass are essentially made of three major polymers; the lignin, cellulose and hemicellulose. Experiments have shown that compared with lignin, cellulose and hemicellulose produced gases more rapidly with higher CO and CH_4 but lower H_2 and CO_2 concentrations, and higher temperature is needed for optimum hydrogen production. Lignin produced more hydrogen than cellulose and hemicellulose cell (Tian *et al*., 2017).

4. 0 IMPLICATIONS OF HYDROGEN FUEL

Hydrogen as an energy carrier can be converted into useful forms of energy. For combustion in internal combustion (IC) engines, jet engines and rocket engines; hydrogen powered combustion engines are about 20% more efficient than gasoline engines (Barbir, 2013; Spath and Dayton, 2003). This is because the thermal efficiency of internal combustion engine can be improved by either increasing the compression ratio or the specific ratio both of which are higher in hydrogen engines (Das, 2016).

Hydrogen combusted with pure oxygen can generate steam with a temperature in the flame zone of above 3000 ^{o}C (Spath and Dayton, 2003). Hydrogen steam generators can be used for industrial steam power supply, for electricity generation and in power plants. Hydrogen steam generator is close to 100% efficient since there are little or no thermal losses and there is no emission other than steam. Gao et al. (2007) estimated that in the near future, there might be entire cities converting to solely hydrogen for heating and cooling.

Hydrogen can be combined with oxygen in an electrochemical reaction in fuel cell to produce electricity (Maleki *et al*., 2016). In the typical IC engine vehicle optimized for a hydrocarbon fuel, only about 15% of the fuel value ends up as kinetic energy moving the vehicle down the road. This value increases to about 25% for an IC engine/electric hybrid (Barbir, 2013). Fuel cell vehicles operating on compressed hydrogen have the potential of achieving over 30% and, unlike the hybrids, would be classed as zero emission vehicles (Dell *et al*., 2014).

In conclusion, gasified biomass can be used to power IC engines, gas turbines and fuel cells, all of which are able to produce electricity at higher efficiency. Therefore, coupling biomass gasifiers with these energy generators has the potential for considerably lowering capital investment than a similarly sized boiler/steam turbine system.

Other energy conversion route of hydrogen includes catalytic conversion to produce heat and conversions involving metal hydrides.

Analysis of biomass gasification options has shown that production of hydrogen is the most economic route for

the conversion of syngas to transportation fuels (Spath and Dayton, 2003). An economic and efficiency evaluation of hydrogen from biomass is therefore important for the implementation of the technologies of the gasification processes. Table 3 lists the hydrogen production costs from biomass gasification using different gasifiers from previous studies. Hydrogen production from other sources aside from biomass gasification are also listed on the table. Biomass gasification seems to be the most cost effective for the production of hydrogen and power aside from steam methane reforming (SMR). SMR is a mature technology that uses natural gas which has a well-defined non varying composition and is delivered via pipeline. However, SMR uses fossil fuel which is prone to depletion, environmental pollution and GHG emission. Biomass gasification on the other hand uses renewables which are available and sustainable. In fact, it has been viewed as an important technology for reducing GHG.

The U.S Department of Energy (U.S. DOE) has set a cost goal for hydrogen at $2-$3/kg including production, transportation and delivery for hydrogen to be cost competitive with fossil fuel. The goal for production cost only was set at $1.10/kg (NREL, 2011; Nikolaidis and Poullikkas, 2017). In fact the goal for biofuels production in the US is 36 billion gallons by 2022 (USA Energy Independence, 2007).

None of the gasification process presented in table 3 met up with this goal. One way to reduce cost of production is to use renewables from nonfood biomass such as agricultural residues, energy crops, woody crops, forestry, mill and wood wastes.

Hydrogen energy technologies are particularly interesting for the developing countries that do not have huge energy infrastructures in place. Cost for distribution such as power transmission lines, pipelines, transportation infrastructure might work against centralized production in developing economy. Hence, hydrogen can be produced from low cost biomass to supply off grid electricity to homes using a portable fuel cell power system. Developing countries may adopt dispersed renewable energy sources using both traditional and advanced technologies for their utilization.

Technology improvements of gasification process may reduce the cost of producing hydrogen from biomass. Advances in biotechnology that will produce high yield, low-cost energy crops are one of such ways. Improvement actions leading to an increase in process efficiency that would significantly enhance the system's performance is another way. This is because increase in hydrogen production from gasification of biomass has been linked to improved exergy efficiency of the gasification process (Zhang et al; 2019a).

Table 3: Hydrogen production cost

Process	H_2 production cost	References
Air gasification in a fluidized bed	2.11USD/kg	Mohamed *et al*., 2011
Steam gasification in fluidized bed with in-situ CO_2 capture	1.91 USD/kg	Inayat *et al*., 2011
Oxygen gasification in a fixed bed and CO-shift at atmospheric pressure	1.69 USD/kg	Lv *et al*., (2008)
Large scale gasification	1.38 USD/kg	Spath *et al*., 2005
Fuel cell Hydrogen	2.76 USD/kg	Ogden, 1999
Electrolysed hydrogen	10 USD/kg	Iwasaki, 2003
Biomass pyrolysis with high pressure	4.28 USD/kg	Iwasaki, 2003
Steam methane reforming	1.25 USD/kg	NREL, 2011

5.0 CONCLUSION

Hydrogen energy system from biomass gasification is a coherent, comprehensive and permanent solution to global energy-economic-environmental problems, and as such deserves support from individual governments, industrial organizations and research institutes. The Hydrogen yield in the syngas composition is influenced by some operating conditions such as steam flow rate and temperature. The choice of materials also has critical influence on the efficiency of the gasification process. Biomass gasification is a renewable and clean energy source with great potentials to replace fossil fuels for hydrogen production. Adopting gasification technology for the main purpose of producing hydrogen may seem expensive but in the long run its benefit might be unquantifiable. Further research efforts to improve the reaction rates and efficiency, reduce the production cost and fast track the large scale production should be encouraged.

REFERENCES

Ahmad, A.A., Zawawi, N.F., Kazim, F.H., Inayat, A., Khasri A. (2016). Assessing the gasification

performance of biomass: A review on biomass gasification process conditions, optimization and economic evaluation. *Renewable and Sustainable Energy Reviews*, 53: 1333-1347.

Ahmed, U., Kim C., Zahid, U., Lee, C. J., Han C. (2017). Integration of IGCC and methane reforming process for power generation with CO2 capture. *Chem Eng Process Intensif.*, 111:14–24.

Ben-Iwo, J., Manovic, V., Longhurst P. (2016). Biomass resources and biofuels potential for the production of transportation fuels in Nigeria, *Renewable and Sustaianble Energy Reviews*, 63: 172-192.

Badwal, S. P. S., Giddey, S., Munnings C. (2013). Hydrogen production via solid electrolytic routes. *Wiley Interdiscip Rev Energy Environ, 2(5), 473-487.*

Barbir, F. (2013). PEM fuel cells: Theory and practice. United Kingdom, Academic Press, 2nd Ed.

Barbuzza, E., Buceti, G., Pozio, A., Santarelli, M., Tosti, S. (2019). Gasification of wood biomass with renewable hydrogen for the production of synthetic natural gas. *Fuel*, 242:520-531.

Brachi, P., Chirone, R., Miccio, F., Miccio, M., Ruoppolo, G. (2018). Entrained-flow gasification of torrefied tomato peels: Combining torrefaction experiments with chemical equilibrium modeling for gasification. *Fuel*, *220*: 744–753.

Cao, L., Yu, I.K.M., Xiong, X., Tsang, D.C.W., Zhang, S., Clark, J.H., Hu, C., Ng, Y.H., Shang, J., Ok, Y.S. (2020). Biorenewable hydrogen production through biomass gasification: A review and future prospects, *Environmental Research*,
doi: https://doi.org/10.1016/j.envres.2020.109547 .

Catalan-Martinez, D., Domine, M. E, Serra, J. M. (2018). Liquid fuels from biomass: An energy self-sustained process integrating H_2 recovery and liquid refining. *Fuel*, 212:353-363.

Chakik F. E, Mikou M. (2017).Effect of operating parameters on hydrogen production by electrolysis of water. *Int J Hydrogen Energy*, 42(40):25550-25557.

Ciferno, J. P.,Marano, J. J. (2002). Benchmarking biomass gasification technologies for fuels, chemicals and hydrogen production. U.S. Department of Energy National Energy Technology Laboratory (Washington, DC); 2002.

Contreras, A., Carpio, J., Molero, M., Veziroglu, T. N. Solar (1999). Hydrogen:an energy system for sustainable development in Spain. *International Journal of Hydrogen Energy*, 24:1041-1052.

Cormos, A.M., Szima, S., Fogarasi, S., Cormos, C.C. (2018).Economic assessments of hydrogen production processes based on natural gas reforming with carbon capture. *ChemEng Trans*, 70:1231–1236.

Das, L.M. (2016).Hydrogen –fueled internal combustion engines In: Compendium of Hydrogen energy, Vol. 3: Hydrogen energy conversion. (Ed Barbir, F., Basile, A., Vesiroglu, T.J.), Wood Head Publishing Series in Energy.

Dell, R.M., Moseley, P.T., Rand, D.A.J. (2014).Towards sustainable road transport. United Kingdom, Academic Press., 1st Ed.

Demirbas, A. (2001). Biomass resource facilities and biomass conversion processing for fuels and chemicals. *Energy conversion management*, 42(11): 1357-1378.

Dincer, I., Acar, C., (2015). A review on clean energy solutions for better sustainability. *Int. J. Energy Res*. 39 (5), 585-606.

Do Sacramento, E.M, De Lima, L.C, Oliviera, C. J., Veziroglu T.N. (2008).A Hydrogen energy system and prospects for reducing emissions of fossil fuels pollutants in the Ceara state Brazil. *International Journal of Hydrogen Energy*, 33:2132-2137.

Gao, N., Li, A., Quan, C., and Gao, F. (2008). Hydrogen-rich gas production from biomass steam gasification in an updraft fixed-bed gasifier combined with a porous ceramic reformer.*International Journal of Hydrogen Energy*, *33* (20): 5430-5438.

Gao,N., Li, A., Quan, C., Qu, Y., Mao, L. (2012). Characteristics of hydrogen-rich gas production of biomass gasification with porous ceramic reforming. *Int J Hydrog Energy*, 37:9610–9618.

Gao, H., Zhen, W., Ma, J., Lu, G., (2017). High efficient solar hydrogen generation by modulation of Co-Ni

sulfide surface structure and adjusting adsorption hydrogen energy.*Appl. Catal. B Environ*., 206: 353-363.

Ghassemi, H., Mostafavi, S. M., Shahsavan-Markadeh, R. (2016). Modeling of high-ash coal gasification in an entrained-flow gasifier and an IGCC plant. *J Energy Eng*, 40:150-152.

Gong, M., Zhu, W., Zhang, H.W, Ma, Q, Su, Y., Fan, Y.J. (2014). Influence of NaOH and Ni catalysts on hydrogen production from the supercritical water gasification of dewatered sewage sludge *International Journal of Hydrogen Energy*, 39:19947-19954.

Hemschemeier, A., Melis, A., Happe, T., (2009). Analytical approaches to photobiological hydrogen production in unicellular green algae. Photosynthesis Research, 102 (2–3): 523–540.

Holladay, J. D., Hu, J., King, D.L., Wang, Y. (2009). An overview of Hydrogen production technologies. Catalysis, 139: 244-260.

Inayat, A., Ahmad M. M., Abdul Mutalib, M. I, Yusup, S. (2010). Effect of process parameters on hydrogen production and efficiency in biomass gasification using modelling approach. *J Appl Sci*, 10:3183–3190.

Inayat, A., Ahmad, M.M, Mutalib, M.A, Yusup, S. (2011). Heat integration analysis of gasification process for hydrogen production from oil palm empty fruit bunch. *Chem Eng Trans* 25:971–976.

Iwasaki W. (2003). A consideration of the economic efficiency of hydrogen production from biomass. *Int J Hydrogen Energy*, 28:939–44.

Kalinci Y, Hepbasli A, Dincer I. (2009). Biomass-based hydrogen production: a review and analysis. *Int J Hydrogen Energy*, 34:8799–8817.

Lewis, M.A., Ferrandon, M.S., Tatterson, D.F, Mathias, P. (2009).Evaluation of alternative thermochemical cycles-part III further development of the Cu-Cl cycle, Int J Hydrogen Energy, 34, 4136-4145.

Li, J., Yin, Y., Zhang, X., Liu, J., Yan, R. (2009). Hydrogen-rich gas production by steam gasification of palm oil wastes over supported tri-metallic catalyst. *Int J Hydrog Energy*, 34:9108–9115.

Liu, Y., Zhu, Q., Zhang, T., Yan, Z., Duan, R. (2020) Analysis of chemical-looping hydrogen production and power generation system driven by solar energy, *Renewable Energy*, https://doi.org/10.1016/j.renene.2020.02.109.

Lu, Y., Jin, H., Guo, L., Zhang, X., Cao, C., Guo, X. (2008). Hydrogen production by biomass gasification in supercritical water with a fluidized bed reactor. *Int J Hydrogen Energy*, 33:6066-6075.

Luo, S., Xiao, B., Hu, Z., Liu, S., Guo, X., He, M.(2009). Hydrogen-rich gas from catalytic steam gasification of biomass in a fixed bed reactor: influence of temperature and steam on gasification performance. *Int J Hydrog Energy*, 34:2191–2194.

Lv, P., Wu, C., Ma, L., Yuan, Z. (2008) A study on the economic efficiency of hydrogen production from biomass residues in China. *Renewable Energy*, 33:1874–1879.

Lv, P. M., Xiong, Z. H., Chang, J., Wu, C. Z., Chen, Y., Zhu, J. X. (2004). An experimental study on biomass air–steam gasification in a fluidized bed. *Bioresour Technol*, 95(1):95–101.

Mahishi, M.R., Goswami, D.Y. (2007). Thermodynamic optimization of biomass gasifier for hydrogen production. *Int J Hydrogen Energy* 32:3831–3840.

Maleki, A., Pourfayaz, F., Ahmadi, M.H., (2016). Design of a cost-effective wind/ photovoltaic/ hydrogen energy system for supplying a desalination unit by a heuristic approach. *Sol. Energy*, 139: 666-675.

McKendry, P. (2002a). Energy production from biomass (part 2): conversion technologies. *Bioresource technology, 83*: 47-54.

McKendry, P. (2002b). Energy production from biomass (part 3): gasification technologies. *Bioresource technology, 83*: 55-63.

McQuillan, B.W., Brown, L.C., Besenbruch, G.E., Tolman, R., Cramer, T., Russ, B.E. (2002). High efficiency generation of hydrogen fuels using solar thermochemical splitting of water. Annual Report, GA-A24972, General Atomics, San Diego, CA.

Mohammed, M.A.A, Salmiaton, A, Wan,Azlina WAKG, Mohammad Amran M.S, Fakhru'l-Razi A.

(2011). Air gasification of empty fruit bunch for hydrogen-rich gas production in a fluidized-bed reactor. *Energy Conversion Management*, 52(2), 1555–1561.

Molino, A., Larocca, V., Chianese, S., Musmarra, D. (2018) Biofuels production by biomassgasification: A review. *Energies* 11(4): 811-842.

Moneti, M., Di Carlo, A., Bocci, E., Foscolo, P.U, Villarini, M., Carlini M. (2016). Influence of the maingasifier parameters on a real system for hydrogen production from biomass. *Int J Hydrogen Energy*, 1–9.

Nanda, S., Isen J., Dalai A.K., Kozinski J.A.(2016a). Gasification of fruit wastes and agro-food residues in supercritical water. *Energy Convers Manag*, 110:296-306.

Nanda, S., Reddy S.N, Dalai, A. K., Kozinski, J. A.(2016b) Subcritical and supercritical water gasification of lignocellulosic biomass impregnated with nickel nanocatalyst for hydrogen production. *Int J Hydrogen Energy*41:4907-4921.

Naterer, G.F., Suppiah, S., Stolberg, L., Lewis, M., Wang, Z., Daggupati, V., Gabriel, K., Dincer, I., Rosen, M.A, Spekkens, P., Lvov, S., Fowler, M., Tremaine, P.,Mostaghimi, J., Easton, E.B., Trevani, L., Rizvi, G., Ikeda, B.M., Kaye, M.H., Lu, L.,Pioro, I., Smith, W.R., Secnik, E., Jiang, J., Avsec, J., (2010). Canada's program on Nuclear Hydrogen Production and the Thermochemical Cu-Cl cycle, *Int J Hydrogen Energy*, 35: 10905-10926.

National renewable energy laboratory (NREL) (2011). Hydrogen production cost estimate using biomass gasification. www.nrel.gov.

Ni, M., Leung, D.Y, Leung, M.K, Sumathy, K. (2006).An overview of hydrogen production from biomass, *Fuel Process Technol*, 87: 461-472.

Nikolaidis, P. and Poullikkas, A. (2017). A comparative overview of hydrogen production processes. *Renew. Sustain. Energy Rev.*, 67: 597–611.

Nikolic, V. M., Tasic, G. S., Maksic, A. D., Saponjic, D.P., Miulovic, S. M., MarcetaKaninski, M. P., (2010). Raising efficiency of hydrogen generation from alkaline water electrolysis - energy saving. *Int J Hydrogen Energy*, 35(22):12369-12373.

Ogden, J. M. (1999).Prospects for building a hydrogen energy infrastructure. *Annu Rev Energy Envision*, 24:227–273.

Orhan, M.F., Ibrahim D., Marc A.R., (2011), Simulation and Exergy Analysis of a Copper-Chlorine Thermochemical Water Decomposition Cycle for Hydrogen Production, *Intl Journal of Hydrogen Energy*, 36, 11309-11320.

Pala, L.P.R., Wang, Q., Kolb, G., Hessel, V.(2017). Steam gasification of biomass with subsequent syngas adjustment using shift reaction for syngas production: an Aspen Plus model. *Renew Energy*, 101:484-492

Pallozzi, V., Di Carlo, A., Bocci, E., Villarini, M., Foscolo, P.U, Carlini, M. (2016). Performance evaluation at different process parameters of an innovative prototype of biomass gasification system aimed to hydrogen production, *Energy Conversion and Management* 130: 34–43

Rapagnà, S., Latif, A. (1997).Steam gasification of almond shells in a fluidised bed reactor: the influence of temperature and particle size on product yield and distribution. *Biomass Bioenergy*, 12(4):281–288.

Qiu, P.H., Du, C.S., Liu, L., Chen, L. (2018). Hydrogen and syngas production from catalytic steam gasification of char derived from ion-exchangeable Na- and Ca-loaded coal. *Int J Hydrogen Energy*, 43:12034-12048.

Safari, F., Javani, N., Yumurtaci, Z. (2018).Hydrogen production via supercritical water gasification of almond shell over algal and agricultural hydrochars as catalysts. *Int J Hydrogen Energy*, 43:1071-1080.

Santos, D. M. F., Sequeira, C. A. C, Figueiredo, J. L. (2013). Hydrogen production by alkaline water electrolysis. *Quim Nova*, 36(8):1176- 1193.

Siedlecki, M., de Jong, W., Verkooijen, A.H.M.(2011). Fluidized bed gasification as a mature and reliable technology for the production of bio-syngas and applied in the production of liquid transportation fuels-a review. *Energies*, 4:389–434.

Sikarwar, V.S., Zhao, M., Fennell, P. S., Shah, N., Anthony, E.J. (2017). Progress in biofuel production from gasification. *Prog. Energy Combust. Sci., 61*: 189–248.

Simonyan, K., Fasina O. (2013). Biomass resources and bioenergy potentials in Nigeria, *Afr J Agric*., 8:4975–4989.

Skoulou, V., Swiderski, A., Yang, W., Zabaniotou A.(2009). Process characteristics and products of olive kernel high temperature steam gasification (HTSG). *Bioresour. Technol*. 100(8):2444–2451.

Spath, P.L., Dayton, D.C. (2003). Preliminary Screening Technical and Economic Assessment of Synthesis Gas to Fuels and Chemicals with Emphasis on the Potential for Biomass- Derived Syngas. National Renewable Energy Laboratory: Golden, CO, TP-510-34929.

Spath, P. L., Aden, A., Eggeman, T., Ringer, M., Wallace, B., Jechura, J. (2005). Biomass to Hydrogen Production Detailed Design and Economics Utilizing the Battelle Columbus Laboratory Indirectly Heated Gasifier. National Renewable Energy Laboratory: Golden, CO, TP-510-37408

Tian, T., Li, Q., He, R., Tan, Z., Zhang, Y. (2017). Effects of biochemical composition on hydrogen production by biomass gasification, *International Journal of Hydrogen Energy* 42: (31) 19723-19732.

USA Energy Independence (2007).Security Act of 2007. *Public Law 2007*, 110–140.

Valente, A., Diego, R.,Dufour, J. (2019). Life cycle sustainability assessment of hydrogen from biomass gasification: A comparison with conventional hydrogen, *International Journal of Hydrogen Energy*, 44(38): 21193-21203.

Wei, L., Yang, H., Li, B., Wei, X., Chen, L., Shao, J., Chen, H.(2014). Absorption-enhanced steam gasification of biomass for hydrogen production: effect of calcium oxide addition on steam gasification of pyrolytic volatiles. *Int J Hydrogen Energy* 2014, 39:15416-15423.

Xiao, R., Jin, B., Zhou, H., Zhong, Z., Zhang, M. (2007). Air gasification of polypropylene plastic waste in fluidized bed gasifier. *Energy Convers Manag*., 48:778–786.

Yanik, J., Ebale, S., Kruse, A., Saglam, M., Yuksel, M. (2007). Biomass gasification in supercritical water: Part 1. Effect of the nature of biomass. *Fuel*, 86:2410-2415.

Yang, R.X., Chuang, K.H., Wey, M.Y. (2018). Effects of temperature and equivalence ratio on carbon nanotubes and hydrogen production from waste plastic gasification in fluidized bed. *Energ Fuel*, 32:5462-5470.

Zhao, Y., Sun, S., Zhou, H., Sun, R., Tian, H., Luan, J. (2010). Experimental study on sawdust air gasification in an entrained-flow reactor. *Fuel Process Technol*, 91:910–914.

Zhang, Y., Li, L., Xu, P., Liu, B., Shuai, Y., Li, B. (2019a). Hydrogen production through biomass gasification in supercritical water: A review from exergy aspect, *International Journal of Hydrogen Energy*, 44(30):15727-15736.

Zhang, Y., Li, L., Xu, P., Liu, B., Shuai, Y., Li, B. (2019b). Exergy analysis of hydrogen production from steam gasification of biomass: A review, *International Journal of Hydrogen Energy*, 44(28): 14290-14302.

DOI: 10.51975/KWZC7505
Journal of the Nigerian Society of Chemical Engineers, 36(1), 2021

POWER RATE LAW BASED CHEMICAL KINETICS AND THERMODYNAMIC MODELING OF AFRICAN PEAR SEED OIL CONSECUTIVE IRREVERSIBLE BASE METHANOLYSIS FOR BIODIESEL PRODUCTION

***Esonye, C.[1], Onukwuli, O. D.[2] and Momoh, S. O.[3]**

[1]*Department of Chemical/ Engineering, Alex Ekwueme Federal University, Ndufu-Alike Ikwo, Abakaliki, Nigeria; eso_vic@yahoo.com.*

[2]*Department of Chemical Engineering, NnamdiAzikiwe University, Awka, Nigeria; onukwuliod@yahoo.com*

[3]*Research and Development Unit, National Agency for Science and Engineering Infrastructure, Abuja, Nigeria.stevemomoh@yahoo.com.*

ABSTRACT

Currently the major challenge of biodiesel application as a replacement to petrodiesel is its industrial production sustainability.Consequently, the successful scale-up of laboratory results in transesterification requires so much information obtained through chemical kinetics.This paper presents the kinetics and thermodynamic study of alkali-homogeneous irreversible methanolysis of seed oil derived from African pear. The transesterification process was carried out from 0-100 minutes at temperature range of 55-65°C. The reaction mixture compositions were ascertained using gas chromatography- flame ionization detector (GC-FID) technique. Rate constants of the triglyceride (Tg), diglycerides (Dg) and monoglycerides(Mg) hydrolysis were in the range of 0.0140- 0.07810 wt%/min and increased with increase in temperature. The rate of reaction was found to increase with increase in temperature. Activation energies were found to be 6.14, 20.01 and 28.5kcal/mol at 55, 60 and 65^oC respectively. Tg hydrolysis to Dg was observed asthe rate determining step while the reaction agreed with second order principles. A biodiesel yield of 93.02% was obtained with cloud point of 10°C , flash point of 125°C , pour point of 4°C , calorific value of 34.4MJ/kg, and cetane number of 54.90 which satisfy EN14214 and ASTM D 6751 standards. Results presented in this report would serve as idealized conditions for industrial scale up of biodiesel production from African pear seed oil.

Keywords:*Kinetics; methanolysis; rate constants; activation energy; African pear seed oil; biodiesel*

1. INTRODUCTION

The challenges on the environment due to the application of fossil diesel have made the application of alkyl esters derived from natural sources indispensable. The physico-chemical characteristics and energy attributes of biodiesel are very similar to those of petrodiesel. Currently, the homogeneous base-catalyzed transesterification using methanol resulting in the corresponding fatty acid methyl esters (FAMEs) is the predominant technique applied for large scale production of biodiesel (Reyero, et al., 2015)). Application of methanol is necessitated by its wide availability and low-cost. The application of homogeneous base catalyst like NaOH and KOH at commercial level is highly encouraged because they possess of higher catalytic capabilitythan acid catalyst which is more corrosive (Wan and Hammed, 2011). The introduction of catalyst neutralization and washing has been among the most important stages of conventional purification steps employed to arrest the challenges of soap formation (Reyero et al., 2015). Also, the challenges of catalyst re-usability and the leaching of support or active sites which causes catalyst loss and decrease of the FAME yield have been serious challenges to heterogeneous catalyst application (Ilgen, 2012).

The major challenge in biodiesel application as a renewable and alternative fuel to petrodiesel is the lack of sustainability of its generation (Wang et al., 2020). The successful scale-up of laboratory results in transesterification requires information obtained through kinetics and optimization studies. Hence, chemical kinetics data are required to arrest the above problem. Chemical kinetics deals with the dynamics of chemical reactions: the rate (velocity) of the process and the way by which the reaction takes place. The rate law is the keystone for the chemical reaction mechanism which helps in describing the relationship between the reaction rate and the concentration of the chemical reactants (Abdel-Latiff. and Abdallah, 2010). Of great importance is the determination of the rate constants as it is highly required in establishing the value of the reaction rate by

applying its rate equation. Of high industrial importance is the chemical rate equation as it is needed in the kinetics application to establish the important conditions of reaction such as optimal pressure, temperature, feed composition, space velocity, degree of conversion and recycling (Abdel-Latiff. and Abdallah, 2010). Many chemical kinetic models previously proposed have not been able to bridge the gap between laboratory and the industry due to their high complexities and the assumption that the base methanolysis is reversible while the usual application of high methanol/oil molar ratio always shift the reaction to the right. This negates the effect of reversible reactions in transesterification process. Additionally, thorough review of the optimization studies of biodiesel production from literature has reported optimal alcohol/oil molar ration to be above 5:1 and this condition cannot promote reversible transesterification process. Also, a detailed review of various kinetic modeling studies of transesterification has proven that the alcohol/ oil molar ratio is always greater than the usual stoichiometric value of 3:1; (6:1)(Ilgen, 2012); (Okullo and Temu 2015); (Noureddini and Zhu1, 999), (4:1-14:1)(Zanette. et al., 2011), (15:1)(Wan and Hammed 2011), (6:1,12:1 and 24:1)(Reyero et al., 2015), (9:1)(Zavarukhin, et al., 2013), (6:1, 8:1 and 10:1)(Orifici. et al 2013), (9:1,12:1 and 15:1)(Patil et al., 2011) and (42:1)(Almgrbi et al., 2014). It is noteworthy that the complexity in kinetic models proposed in the above reports based on reversible consecutive mechanism challenges their industrial translation while simplified kinetic models suffice for practical purposes. Consequently, methanolysis reaction has been proposed to constitute three consecutive irreversible stages, especially by the usual condition of using high methanol to oil ratio (>3:1) which shifts the reaction methyl to the right (Ilgen, (2012); Darnoko and Cheryan (2000)

There are some researches that investigated on the reaction kinetics of various vegetable oil transesterification (Menkiti et al 2017) and few on African pear seed oil. The reversible models of kinetics of African pear seed oil on the basis of heterogeneous catalysis [Onukwuli and Ude 2018), its esterification and transesterification (Esonye. et al 2018) have been reported but this study presents the kinetics of methyl ester production from non-conventional non-edible tropical seed of African pear on the basis of irreversible consecutive mechanisms. Most seed oil transesterification kinetics presented earlier dealt on complex three-step. Before now, the seed oil from African pear is treated as a waste after consuming its fatty and juicy pulp (Bull and George, 2015). Also, African pear is a perennial plant with high seed oil content in the seed with good productivity per hectare (Ogunsuyi, 2015; Bull and George2015) and thus satisfies the EU stipulations for biodiesel feedstock. Consequently, this research proposes the evaluation Aof the kinetics of biodiesel production from African pear seed oil (APSO) on the basis of irreversible consecutive mechanism.

2. MATERIALS AND METHODS

2.1 Materials.

The materials used in this research include sodium hydroxide (99%, Sigma-aldrich), potassium hydroxide (lobachemie, 85%), methanol (Merck, Germany, 99.5 % purity), carbon tetrachloride (chloroform), Wij's solution (iodine monochloride), potassium iodide solution and phenolphthalein (Merck Germany. The fruit seed biomass was bought from Ochanja market in Onitsha city in Anambra state of Nigeria and the seed oil was extracted by solvent extraction method using hexane.

2.2 Physico-chemical characterization of the seed oil and the biodiesel

This stage of the experiment has been conducted and reported previously (Esonye et al., (2018). The properties of the African pear seed oil were determined in accordance with Association of Official Analytical Chemists method (AOAC, 1990), the acid value by AOAC Ca5a-40, saponification value by AOAC 920:160; iodine value by AOAC 920:158 and peroxide value by AOAC 965.33) while the viscosity was determined by using Oswald viscometer apparatus, the density by using density bottle and moisture content by the Rotary evaporator oven (BTOV 1423). The ash content was evaluated by heating to dryness in Veisfar muffle furnace and the refractive index was measured using Abbe refractometer (Model: WAY-25, Search tech. Instruments). The fuel properties of the synthesized biodiesel were determined by ASTM standards: the kinematic viscosity was determined by ASTM D-445 method, the density was determined by ASTM D-1298 method, and the pour point determination was made using ASTM D-97 methods. The flash point of the fuel was determined as ASTM D-93, the value of cloud point was estimated according to ASTMD-2500, and acid value was measured following the ASTM D-664 method. The calorific value and cetane number were calculated according to the correlation developed by Bull and George, (2015).

2.3 Kinetic Study

The rate of reaction and its mechanism as regards the transesterification process of the seed oil were investigated by considering irreversible conditions.

2.4 Equation of transesterification reaction

Darnoko and Cheryan, (2000) have reported that transesterification reaction mechanism includes three consecutive irreversible reactions that yield fatty acid diglycerides and monoglycerides as intermediates. Equation (4) is the summary of Equation (1) to (3), which represents the stages of the reaction.

$$Tg + R'OH \underset{\rightarrow}{}^{k_1} Dg + FAME \quad (1)$$

$$Dg + R'OH \underset{\rightarrow}{}^{k_2} Mg + FAME \quad (2)$$

$$Mg + R'OH \underset{\rightarrow}{}^{k_3} Gl + FAME \quad (3)$$

$$\begin{matrix} CH_2OCOR \\ CHOCOR \\ CH_2OCOR \end{matrix} + \quad 3ROH \leftrightarrow \quad \begin{matrix} CH_2OH \\ CHOH \\ CH_2OH \end{matrix} + \begin{matrix} R'COOR \\ R''COOR \\ R'''COOR \end{matrix} \quad (4)$$

Triglycerides Alcohol Glycerol FAME

Where FAME is fatty acid methyl ester

2.5 Irreversible model assumptions

Since simplified kinetic models suffice for practical purposes, experimental data were processed under the following assumptions (Ilgen, 2012; ,Patil et al., 2011; Darnoko and Cheryan, 2000):

1. The methanolysis reaction is constituted by three consecutive stages but assumed irreversible because of the excessive presence of methanol in the reaction.
2. The free fatty acid neutralization was insignificant since the free fatty acid was negligible.
3. The saponification reaction was considered insignificant because of low acid value of the oil.

2.6 Experimental procedure

Experiments were designed to determine the reaction rate constants. A 6:1 molar ratio of methanol to oil was used in all the experiments. To examine the temperature dependency of the reaction rate constants, reactions at 55, 60 and 65˚C were studied. The oil obtained from the esterification the seed oil as previously reported by the authors (Esonye et al., 2019) was used in this experiment. All reactions were carried out at atmospheric pressure with 0.20wt% sodium hydroxide as catalyst, methanol/oil molar ratio of 6:1 at a stirring speed of 140rpm. As reaction progresses, 2ml aliquot sample was withdrawn with a disposable pipette through an opening on the top of the reactor. The samples were collected in 10ml test tubes and kept in an ice bath at 5˚C prior to use to quench the reaction. Samples were withdrawn at specified time intervals (0, 0.3, 0.5, 2, 4, 6, 10, 20, 40, 60, 80 and 100 minutes). The composition of sample was determined by gas chromatography (GC) on Perkin Elmer Claurus 600 model FID to ascertain the amount of triglycerides, diglycerides, monoglycerides, total methyl esters and glycerol content in the biodiesel production batch reaction system. The GC operating specifications are given in Table 1. The diglycerides and monoglycerides contents were minimal (< 3%), while the amounts of triglycerides were above 94%.

Table 1: Operating conditions of gas chromatography analysis .

SN	Item	Condition
1	Column	5"x1/4" internal diameter (i.d), glass column packed with 10% silica 10°C on 80-100mesh chromasorb HP at a temperature of 180°C
2	Detector	Flame Ionization Detector (FID),
3	Column Temperature	185°C (set point = 150°C , increment = 35°C)
4	Nitrogen flowrate	30 ml/min.
5	Hydrogen flowrate	20lb/in^2
6	Air Pressure	12lb/in^2
7	Sample size	0.3µl
8	Attenuation	2x10 ^{4}
9	Backing off range	x100

2.7 Second –order irreversible model

The best kinetic model for an irreversible model has been proposed to be a second-order based on Tg hydrolysis especially during the early stages of the reaction (Darnoko and Cheryan, 2000). To test the above report, a model developed based on Tg hydrolysis and the second-order reaction rate for Tg would be as shown in Equation (5) (Darnoko and Cheryan 2000, Levenspiel, 1999)

$$\frac{-d[Tg]}{dt} = k[Tg]^2 \quad (5)$$

Integrating and rearranging of Equation (5) by integration yields Equation (6).

$$k_{Tg}t = \frac{1}{[Tg]} - \frac{1}{[Tg0]} \quad (6)$$

Where k is the overall rate constant, t is the reaction time, Tg_0 is the initial triglyceride concentration.

A plot of reaction time (t) against $\frac{1}{[Tg]}$ will give a straight line if the model is valid.

Where k is the overall rate constant, t is the reaction time; Tg_0 is the initial triglyceride concentration. A plot of reaction time (t) against $\frac{1}{[Tg]}$ will give a straight line if the model is valid. Similar approach was applied on the monoglycerides and diglycerides hydrolysis to get Equations (7) and (8).

$$k_{Dg}\,t = \frac{1}{[Dg]} - \frac{1}{[Dg_0]} \quad (7)$$

$$k_{Mg}\,t = \frac{1}{[Mg]} - \frac{1}{[Mg_0]} \quad (8)$$

2.7 First-order irreversible model

To determine the kinetics of the reaction based, the effect of reaction temperature and time were measured.
It was assumed that the catalyst was used in sufficient amount with respect to oil to shift the reaction equilibrium towards the formation of fatty acid methyl esters. Thus, the reverse reaction could be ignored and change in concentration of the catalyst during the course of reaction can be assumed to be negligible [Esonye, C, et al (2019)]. Also, since the concentrations of both Dg and Mg were found to be very low (Dg<2.9wt%, Mg<1.45wt %) compared to those of Tg (Tg>94wt%) in the crude vegetable oils used in this research, the reaction could be assumed to be a single-step transesterification (Levenspiel, 1999). Therefore, the rate law of the transesterification reaction for forward reaction can be expressed by Equation (9) (Zhang et al 2010).

$$-r_{Tg} = \frac{-d[Tg]}{dt} = k'.[Tg].[ROH]^3 \quad (9)$$

Where [Tg] is the concentration of triglycerides and [ROH] that of methanol and k′ is the equilibrium rate constant. However, due to the high molar ratio of methanol to oil, the change in methanol concentration can be considered as constant during reaction. This means that by taking methanol in excess, its concentration does not change the reaction order and it behaves as a first-order chemical reaction. Hence, the reaction would obey pseudo-first order kinetics (Zhang, et al., 2010) and finally, the rate expression can be written as in Equation (10).

$$-r_{Tg} = \frac{-d[Tg]}{dt} = k.[Tg] \quad (10)$$

Where k is modified rate constant and $k = k'[ROH]^3$. Assuming that the initial triglyceride concentration was $[Tg_0]$ at time t =0, and at time t it falls down $[Tg_t]$. The integration of Equation (10) from t = 0, $[Tg]= [Tg_0]$ to t = t, $[Tg] =[Tg_t]$ gives Equation (11)[14]:

$$-\ln[Tg] + \ln[Tg_0] = kt \quad (11)$$

Based on the above considerations, the rate data from the seed oil of African pear transesterification reaction was fit into Equation (11) to test this rate equation. Hence, -ln[Tg] was plotted against time. In this procedure, the weight percentage of Tg was used as concentration because $[Tg]_0/[TG]$ is a concentration ratio and its value is independent of units, provided that the same units are used for both $[Tg]_0$ and [Tg]. Least-square approximation was applied in fitting a straight line to the experimental data, and in each case the coefficient of determination (R^2) was determined.

2.8 Thermodynamic properties determination

Activation energies of the reaction taking place were estimated using the calculated rate constants and temperatures at which they were observed in Arrhenius equation (Eqn. 12).

$$\log_{10}k = \frac{-Ea/2.303R}{T} + A \quad (12)$$

Where E_a = Activation energy, R = Gas constant, A = Arrhenius constant or frequency factor

3. RESULTS AND DISCUSSIONS

3.1 Seed oil and biodiesel characterization

The physico-chemical parameters of the APSO and APSOME are shown in Table 2. The oil content is a key factor influencing the choice of plant seeds as potential feedstock for biodiesel and other industrial products. The percentage oil yield from African pear is very encouraging for biodiesel purposes when compared with most oil feedstocks. It is observed that the seed has high oil yield (>56%), though with high free fatty acid (FFA). High FFA in oils results in losing the oil to soap rather than to biodiesel (Mushtaq et al., 2014). The high FFA

gave the need to apply two - step transesterification which brought down the FFA to 0.16, at 65 °C reaction temperature and 100 minutes esterification time, in order to prevent soap formation which lowers the biodiesel yield (Esonye et al 2019). The results of moisture content obtained for APSO is quite low and would therefore promote high yield of biodiesel, prevent oxidation rancidity and sustain its shelf life (Menkiti et al., 2017). APSOME showed slight decrease in the iodine values obtained from the parent seed oil. The iodine value according to EN 14214 (European committee for standardization) should be less than 120 g I_2/100 g sample for the seed oil to be suitable as feedstock for biodiesel production while oils having high unsaturation of fatty acids, when heated are prone to polymerization of the glycerides, causing formation of deposits and thereby compromising oxidative stability (Birla et al 2012). Peroxide value is an index of rancidity and hence provides information on oil quality and stability. The value obtained clearly suggests that the seed oil is stable and may not readily become rancid during storage.The specific gravity value is close to the range of 0.87 – 0.90 for biodiesel. It is expected to promote effective functioning of the injection engines through maintaining the optimal air to fuel ratio required for efficient combustion and low particulate matter emissions. The viscosity result is consistent with 3.70 cp for APSO as reported in (Ogunsuyi 2015). Viscosity is important in determining optimum handling, storage and operational conditions because biodiesel fuel need to have suitable flow characteristics to ensure that adequate supply reaches injectors at different operating temperatures. The values obtained is very optimal and would prevent fuel filters clogging, formation of droplets on injection which causes poor atomization and provide sufficient lubrication for precision fill of the fuel injection pumps (Atabani , et al., 2012). Moreover, the viscosities of the seed oil decreased considerably after transesterification. The seed oil and the methyl ester have favorable values for smoke point, titre, flash point and cloud point and this would translate to high biodiesel potentials. The cold flow properties of the methyl esters were measured by determination of cloud point (CP) and pour point (PP). Specifications for CP and PP are not in the biodiesel standards of DIN 14214 though ASTM D6757 requires that CP be reported probably because each country has different climatic conditions. As reported here, APSOME has values which are quite within ASTM D6757 standards and this shows that the produced FAME would perform well in very cold and temperate regions.The ash content of the methyl ester is lower than the values obtained from the corresponding vegetable seed oil sample showing improved fuel quality because of the transesterification process. The calorific value is below diesel fuel ASTM D 975 standards but within the limit of EN DIN14214 standard. The cetane number (CN) is above the standard set for petrol diesel. This could be explained to be due to higher oxygen content which is typical of biodiesel fuel. The quality of the oil and biodiesel compared well with result of other studies in the literature (Ogunsuyi, 2015).

Table 2: Physico-chemical parameters of APSO and its biodiesel in relation with standards

Parameters	APSO	APSOME	Standards		
			ASTM D 9751	**ASTMD 6751**	**EN 14214**
Yield (wt%)	56.30	93.025	-	-	-
Colour	Pale yellow	Light brown	-	-	-
Specific gravity	0.8875	0.8570	0.850	0.880	0.86 -0.90
Moisture content (%)	0.53	0.030	-	-	-
Refractive Index	1.4369	1.4279	-	-	-
Acid value (mgKOH/g)	13.98	0.32	0.062	0.50	0.50
Free fatty acid (wt%)	7.89	0.16	0.31	0.25	0.25
Iodine value (mgKOH/g)	51.96	45.21	42-46	-	120 max
Peroxide value (milli eq. oxy/kg)	1.79	-	-	-	-
Saponification value (mgKOH/g oil)	254.72	243.51	-	-	-
Ash content (%)	1.65	0.11	0.01	0.02	0.02
Viscosity (mm^2/s)	5.82	2.34	2.6	1.9-6.0	3.5-5.0
Smoke point (^oC)	30	24	-	-	-
Titre value (^oC)	35	-	-	-	-

Parameters	APSO	APSOME	Standards		
			ASTM D 9751	**ASTMD 6751**	**EN 14214**
Fire point (^{o}C)	40	27	-	-	-
Flash point (^{o}C)	147	125	60-80	100-170	120
Cloud point (^{o}C)	10	10	-20	-3 to 12	-
Pour point (^{o}C)	-6	4	-35	-15 to -16	-
Calorific value (KJ/Kg)	-	34,391.50	42-46	-	35
Conductivity (Us/CM)	-	0.87	-	-	-
Cetane index	-	56.98	-	-	-
Cetane number	-	54.90	40-55	47 min	51 min

3.2 Chemical Kinetics Result

Fig. 1(A-C) shows the progress of the transesterification reaction of African pear seed oil for reaction temperatures of 50°C, 60°Cand 65°C. The catalyst concentration was 0.2wt % of NaOH and methanol/ oil ratio of 6:1 at mixing speed of 140rpm. The initial stage of the reaction produced fatty acid methyl esters (FAMEs) rapidly. The rate then reduced and finally reached almost equilibrium in about 80 minutes for all the temperatures. It is observed in Fig.1 that the glycerol concentration increased with increase in FAME but was not in relative proportion (without a constant factor). This could be as a result of the intermediate products (Dg and Mg). Also, the triglycerides concentration reduced as the reaction progresses. The Tg concentration after 60 minutes was less than 15% for all the temperatures. The highest concentration of Dg and Mg were observed in the first 2 minutes for APSO after which they started decreasing until after 80 minutes when they started being almost at equilibrium. The values of Tg was greater than Dg and Dg was greater than Mg values for all the temperature. It was observed in Fig 1 that the higher the temperature, the lower the values of Tg, Dg and Mg for respective reaction times but the higher the temperature, the higher the values of FAME (Fig. 2). This could be probably because as the temperature moves from 55°C towards the 65°C, the closer it gets to the boiling point of methanol (68°C) which could give better reaction condition for higher conversion of glycerides (Fig. 1).

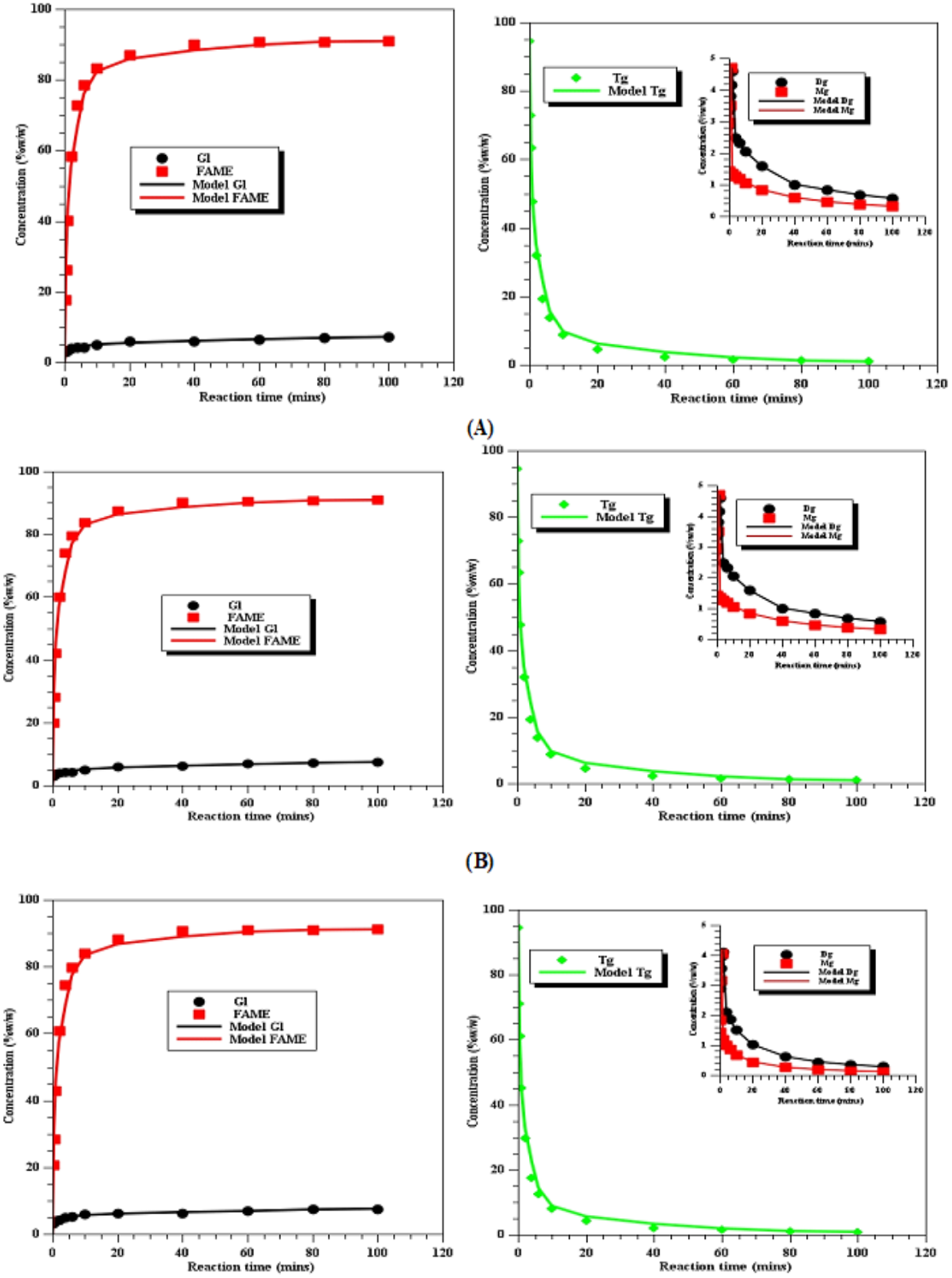

Fig. 1: Composition of Transesterification reaction products at 65°C (A). 60°C (B) and 55°C (C).

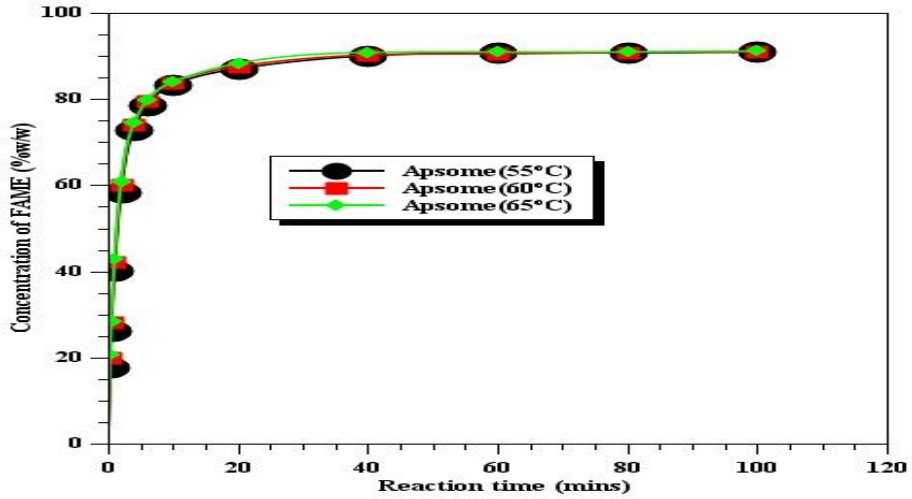

Fig. 2: Effect of reaction temperature on the transesterification reaction.

Fig. 3 shows a clearer reaction trend of the Dg and Mg at the initial stages of the reaction time (0-10 minutes). The trends show an agreement with a typical progress trend observed in consecutive reaction systems on the intermediates. It was observed that the concentration of the intermediates (Mg and Dg) increased as the concentration of triglycerides (Tg) decreased. This continued until about 2.0 minutes of reaction time when maximum intermediate concentrations were reached. After this the decomposition of the intermediates becomes more rapid than their formation and their concentration drops. The maximum points of last intermediates (Dg) were found to be 4.59, 4.20 and 4.10 wt% at 55°C, 60°C and 65°C respectively which correspond to the point of inflection of final product (FAME) of 58.32, 60.15 and 60.84wt% for 55°C, 60°C and 65°C respectively at 2.0 minutes.

The plot of the inverse of triglyceride oncentration against time for the three temperatures is shown in Fig. 4. The slope is k_{Tg} ($wt\%^{-1}min$). The same trends observed in Figure 3 were observed in the case of the intermediates. It is observed that k increased with temperature. The plots equally validate the second order model proposed considering the fact that at all the temperatures the plots agreed with the proposed model equation. This is supported by the high coefficient of determination (all were above 0.97). Fig. 5 shows the Arrhenius plots for the three temperatures to determine the activation energies. It contains the plots of the logarithm of rate constants against the inverse of temperature in Kelvin. The results of the activation energies and rate constants are presented in Table 3.

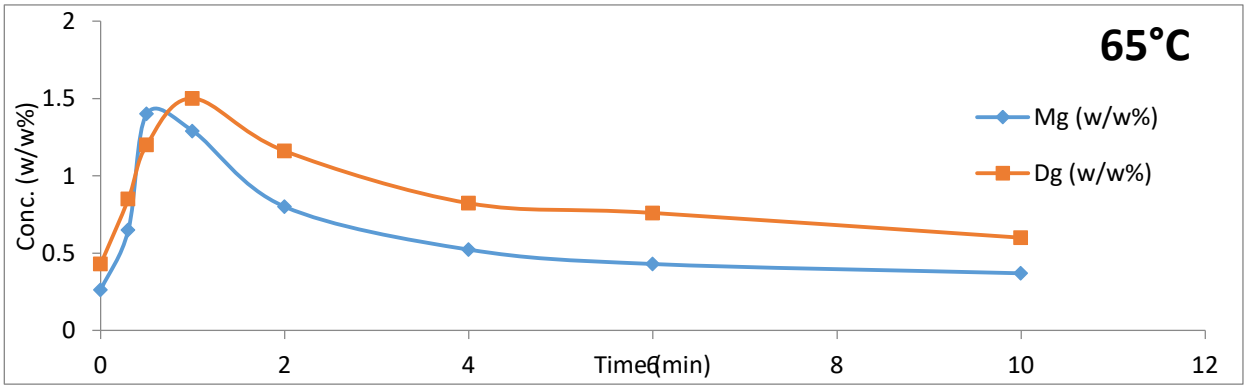

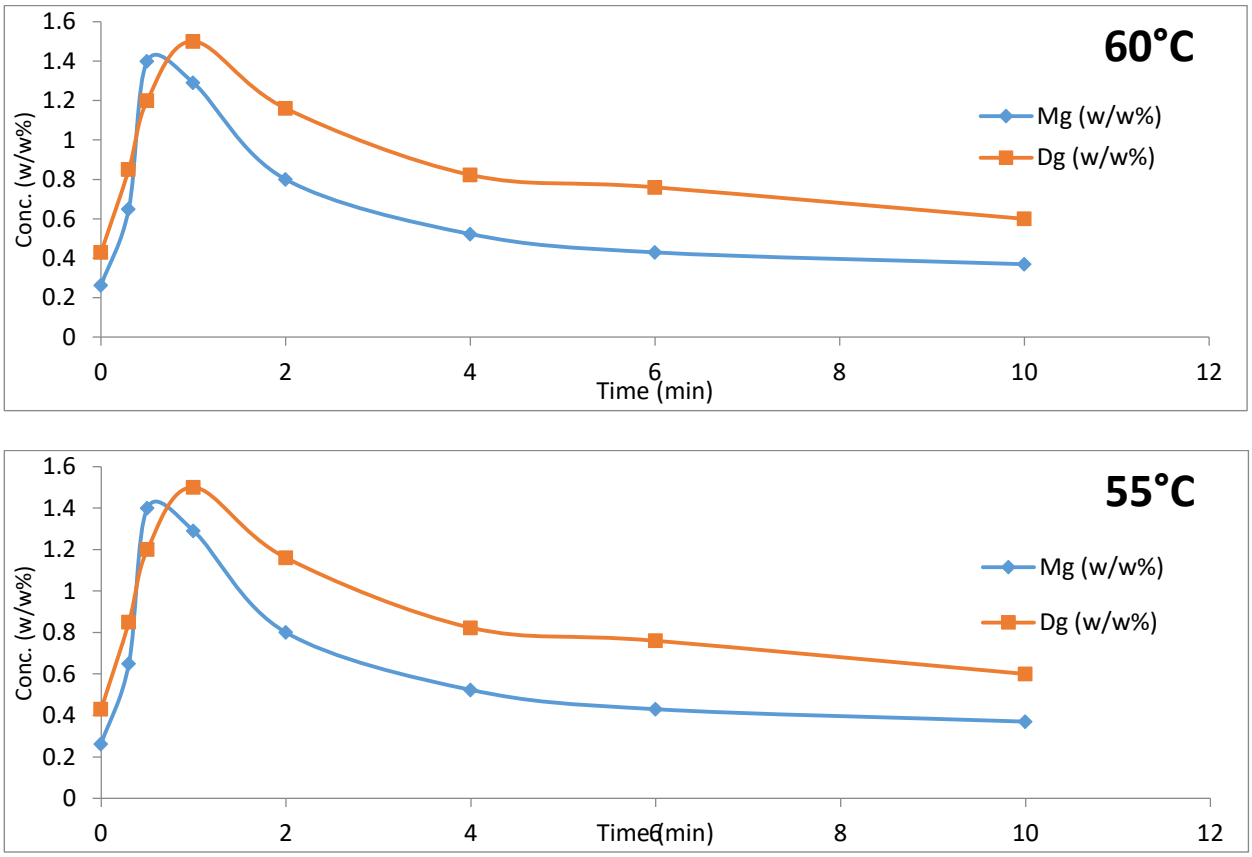

Fig. 3: Progress of intermediates at various temperatures at the initial stage.

Table 3: Summary of the kinetics result for second-order irreversible reaction

Glyceride	Temperature(T)			Rate constant, k (wt%/min)	Log k	Activation energy (Kcal/mol.)
	(°C)	(K)	1/T x10^3(K^{-1})			
Tg ⟶ Dg	55	328	3.05	0.01040	-1.98	6.14
	60	333	3.00	0.01120	-1.95	
	65	338	2.96	0.01160	-1.93	
Dg ⟶ Mg	55	328	3.05	0.01404	-1.85	20.01
	60	333	3.00	0.01460	-1.83	
	65	338	2.96	0.03170	-1.50	
Mg ⟶ Gl	55	328	3.05	0.02470	-1-61	28.50
	60	333	3.00	0.04730	-1.32	
	65	338	2.96	0.07810	-1.11	

DOI: 10.51975/KWZC7505
Journal of the Nigerian Society of Chemical Engineers, 36(1), 2021

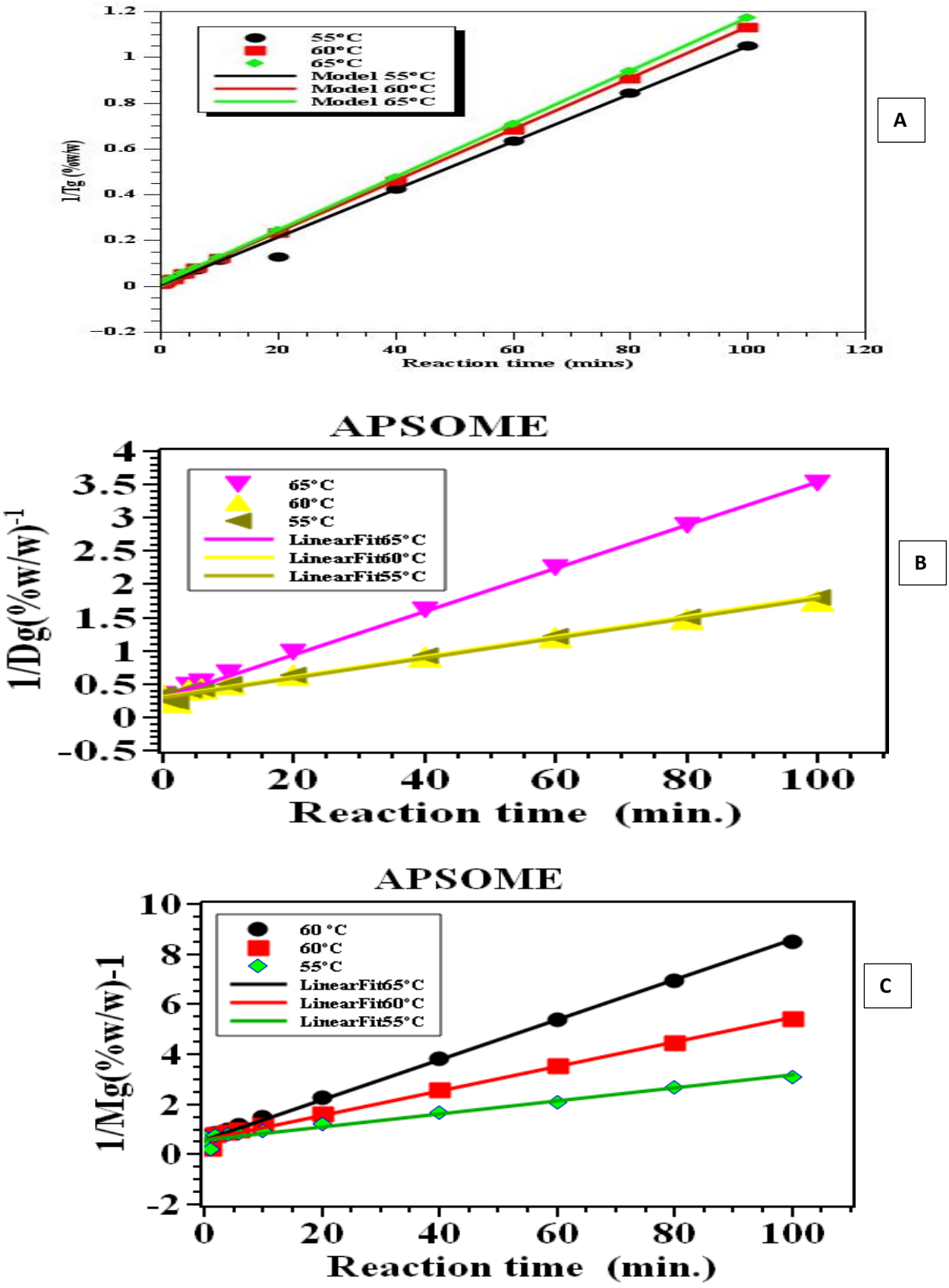

Fig. 4: Second – order reaction irreversible model of triglycerides (A), diglycerides (B) and monoglycerides (C) hydrolysis

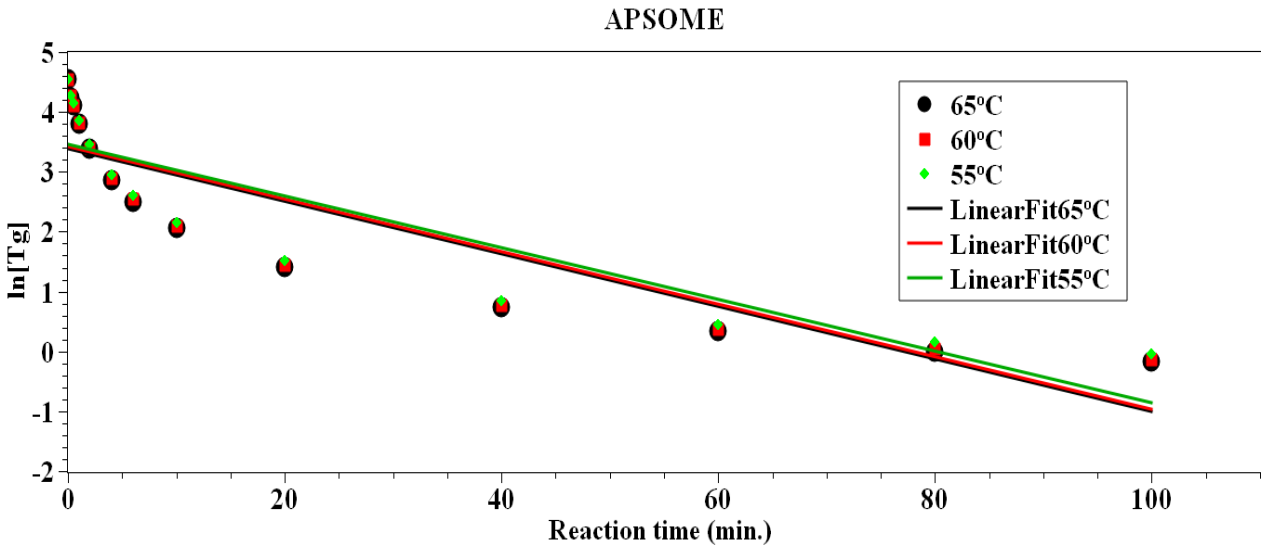

Fig. 5: First – order reaction irreversible model of triglycerideshydrolysis

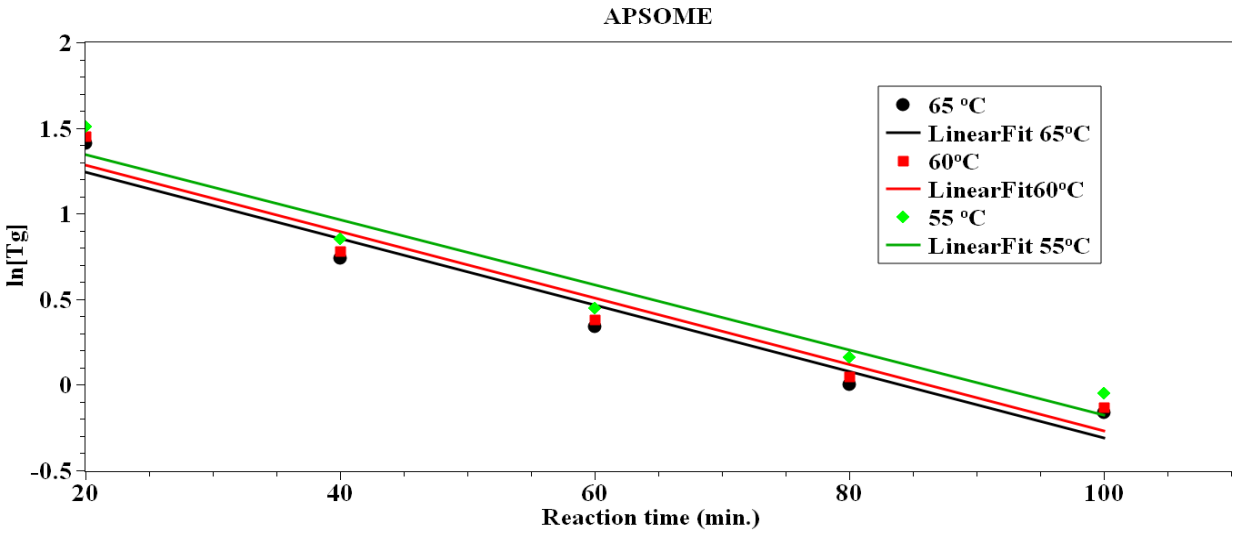

Fig. 6: First – order reaction irreversible model of triglycerides of later stage hydrolysis.

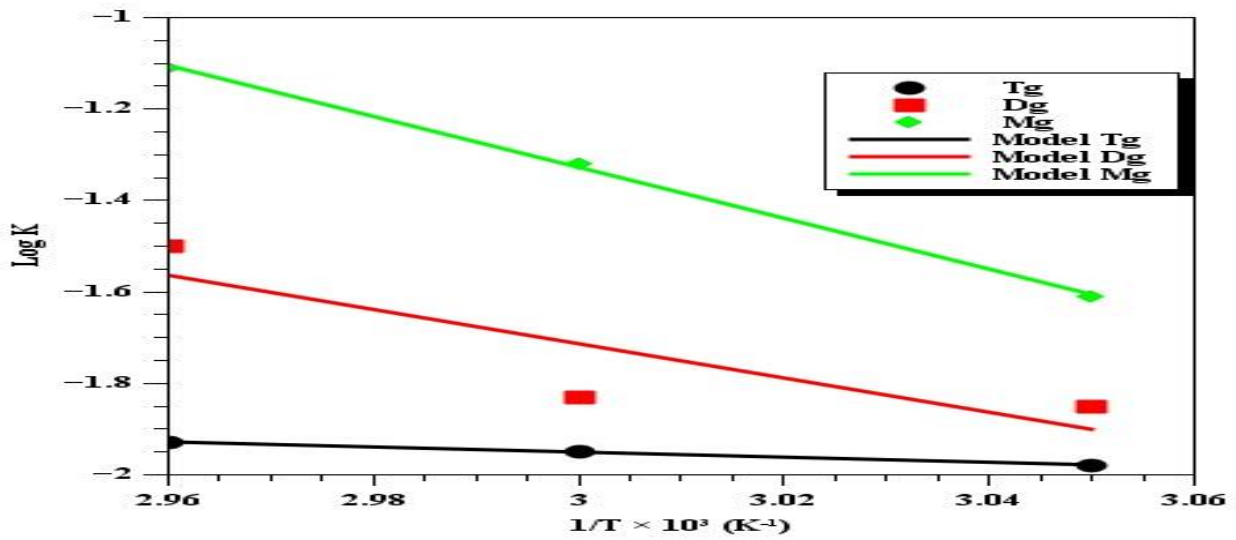

Fig. 7: Arrhenius plot of second order irreversible model reaction rate versus temperature.

Although, the kinetics of base-catalyzed transesterification of African pear seed oil is not widely documented in the literature, the results obtained in this study is comparable withprevious works on other feedstocks. The values 14.7 and 14.2 kcal/min obtained for Tg and Dg hydrolysis of palm oil has been reported in literature (Darnoko and Cheryan 2000) at same temperature. The values of rate constants for the Tg hydrolysis obtained in this research is about 4 times higher than that determined in (Darnoko and Cheryan, 2000) for palm oil at same conditions and about 2 times lower than the values reported in (Reyero et al., 2015) on the kinetics of NaOH catalyzed transesterification of sun flower oil with ethanol.

Also, the percentage conversion of Tg recorded for the seed oils ranged from 89-91% and this is agreement with 91% obtained by Zhang et al., (2010) and 98% obtained in (Darnoko and Cheryan 2000) after 1hour. The model predicts that maximum monoglycerides yield decreases as the reaction temperature increases. This could be due to the fact that the conversion of monoglycerides into glycerol has the highest activation energy among the three transesterification steps. The results show that kinetic constants of the first step (hydrolysis of Tg into Dg and biodiesel) has the smallest values. It is therefore slowest and the rate determining step. It is observed that k increased with temperature. The values of rate constants were used to determine the Arrhenius activation energy from the plots of reaction rate constant (k) versus the reciprocal of absolute temperature (T). Dg and Mg relationship with time followed the same trend with that of Tg. The lower activation energies obtained for the triglycerides hydrolysis indicate that temperature has a profound impact on the reaction according to kinetic theory. Then the higher activation obtained for monoglycerides hydrolysis clearly shows that higher temperature favours the reaction step more than the other steps with lower activation (for multiple reaction). The positive value of the activation energy supports the exothermic nature of transesterification process (Reyero, et al., (2015). The increase in k with temperature follows the magnitude of $k_{Mg}>k_{Dg}>k_{Tg}$ and in agreement with reports of Darnoko and Cheryan (2000). It was observed that triglycerides are the major constituents of the three tropical oil (T_g>94.0%). Similar results have been reported by Kumar *et al.,* (2011), who obtained 92-93% of Tg for mahua oil and 90-92% for *jatropha* oil. However, the results are in contrast to the composition of pongamia oil with Tg, Dg and Mg found to be in the ratio of 42:26:11 (Mushtaq et al., (2014).

3.3 First-order irreversible model

By ignoring the intermediate reactions of diglyceride and monoglyceride, the three steps have been combined in a single step (Birla et al., 2012). However, due to the high molar ratio of methanol to oil, the change in methanol concentration can be considered as constant during reaction. This means that by taking methanol in excess, its concentration does not change the reaction order and it behaves as a first order chemical reaction (Zhang, et al 2010). Least-square approximation was applied, in fitting a straight line to the experimental data, and in each case the coefficient of determination (R^2) was determined. The overall pseudo rate constants determined from the slopes of the straight line plots of ln [Tg] against t shown in Figure 7 are presented in Tables 4. As can be seen from Figure 6, in the reactions conducted at 55, 60 and 65°C, there was a decrease in the coefficient of determination for the pseudo first-order kinetic model. The coefficient of determination is especially important because the value of R^2 x100 represents the percentage of original uncertainty as explained by the linear model. Figure 5 shows that the reaction at these temperatures does not fit the pseudo first-order reaction kinetic model better. This is supported by the lower values of coefficient of determination obtained from the first-order fitted plots (R^2< 0.80) against high coefficient of determination obtained on the second-order irreversible kinetic model (R^2 > 0.97). Similar results have been reported on the kinetics of hydrolysis of nigella sativa (*black cumin*) seed oil catalyzed by native lipase in ground seed where pseudo first-order rate equation at 20, 30 and 40°C; and the pseudo second-order equation at 50, 60 and 70°C (Dandikand Aksoy, 1992). Therefore, it could be that hydrolysis of some oils to methyl esters follows first-order irreversible kinetic models at low temperature ranges (20-40°C). The low temperature ranges is reported to favour the activity of native lipase better than at higher temperatures and this resulted in different mechanisms. But such low temperatures would not favour maximum ester yield in this study because they are far below the reported optimum temperature (Darnoko and Cheryan 2000). Darnoko and Cheryan (2000), has observed that at latter reaction stages (beyond 30 mins) of palm oil hydrolysis to methyl ester, the first-order or zero-order reaction model is the best fitted. Similar observation was made on this study where as from 20 minutes reaction, the reaction follows first-order model with high coefficient of determination (R^2 > 0.94). This is shown in Figure 6. These stages showed low reaction rate due to reduction in the reactants concentration. It implies that at low temperatures and

latter stages of methanolysis of the vegeatble oilsprogesses very slowly and follow first-order kinetic model.

Table 4: First-order model reaction rate constant for APSOME.

Glyceride	Temperature (°C)	Reaction rate constant (min^{-1})	R^2
Triglyceride	55	0.0431	0.80
	60	0.0437	0.80
	65	0.0439	0.80

CONCLUSION

Chemical Kinetic model has been developed for the NaOH – catalyzed methanolysis of African pear seed oils. The second order model describes very well the effects of temperature on the oil conversion and yields of final (biodiesel and intermediate Tg and Mg) transesterification products on irreversible basis. The kinetics of base-catalyzed methanolysis of APSO studied at three different temperatures (65˚C, 60˚C and 55˚C) showed no initial lag phase (usually attributed to mass transfer) in the conversion of Tg. The seed oil conversion increased with increase in temperature. The initial time of reaction recorded high conversion. At about 40 minutes, complete conversion was achieved. The rate constants for APSO methanolysis showed highest values for Mg hydrolysis. However, there was obvious increase in rate constants with increase in temperature.

NOTATIONS

[Al]	Alcohol concentration
Al	Alcohol
APSO	African pear seed oil
APSOME	African pear seed oil methyl ester
A	Arrhenius constant
Dg	Diglycerides
[Dg]	Diglycerides concentration
E_a	Activation energy (kcal/min)
FAAE	Fatty acid alkyl ester
FAEE	Fatty acid ethyl ester
FAME	Fatty acid methyl ester
Gl	Glycerol
[Gl]	Glycerol concentration
k_1-k_3	Rate constants (wt%/.min)
Mg	Monoglycerides
[Mg]	Monoglycerides concentration
T	Temperature (K or °C)
t	Time (minutes)
Tg	Triglyceride
[Tg]	Triglyceride concentration

ACKNOWLEDGEMENT

The authors would like to thank the staff and management of the National Centre for Energy Research and Development (NCERD), University of Nigeria Nsukka, National Research Institute for Chemical Technology (NARICT), Ahmmadu Bello University (ABU), Zaria, and PZ/NOTAP Chemical Engineering laboratory of Alex Ekwueme Federal University, Abakaliki, Nigeria for the availability of the laboratory facilities, apparatus and analytical equipment.

REFERENCES

Abdel-Latiff, A. C. and Abdallah, L. A. (2010).Two optimization methods to determine the rate constants of a complex chemical reaction using FORTRAN and MATLAB.American Journal of Applied Sciences. 7(4):509-517.

Almgrbi, A. M., Hatami, T., Glisic, S. B. and Orloric, A. M. (2014).Determination of kinetic parameters for complex tranesterification reaction by standard optimization methods. Hem. Ind. 68(2): 149-159.

AOAC, (1990). Official methods of analysis, (13th Edition), Association of Official Analytical Chemists, Washington, DC.

Atabani, A. E., Silitonga, A.S., Irfan, A.B., Mahlia, T.M. I., Masjuki, H. H. and Mekhilef, S. A. (2012). comprehensive review on biodiesel as an alternative energy resource and its characteristics. *Renewable and Sustainable energy review*, 16: 2070- 2093.

Birla, A., Singh, B., Upadhyay, S. and Sharma, Y. (2012). Kinetics studies of synthesis of biodiesel from waste frying oil using a heterogeneous catalyst derived from snail shell. Bioresource Technol., 106: 95-100.

Bull, O. S.; George, D. Mc.(2015) Assessment of fuel properties of biodiesel obtained from African Pear (Dyacrodes edulis) seed oil, *Int. J. of Advanced research in Science, Engineering and Technology*, 2 (10), 894-898.

Dandik, L. and Aksoy, H. A. (1992). The kinetics of hydrolysis of Nigella sativa (Black Cumin) seed oil catalyzed by native lipase in ground seed. JAOCS, 69, (12), 1239-1240.

Darnoko, D.; Cheryan, M (2000) Kinetics of palm oil transesterification in a batch reactor, *J. Am. Oil Chem.* Soc. 77, 1263-1267.

Esonye, C., Onukwuli, O. D. & Ofoefule, A. U. (2019) Chemical Kinetics of a Two-step Transesterification of Dyacrodes Edulis Seed Oil Using Acid-Alkali Catalyst. Chemical Engineering Research and Design, 145, 245-257. http://dx.doi.org/10.1016/j.cherd.2019.03.010.

Esonye, C.,Onukwuli, O. D.; Ofoefule, A. U. **(**2018). Modeling of Biodiesel Yield from African Pear Seed (*Dyacrodes edulis*) oil using Artificial Neural Networks, *Journal of the Nigerian Society of Chemical Engineers (JNSChE)*. 33(1), 26-30.

Ilgen, O. (2012). Reaction kinetics of dolomite catalyzed transesterification of conola oil and methanol .Fuel Processing Technology 95, 62-66.

Kumar, G. R.; Ravi, R.; Chadh, A. (2011) Kinetic Studies of Base-catalyzed transesterification reaction of non edible oils to prepare Biodiesel; The effect of co-solvent and temperature, *Energy and Fuels* 25, 2826-2832.
Levenspiel, O. (1999) Chemical Reaction Engineering, 3rd edition, McGraw-Hill.

Menkiti, M. C., Ocholi, O. and Agu, C. M., (2017). Production of environmentally adapted lubricant basetock from jatropha curcas specie seed oil. Int J Ind Chem DOI 10.1007/s40090-017-0116-1.

Mittelbach, M.(1996). Diesel fuel derived from vegetable oils: specification and quality control of biodiesel. *Bioresource Technol*. 56,7-11.

Mushtaq, A, Shazia, S., Lee, K.T., Ahmed, Z.A., Haleema, S., Muhammed, Z., Taibi Ben, H., Muhammed, A.A.& Rasool, B.T.(2014). Distaff Thistle Oil : A possible new non-edible feedstock for biogas energy. *International Journal of Green Energy*, 10: 1-27.

Noureddini, H and Zhu, D.(1999). Kinetics of transesterification of soybean oil. J.A.O.C.S. 74:1457-1462.

Ogunsuyi, H. O.(2015) Production of biodiesel using African pear (*Dyacrodes edulis*) seed oil as a feed stock, *Academia Journal of Biotechnology*, 3(5), 085-092
Okullo, A.A and TemuA.K(2015).Modelling the kinetics of *jatropha* oil transesterification. Energy and Power Engineering. 7:135-143: doi:10.4236/epe2015.74013.

Onukwuli, O. D. and Ude, C. N. (2018).Kinetics of *Dyacrodes edulis* seed oil (APO) methanolysisCatalyzed by Phosphoric acid-activated Kaolin clay. Appl. Petrochem Res. https://doi.org/10.1007/513203-018-0210.0

Orifici. L.I., Bhal, C.D., Gely, M.C., Bandoni, A and Pagano, A.M(2013) Modelling and simulation of biodiesel production in a pilot continous reactor.Mecanica Computcional XXXII: 1451-1461.

Patel, V. (1999).Cetane Number of New Zealand diesel, Report, office of Chief Gas Engineer, Energy Inspection Group.Ministry of Commerce Press, Wellington, New Zealand.

Patil, P., Gude, V.G., Pinappu, S and Deng, S(2011). Transesterification kinetics of *Camelina sativa* oil on metal oxide catalyst under conventional and microwave heating conditions. Chemical Engineering Journal. 168:1296-1300.

Reyero, J. G.; Arzamendi, S.; Zabala, M. L.; Gandia, P. (2015) Kinetics of NaOH-catalyzed transesterification of sun flower oil with ethanol to produce biodiesel, *Fuel Processing Technology* 129, 147-155.

Vujicic, D., Comic, D., Zarubica, A., Micic, R., & Boskovi, G., 2010. Kinetics of biodiesel synthesis from sunflower oil over CaO heterogeneous catalyst.*Fuel* 89, 2054– 2061.

Wan, Z and Hammed, B. H. (2011). Transesterification of palm oil to methyl esters on activated carbon supported calcium oxide catalyst. Bioresource Technology 102, 2659-2664.

Wang, Y; Seo, B; Wang, B; Zamel, N; Jiao, K. and Adroher, X, C. (2020). Fundamentals, materials and machine learning of polymer electrolyte membrane fuel cell technology. Energy and AI, 1: 100014. Doi.org/10.1016/jegyai..

Zanette A. F., Barella,R.A., Pergher, S.B. C, Treichel, H., Oliveira, D., Mazatti, M.A., Silva, E.A., and Oliveira J.V(2011). Screening, optimization and kinetics of *jatropha curcas*oil transesterification with hetrogeneous catalysts. Renewable Energy 36:726-731.

Zavarukhin, S.G., Ivanova, A.S., Kukushkin R.G., Yuhebedev, M., Simonov, A.N., Sheristyuk, O. V., Yakovlev, V.A. and Trusov, L.J(2013). Kinetics of barium-aluminium oxide catalyst with the methanol pressure taken into account.Biocatalysis. 5(4):342-349.doi:10.1134/s207005413040090.

Zhang, L., Sheng, B., Xin, Z., Liu, Q., and Sun, S., (2010). Kinetics of transesterification of palm oil and dimethyl carbonate for biodiesel production at the catalysis of heterogeneous base catalyst.Bioresource.Technol. 101, 8144–8150.

DOI: 10.51975/SQYB7600
Journal of the Nigerian Society of Chemical Engineers, 36(1), 2021

THERMAL AND OVERPRESSURE HAZARDS MODELLING AND SIMULATION: A CASE STUDY OF REFINERY FIRED HEATER

Jamilu, H.[1], Abubakar-Zaria, U.[1,*] and Shuwa, S. M. [1]
[1]Department of Chemical Engineering, Ahmadu Bello University, Zaria
*Correspondence: E-mail: uabubakar@abu.edu.ng and augayya@yahoo.com ; Tel.: +2348033690787

ABSTRACT

Crude oil-fired heaters are associated with considerable fire and explosion hazards. The heaters present higher risks at later operational life due to ageing, wear and obsolescence. It is therefore important to re-evaluate such heaters to determine the adequacy or otherwise of the existing safeguards. This paper presents results of studies on hazard levels in aged fired heaters through quantitative consequence modeling method. A number of credible failure scenarios were considered. In particular, characteristics of potential jet fires due to Liquefied Petroleum Gas (LPG) leaks from hole sizes: 15, 30, 50 and 100 mm were investigated. For the 100 mm hole size, it was found that thermal radiation level of up to 37.5 kW/m^2 could be experienced within 25 m radius of the heater, which is enough to affect nearby operators severely and could also adversely affect critical pieces of equipment around. Fireball potential with peak thermal density of about 12.5 kW/m^2 was also observed within 2 m radius. For the 100 mm hole size, lower flammability limit of the fuel could be attained within 16 m downwind which poses flash fire risks. Overpressures of 1.02, 1.14 and 1.21 bar could be experienced at 30, 6 and 4 m respectively away from the fired heater which could result in partial demolition of structures that are within the radius.Overall, the results indicate that the risk profile is very sensitive to leak sizes, operating and atmospheric conditions as well as the fuel quantity being held, among others. For the chosen case study, higher integrity protection layers, in form of safety instrumented systems, relief, blow down and alarm systems, are recommended.

Keywords: *Downwind distance; Consequence modeling; Radiation intensity; Flame length; Overpressure; Toxicity; Liquefied Petroleum Gas.*

INTRODUCTION

Fire is the most frequently reported process-related incident in Nigerian petroleum industry (DPR annual report, 2017). Fire may result in no damage/loss, medium to catastrophic damage/loss, depending upon the fire characteristics (type of fire, mode of occurrence and potential of escalation). Leakage or spillage of flammable material can lead to a fire that is triggered by any number of potential ignition sources (sparks, open flames, etc.). Depending upon the types of leakage scenarios, fires are mainly categorized into four types, jet fire, pool fires, flash fires and fire balls, therefore there is need to study the risk associated with fire (Niazi *et al*. 2006). Figure 1 is a schematic flowchart showing a typical risk assessment process.

Consequence analysis predicts magnitude, direction vulnerability zones of negative effects of incidents. Once these zones are identified, the risk analysis suggests measures of mitigation or prevention that can be proposed to eliminate damage to plant and potential injury to personnel. Estimation of vulnerability zone of such an incident plays an important role in preparing a realistic emergency plan (Pula *et al*., 2005). Consequence modelling refers to the calculation or estimation of numerical values (or graphical representations of these) that describe the credible physical outcomes of loss of containment scenarios involving flammable, explosive and toxic materials with respect to their potential impact on people, assets, or safety functions (Assessment Directory, 2010).

Estimation of vulnerability zone due to credible scenarios via consequence analysis would play important role in preparing realistic preventive and mitigative measures- including emergency response and evacuation plan. Physical models can be used to estimate hazards zones in case of accidents (Osman *et al*., 2015). For these reasons, it is important to determine consequences due to accidental leak or rupture of a component at various locations around the heater. The following section highlights the methodology involved in this study.

This work sets out to model and simulate the consequences due to liquefied petroleum gas leakage

from fuel pipe supplying one of the fired heaters of Kaduna Refining and Petrochemical Company (KRPC). Further details on this case study are given below.

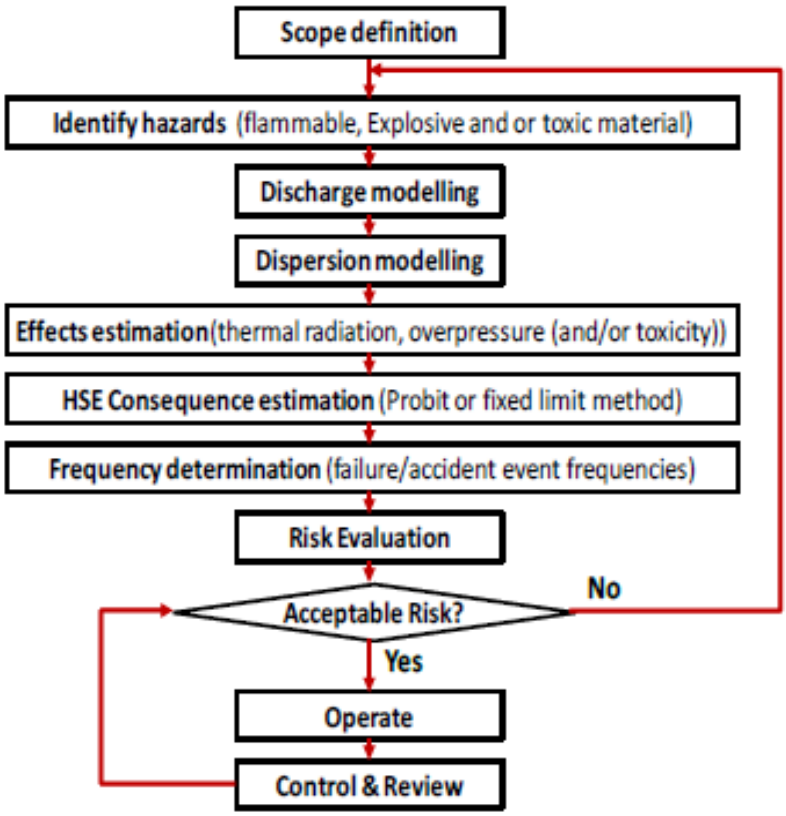

Figure 1. Typical risk assessment procedure (Abubakar *et al*., 2017)

Case Study of Kaduna Refining and Petrochemical Company (KRPC)

The crude heating section (Fired Heater 10H01) is one of the most hazardous sections of the Crude Distillation Unit 1 (CDU-1). This is where the crude is heated to distillation temperature before it is finally charged into the fractionator. This is because the fired heater contains naked flames and handles crude in the pipe which is highly flammable. In this work, the emphasis was on hazard resulting from fire that is associated with crude discharge fired heater (10H01) of KRPC (CDU-1 Manual, 1978).

The fired heater is an exchanger that transfers heat from the combustion of fuel to fluids contained in tubular coils within an internally insulated enclosure. The fired heaters are an essential component of CDU-1 of the KRPC. The functions served by fired heaters in chemical plants are many, these include: simple heating or provision of sensible heat and raising the temperature of the charge to heating and partial evaporation of the charge, where equilibrium is established between the unvapourised liquid and the vapour. The charge leaves the furnace in the form of a partially evaporated liquid in equilibrium. Fired heaters may also be used to provide the heat required for cracking or reforming reactions. Fired heaters process fluids flowing inside tubes mounted inside the furnace, the fluid is heated by gases produced by the combustion of a liquid or gaseous fuel. The major advantage of fired heaters is the achievement of continuous operation (Garg, 1997). These heaters are widely used for heating purposes in petroleum refining, petrochemical plants and other chemical process industries.

Fired heaters present high safety risks as the process streams contain highly flammable hydrocarbons with potential catastrophic fire incidents. Due to ageing (over 30 years after commissioning of the refinery), wear and obsolescence, the fire risk profile of the crude charge

fired heater (10H01) of KRPC within the CDU-1 needs to be reevaluated. For instance, in the year 2017 there was explosion at fired heater 12H01 at KRPC due to tube rupture which led to the breakdown of the unit for about two years. Therefore, it is important to determine the vulnerability zone of other heaters in the company.
Table 1 presents the potential effects due to a number of radiation intensity levels. The table is usually used to estimate potential thermal damages/impacts.

Table 1. Effect of Various Radiation Intensities

Intensity of heat radiation kw/m^2	Potential effect
1.6	Insufficient to cause discomfort for long exposure
2.2	Threshold pain. No reddening or blister
4.2	First degree burn
8.3	Second degree burn
10.8	Third degree burn
15.0	Piloted ignition of wood
25.0	Spontaneous ignition of wood
4.0	Glass crack
12.0	Plastic melt
19.0	Cable insulation degrade
37.5	Damage to process equipment
100.0	Steel structure fail

Source: (AIChE/CCPS, 2000)

Table 2 presents certain pressure levels and the corresponding potential overpressure effects and could be used to predict the damages resulting from a range of explosion overpressures.

Table 2: Overpressure Effects of Explosion

Pressure (psig)	Damage
0.02	Annoying noise (137 dB if of low frequency 10-15 Hz).
0.03	Occasional breaking of large glass windows already under strain.
0.04	Loud noise (143 dB), sonic boom glass failure.
0.1	Breakage of small windows under strain.
0.15	Typical pressure for glass breakage.
0.3	“Safe distance” (probability 0.95 no serious damage beyond this value).
0.4	Limited minor structural damage.
0.5-1.0	Large and small windows usually shattered; occasional damage to window.
0.7	Minor damage to house structures.
1.0	Partial demolition of houses, made uninhabitable.
1-2	Corrugated asbestos shattered; corrugated steel or aluminium panels, fastenings.
1.3	Steel frame of clad building slightly distorted.
2	Partial collapse of walls and roofs of houses.

Pressure (psig)	Damage
2-3	Concrete walls, not reinforced, shattered.
2.3	Lower limit of serious structural damage.
2.5	50% destruction of brickwork of houses.
3	Heavy machines in industrial building suffered little damage; steel frame.
3-4	Frameless, self –framing steel panel building demolished; rupture of oil storage.
4	Cladding of light industrial buildings ruptured.
5	Wooden utility poles snapped; tall hydraulic press in building slightly damaged.
5-7	Nearly complete destruction of houses.
7	Loaded train wagons overturned.
7-8	Brick panels, 8-12 in. thick, not reinforced, fail by shearing or flexure.
10	Probable total destruction of buildings, heavy machines tools moved and badly damaged, very heavy machine tools (12,000lb) survived

Source: MS. K.G.O.C Terminals PVT LTD

The consequence modelling involves three major steps. Firstly, the discharge calculations are carried out to determine the release characteristics for the hazardous chemicals (including depressurization to ambient). Scenarios which may be modelled include: releases from vessels (leaks or catastrophic ruptures), short pipes or long pipes and releases of combustion products following a warehouse fire. Thermo-physical states considered include releases of sub-cooled liquid, superheated liquid and/or vapour phase releases. Other conditions often considered are: unpressurized/pressurized releases, continuous, time-varying and/or instantaneous releases (Witlox, 2010).

Secondly dispersion calculations are carried out to determine the concentrations of the hazardous chemical when the cloud travels in the downwind direction. This includes effects of jet, heavy-gas and passive dispersion. In the case of a two-phase release, material rainout may occur, hence pool formation/spreading and re-evaporation may also have to be modelled. Also, effects of indoor dispersion (for indoor releases) and building wakes can be accounted for (Witlox, 2010).

Thirdly, toxic or flammable calculations are carried out. For flammables, ignition may lead to fireballs (for instantaneous releases), jet fires (for pressurised flammable releases), pool fires (after rainout) and vapour cloud fires or explosions. Radiation calculations are carried out for fires, while overpressure calculations are carried out for explosions.

For each event, the probability of fatality is determined using toxic or flammable PROBIT function given in equation 1.

$$P_r = -36.38 + 2.56 * \ln (t * q^{4/3}) \quad \ldots\ldots . (1)$$

Where q is the radiation heat flux, t is the time of exposure and Pr is the PROBIT function for heat radiation lethality (Pula et al., 2005).

Probability of fatality (in percentage) can be calculated from equation 2, (CCPS 2000)

$$P = 50[1 + \frac{P_r - 5}{|P_r - 5|} \text{erf} (\frac{|P_r - 5|}{\sqrt{2}}) \quad \ldots\ldots (2)$$

Expected fatality can be calculated from equation 3

$$Expected\ fatality = P * N(exposed\ people) \quad \ldots\ldots\ldots (3)$$

Determination of the parameters such as flame dimensions, release rates, heat flux and distances to radiation levels is an important aspect of the risk assessment process (Abubakar et al., 2017).

METHODOLOGY

This work applies Process Hazard Analysis Software Tool (PHAST). Key data/information and some fundamental assumptions used are presented in Table 3.

Table 3: Required input parameters and specification

Parameter	Specification	Reference
Location under consideration	KRPC	
Case study location coordinate & date	10.41159 N,7.49065 E 28/02/2019, 2pm	Measured
Wind speed	5 m/s maximum	Measured
Wind direction	SSW/208.150 upper angular limit	Measured

Solar radiation flux	1 kW/m^2	Measured
Ambient temperature	28 ^{0}C maximum	Measured
Pasquill stability	Class D	Measured
Humidity	78 %	Measured
Cloud cover	67 % cloud level	Measured
Altitude	620 m	
Pipe diameter	0.16m	Measured
Height/elevation	2.65 m	Measured
Temperature at burner	45 ^{0}C	CDU-1 Crude Charge heater (10H01) Design Specification
Pressure at burner	1.5 bar + 1 bar atm	"
Phase/state of release	Liquid	"
Inventory/consumption rate	0.35 kg steam/kg oil	"
Leak sizes identified	15 mm, 30 mm, 50 mm and 100 mm	"
Assumption	Unbreaking end of a pipe is connected to an infinite tank source	
Softwares	PHAST 7.2 and ALOHA 5.4.7	Internet

These input data were used in the identified scenario i.e. LPG leak as shown in Figure 2 and was simulated. After the simulation, the result of the different fire models was selected and analyzed considering wind speed and atmospheric stability.

The scenario was selected after careful study of the design and operating principles of the fired heater. Leak sizes were selected based on literature and KRPC maintenance record (further details given in Table 3). The simulation exercise was based on a range of fire models, available in PHAST - considering wind speed and atmospheric stability. The consequence study results were analyzed for the different leak sizes, injuries potentials and catastrophic equipment damage within the study perimeter.

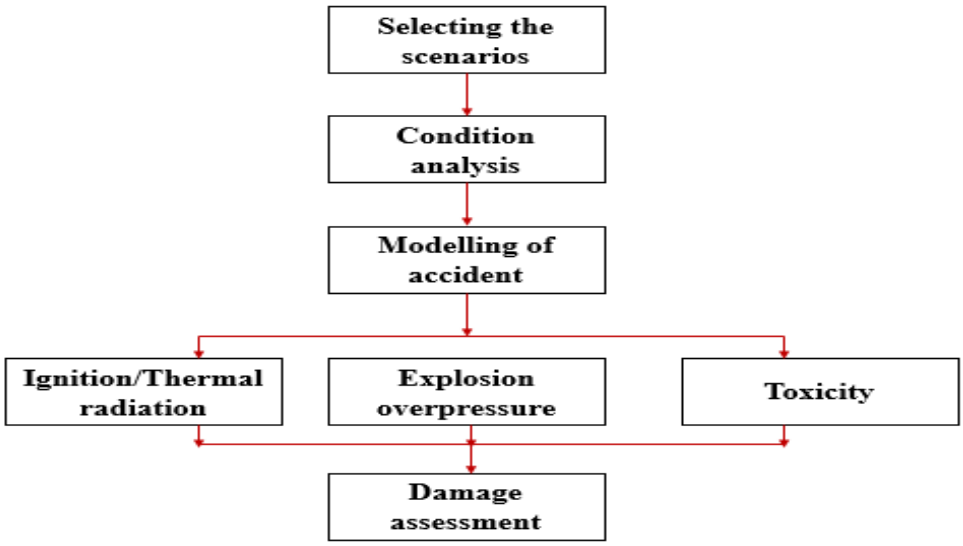

Figure 2: Research Methodology (adopted from Mohammad *et al.*, 2018)

A number of other input details including: wind direction, solar radiation flux, ambient temperature, Pasqual stability, humidity and Cloud cover were specified to reflect the situation under study (Table 3).

RESULTS AND DISCUSSIONS

Table 4 gives the jet fire flame length and downwind distance at which 4.0, 12.5 and 37.5 kW/m^2 radiation intensities are likely to be experienced.

Table 4: Jet fire downwind distance to experience defined radiation levels, for Weather Category 5/D

Scenario	Down Distance [m]to Radiation Levels			
	Flame length	4 kW/m^2	12.5 kW/m^2	37.5 kW/m^2
15mm Leak	5.29	n/a	n/a	n/a
30mm Leak	9.956	10.95	n/a	n/a
50mm Leak	15.7	20.65	15.53	n/a
100mm leak	27.26	40.77	32.55	25.41

Figure 3 gives the radiation levels and respective downwind distance for jet fire

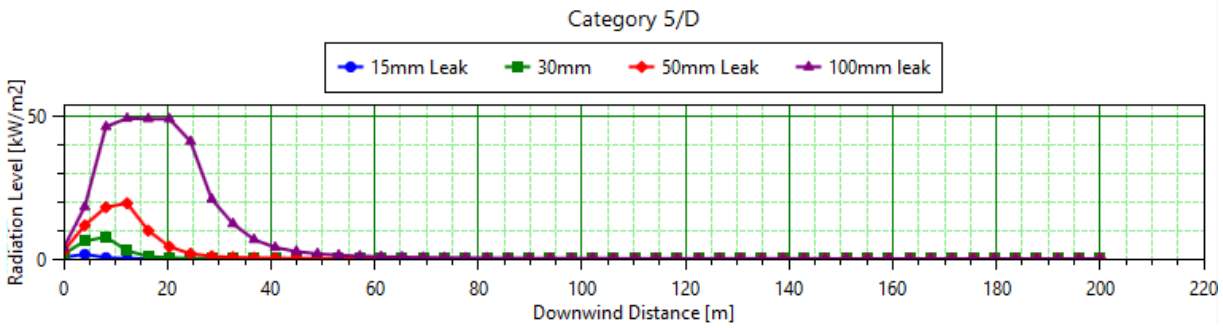

Figure 3: Radiation vs Distance for Jet fire

For Jet Fire, using PHAST the radiation level was plotted for the leakage sizes of 15, 30, 50, and 100 mm in 5/D climate weather as shown in Figure 3, the result of the flame length, radiation levels and calculated distance in downwind direction are presented in Table 4. As depicted in Table 4, the 100 mm leak size has the highest flame length followed by 50 mm, 30 mm and least 15 mm leak size. 4, 12.5 and 37.5 kW/m^2 intensity could not be experienced at 15 mm leak size, 12.5 and 37.5 kW/m^2 intensity could not be experienced at 30mm leak size, 37.5 kW/m^2 could not be experienced at 30 mm leak size and all the defined radiation levels could be experience at 100 mm leak size.

The following equipments; 51-31A, LAB flare knockout drum 90T01, VDU heater 15H01, NHU heater11H01, CRU heater 12H01 column10C01, column 10C07, desalter 10DO3, and heat exchangers 20E0C were identified to be surrounding the heater at approximate and respective distances of 80, 55, 30, 150, 181, 16, 43, 92, 166 and 200 m away from the heater (10H01) as shown in Plate 3. Hence 10C01 fractionator that is in the wind direction could experience 37.5 kW/m^2 radiation at 100 mm leak size which could result in catastrophic damage of the column while 10C07 may experience 4 kW/m^2 radiation intensity which could result in first degree burn on the personnel around as highlighted in Table 1 and could also trigger another accident. It can be observed that radiation consequences are concentrated more toward the downwind direction due to flame tilt caused by the wind as equally reported by (Pula *et al*., 2005). Table 5 gives the fireball downwind distance to experience 4, 12.5 and 37.5 kw/m^2 radiation intensities and fireball diameter.

Table 5: Fireball downwind distance to experience defined radiation levels, for Weather Category 5/D

Scenario	Down Distance [m]to Radiation Levels			
	4 kw/m^2	**12.5 kw/m^2**	**37.5kw/m^2**	**Fireball Diameter**
15mm Leak	7.128	1.756	n/a	4.607
30mm Leak	7.128	1.756	n/a	4.607
50mm Leak	7.128	1.756	n/a	4.607
100mm leak	7.128	1.756	n/a	4.607

Figure 4 gives radiation levels and respective downwind distance for fireball

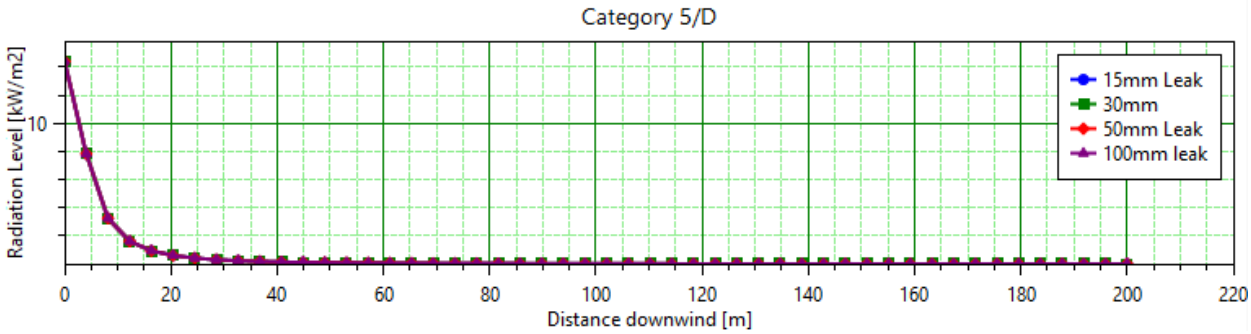

Figure 4. Radiation vs. Distance for Fireball

For the fireball, 15, 30, 50 and100 mm leak size show the same fire ball diameter of 4.607 m also the same downwind distance of 7.128 m to 4kw/m^2 intensity level, and 1.756 m to 12.5 kw/m^2 intensity. 37.5 kw/m^2 intensity could not be experienced for the different leak sizes as shown in Figure 4 and Table 5. The 12 kW/m^2 radiation intensity which could be experienced up to a distance of 1.756m from the epicenter may result in damaging of plastic materials and second degree burn to operators that are within the radius.

Table 6 gives scenarios downwind distance to lower and upper flammability limit of flash fire

Table 6: Flash fire downwind distance to defined concentrations, for Weather Category 5/D

Scenario	Down Distance [m]to LFL, LFL Fraction and UFL		
	LFL[m]	LFL[Fractions]	UFL
15mm Leak	3.211	5.644	0.6181
30mm Leak	5.17	10.45	1.224
50mm Leak	9.92	16.15	2.026
100mm leak	16.25	22.46	4.01

Figure 5 shows the flash fire envelope downwind distance for different scenarios at concentration of 8000 ppm

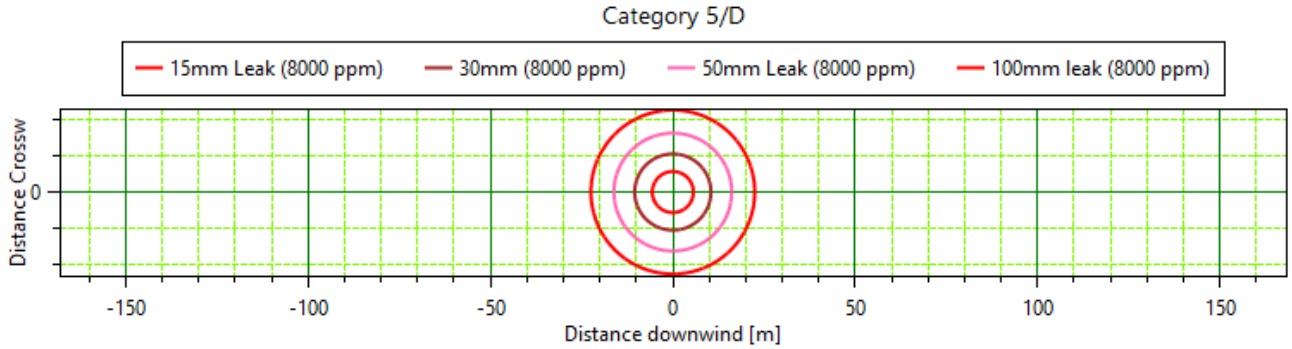

Figure 5: Flash Fire Envelope

Figure 5 shows that 15, 30, 50 and 100 mm leak sizes have the maximum downwind distances to Lower Flammability Limit (LFL) of 5. 64, 10.45, 16.15 and 22.46 m respectively with 100 mm leak scenario having the highest distance, the increase of LFL is due to increase in leak size. The LFL gives an idea on where the ignition could start below which no ignition is expected stoichiometrically. The flash fire envelope at concentration of 8000 and 16000 ppm for different scenarios is shown in Plate I.

Plate I: 10H01 LPG Fuel Pipe Flash Fire Envelope (on KRPC Arial Map)

Table 7 gives downwind distance to defined explosion overpressure for the different scenarios.

Table 7: Late explosion overpressure downwind distance to experience defined overpressures, for Weather Category 5/D

Scenario	Max. Distance [m]to Overpressure		
	1.02068 bar	**1.1379 bar**	**1.2068 bar**
15mm Leak	0	0	0
30mm Leak	25.15	12.94	12.21
50mm Leak	29.01	13.7	12.77
100mm leak	0.0	0.0	0.0

From Table 7, it can be seen that none of the three pressure levels was observable in the case of the 15 mm leak size which suggests that the concentration falls below the Lower explosive Limit. The Upper explosive limit was also exceeded in the case of the 100 mm leak size hence there was no explosion. However, both 30 and 50 mm leak cases fell within the explosive limits.

The 1.2068 bar overpressure could result in minor damage to structures, partial demolition of houses and shattering of corrugated asbestos as highlighted in Table 2.

Table 8 gives downwind distance to defined explosion overpressure for the different scenarios

Table 8: Maximum overpressure distance to experience defined overpressures, for Weather Category 5/D

Scenario	Max. Distance [m]to Overpressure		
	1.02068 bar	**1.1379 bar**	**1.2068 bar**
15mm Leak	0	0	0
30mm Leak	30.3	5.9	4.4
50mm Leak	38.0	7.4	5.5
100mm leak	0.0	0.0	0.0

For leak size 30 mm, overpressures of 1.02, 1.14 and 1.21 bar could be experienced at about 30, 6 and 4 m respectively away from the fired heater which could result in partial demolition of structures that are within the radius as highlighted in Table 2. For the 15 and 100mm leak size, all the overpressure scenarios (1.02 - 1.21 bars) may be experienced right at the epicenter.

CONCLUSION

From the results presented above, it can be seen that the 30m radius (with the crude oil fired heater at the epicenter) is particularly vulnerable to both fire and overpressure impacts. In particular, radiation level of up to 37.5 kW/m^2 could be experienced 25m away from the fired heater in the downwind direction. This radiation level is fatal and could damage process equipment catastrophically. Also, there is potential for ignition up to 16m away from the fired heater. Flame length and downwind distance to radiation intensity of a jet fire increase with increase in leak size. Overpressures of 1.02, 1.14 and 1.21 bar could be experienced at 30, 6 and 4 m respectively away from the fired heater which could result in partial demolition of structures that are within the radius. Leak size plays a significant role in fire accident. Therefore, leak should be prevented by minimizing number of joints, elbows, bend, using corrosion resistant pipes and proper maintenance practice. Ignition sources, such as sparks, hot surfaces and open flames should be eliminated within the 30 m radius (at least). Robust protective layers such as bund/dike, efficient emergency response plan and high integrity safety instrumented systems should be put in place to prevent/mitigate the thermal and overpressure incidents.

REFERRENCE

Abubakar, U., Hamisu A. A., Sabiu B. and Dan-asabe B. (2017). Effects of Operating Conditions on Gas Release Thermal Consequences: a case study of the Trans-

Saharan Gas Pipeline. *Nigerian Journal of Technological Research,* 12(2), 27-33.

AIChE/CCPS, Guideline for chemical process quantitative risk analysis, second edition, New York, 2000.

Assessment, R., & Directory, D. (2010). Consequence modelling, international association of oil and gas producers, United Kingdom, www.ogp.org.uk.

Crude Distillation Unit 1 (CDU-1) Crude Charge heater (10H01) Design Specification (1978). Kaduna refining and petrochemical company (KRPC) Ltd. Ident No. 10H01-024

Department of Petroleum Resources (DPR), 2017 Nigerian Oil and Gas Industry Annual Report.

Garg, A. (1997). Optimize Fired Heater Operations to Save Money. *Hydrocarbon Processing*, 76, 97-112.

Garg, A. (1997). Optimize Fired Heater Operations to Save Money. *Hydrocarbon Processing*, 76, 97-112.

Mohammad H. B., Somayeh F. D., Roohalah H., Sayed M. J. and Alireza K., (2018). Modelling the Consequences of Explosion, Fire and Gas Leakage in Domestic Cylinders Containing LPG: Annals of Medical and Health Sciences Research January2018 Vol 8 Special Issue 184

MS. K.G.O.C Terminals PVT LTD. 'Quantitative Risk Analysis of Bulk Liquid Storage Terminals' SY. no: 274P, 275P, 236/2CP, 239/2P & 249/2P, Visakhapatnam, Andhra Pradesh, India

National oceanic and atmospheric administration(NOAA), United Sate, retrieved 25th July 2020 from https://response.restoration.noaa.gov/oil-and-chemical-spills/chemical-spills/resources/acute-exposure-guideline-levels-aegls.html#whatare

Niazi, U.M., Nasif, M.S., Muhammad, M.B. and Imran, M., (2006). Modeling of Pool Fire and Injury Prediction Considering Different Wind Speeds and Directions in Offshore Platform. *ARPN Journal of Engineering and Applied Sciences*,13000-13005.

Osman, K., Geniaut, B., Herchin, N., & Blanchetiere, V. (2015). A review of damages observed after catastrophic events experienced in the mid-stream gas industry compared to consequences modelling tools, ICHEME Release, 160, 1–12.

Pandya, N., Marsden, E., Floquet, P., & Gabas, N. (2008). Toxic release dispersion modelling with PHAST: parametric sensitivity analysis.

Pula, R., Khan, F.I., Veitch, B. and Amyotte, P. R., 2005. Revised fire consequence models for offshore quantitative risk assessment. *Journal of loss prevention in the process industries*, 18(4-6), 443-454.

Witlox, H. W. M., 2010. Overview of Consequence Modelling in the Hazard Assessment Package Phast. Assessment, (January 2010), 1–8.

JOURNAL OF THE NIGERIAN SOCIETY OF CHEMICAL ENGINEERS

INSTRUCTION TO AUTHORS

1. TYPES OF PUBLICATION

The Journal of the Nigerian Society of Chemical Engineers will publish articles on the original research on the science and technology of Chemical Engineering. Preference will be given to articles on new processes or innovative adaptation of existing processes. Critical reviews on current topics of Chemical Engineering are encouraged and may be solicited by the Editorial Board. The following types of articles will be considered for publication:

a. Full length **articles or review papers**.
b. **Communication** – a preliminary report on research findings.
c. **Note** – a short paper describing a research finding not sufficiently completed to warrant a full article.
d. **Letter to the Editor** – comments or remarks by readers and/or authors on previously published materials.

The authors are entirely responsible for the accuracy of data and statements. It is also the responsibility of authors to seek ethical clearance and written permission from persons or agencies concerned, whenever copyrighted material is used.

For now the journal is published twice in a year, March/April and September/October.

2. MANUSCRIPT REQUIREMENTS

a. The **Manuscript** should be written in clear and concise English and typed in Microsoft Word using double spacing on A4-size paper, Times New Romans font and 12 point. A full length article or review should not exceed 15 pages. Margin should be Normal (i.e. 2.54cm for Top, Bottom, Left & Right margins).
b. The **Manuscript** should be prepared in the following format: Abstract, Introduction, Materials and Methods, Results, Discussion, Conclusion, Acknowledgements, and References..
c. The **Manuscript** must contain the full names, address and emails of the authors. In the case of multiple authorship, the person to whom correspondence should be addressed must be indicated with functional email address. As an examples, authors' names should be in this format:
Momoh, S. O., Adisa, A. A. and **Abubakar, A. S.**

If the addresses of authors are different, use the following format:

***Momoh, S. O.[1], Adisa, A. A.[2]** and **Abubakar, A. S.[3]**

Use star * to indicate the corresponding author.

d. **Symbols** should conform to America Standard Association. An abridged set of acceptable symbols is available in the fourth edition of Perry's Chemical Engineering Handbook. Greek letters, subscripts and superscripts should be carefully typed. A list of all symbols used in the paper should be included after the main text as **Nomenclature**.
e. All **Units** must be in the SI units (kg, m, s, N, etc).
f. The **Abstract** should be in English and should not be more than 200 words. The Abstract should state briefly the purpose of the research, methodology, results, major findings and major conclusions. Abstracts are not required for Communications, Notes or Letters.
g. **Citation** must be in the Harvard Format i.e. (Author, Date). Examples are (Smith, 1990) or (Jones et al, 2011). (Kemp, 2000) demonstrated that …..; (Mbuk, 1985; Boma, 1999; Sani, 2000) if more than two authors. (Telma, 2001a), (Telma, 2001b); etc if the citation have the same author and year of publication.
For more information on Harvard Referencing: Guide visit
http://www.citethisforme.com/harvard-referencing
h. **References** must also be in the Harvard Format i.e. (Author, Date, Title, Publication Information). References are listed in alphabetical order. Examples are shown below:
Haghi, A. K. and Ghanadzadeh, H. (2005). A Study of Thermal Drying Process. *Indian Journal of Chemical Technology*, Vol. 12, November 2005, pp. 654-663

Kemp, I.C., Fyhr, C. B., Laurent, S., Roques, M. A., Groenewold, C. E., Tsotsas, E., Sereno, A. A., Bonazzi, C. B., Bimbernet, J. J. and Kind M.(2001). Methods for Processing Experimental Drying Kinetic Data. *Drying Technology*, 19: 15-34.

i. **Tables** should contain a minimum of descriptive materials. Tables should be numbered in Arabic numerals (1, 2, 3, etc), and should be placed at the referenced point with captions (centralised) placed at the top of the table.
j. **Figures**, charts, graphs and all illustrations should be placed at the referenced point, numbered in Arabic numerals (1, 2, 3, etc) and incorporated in the text. Caption for Figures should be placed at the bottom of the Figure (centralised). Lettering set or symbols should be used for all labels on the figures, graphs, charts, photographs even when drawn in colours. (Note that figures drawn in colours may be unreadable if printed in black and white).

k. **Equations** should be typed using MS Word Equation Editor and should be centred with number (in Arabic numeral) at the right margin.
l. Wherever possible, **Fractions** should be shown using the oblique slash. E.g. x/y
m. **Footnotes** should not be incorporated in the text.
n. **Acknowledgements** should appear at the end of the paper, before the list of references.

3. SUBMISSION OF MANUSCRIPTS

Manuscripts should be submitted by sending a Microsoft Word document (taking into account the Manuscript Requirements described in section 2 above) to the following email address: nschejournal@yahoo.com and copy stevmomoh@yahoo.com**.**

All correspondences are directed to the Editor-in-Chief using the submission emails addresses: nschejournal@yahoo.com and copy stevmomoh@yahoo.com. Meanwhile the online submission of articles on the journal website will soon be ready.

Authors should note that:

a. All authors listed in the manuscript have significantly contributed to the research.
b. All authors are obliged to provide retractions or corrections of mistakes.
c. All references cited are listed and financial support acknowledged.
d. It is forbidden to publish same research in more than one journal.

The fee charged for paper review and publication will be borne by the authors as follows:

a. Manuscript Review charges = N6,500 payable by both Members and Non-Member. Overseas is $30.00.
b. Publication Charges = N10,000 payable by Non-Members and Members who are not financially up-to-date. Overseas is $40.00.
c. Members would only get one (1) Journal free and buy the other if they so wish.
d. Corresponding Author whose paper is published on a particular edition would get one (1) free copy on behalf of all the co-authors. Other co-authors will buy if they so wish.

All fees are paid after the paper had been accepted for publication. These charges may be reviewed from time to time by the Governing Board of Directors of the Society.

4. ACCEPTED PAPERS

On acceptance, authors will be required to submit a copy of their manuscripts using Microsoft Word by emails to nschejournal@yahoo.com and copy stevmomoh@yahoo.com.

The following additional information should be observed for accepted papers: (i) Typed in Microsoft Word using 1.15 spacing on A4-size paper, Times New Romans font and 10 point; (ii) Margin should be 2.54cm for Top & Bottom; 2.20cm for Left & Right margins; (iii) The abstract should be one column document while the body of the manuscript should be double columns with 0.5cm gutter spacing except some tables and figures that may have to go in for one column document.

5. PUBLICATION

Full NSChE Journal edition in hard copy will be published twice annually – March/April Edition and September/October Edition.

6. REPRINT

Reprints are available on request at a moderate fee per page. Orders must be placed before the paper appears in Print.

7. READER'S INFORMATION

The papers are wholly the view of their author(s) and therefore the publisher and the editors bear no responsibility for such views.

8. SUBSCRIPTION INFORMATION

The subscription price per volume is as follows:

a. Individual Reader - N3,000.00
b. Institutions, Libraries, etc.- N5,000.00
c. Overseas Subscription - $100.00

Request for information or subscription should be sent to the Editor-in-Chief through the following emails addresses: nschejournal@yahoo.com and copy stevmomoh@yahoo.com.

9. COPYRIGHT NOTICE

By submitting your manuscript to the Journal, you have agreed that the copyright of the published material belongs to the journal.

10. PRIVACY STATEMENT

The names and email addresses entered in this journal site will be used exclusively for the stated purposes of this journal and will not be made available for any other purpose or to any other party.